

**3D-PRINTED MULTIPROBE ANALYSIS
SYSTEM FOR SOLAR FUEL RESEARCH; DESIGN,
FABRICATION AND TESTING**

**A Thesis Submitted to
the Graduate School of Engineering and Sciences of
İzmir Institute of Technology
in Partial Fulfillment of the Requirements for the Degree of
MASTER OF SCIENCE
in Energy Engineering**

**by
İpek HARMANLI**

**December 2016
İZMİR**

We approve the thesis of **İpek HARMANLI**

Examining Committee Members:

Ass. Prof. Dr. Engin KARABUDAK
Department of Chemistry, İzmir Institute of Technology

Prof. Dr. Mehtap EMİRDAĞ EANES
Department of Chemistry, İzmir Institute of Technology

Ass. Prof. Dr. Ceylan ZAFER
Department of Solar Energy, Solar Energy Institute, Ege University

26 December 2016

Ass. Prof. Dr. Engin KARABUDAK
Supervisor, Department of Chemistry
İzmir Institute of Technology

Ass. Prof. Dr. Özgeç EBİL
Co-advisor, Department of Chemical
Engineering, İzmir Institute of Technology

Prof. Dr. Gülden GÖKÇEN AKKURT
Head of the Department of Energy
Engineering

Prof. Dr. Bilge KARAÇALI
Dean of the Graduate School of
Engineering and Sciences

ACKNOWLEDGEMENTS

There are a number of people without whom it would not have been possible to complete this master thesis and to whom I am grateful.

To my supervisor, Ass. Prof. Dr. Engin KARABUDAK, for his full support, expert guidance, understanding and encouragement over the last year and a half. His in-depth knowledge and patience made it possible to complete this thesis and I cannot image this study could not be finished without his endless help. I am extremely grateful being part of a work team of his research group.

Besides my advisor, I would like to thank to rest of my thesis committee: Prof. Dr. Mehtap EMİRDAĞ EANES and Ass. Prof. Dr. Ceylan ZAFER.

To members of Karabudak Research Group, Uğur SOĞUKKUYU, Mert KOÇ, Mehmet Onur CİRİT, Özge Sevin KESKİN, Fetiye Esin YAKIN and Alaaddin GICI for their help, great patience and motivation at all times. They are always with me when I feel desperate and they are always there for me when I need them.

To Mehtap EMİRDAĞ EANES and her research group, for their technical support and providing $PbVO_3Cl$ for this research which are the vital part of this study. To Assoc. Prof. Dr. Volkan CECEN for guidance in academical writing. Also, to Ass. Prof. Dr. Haldun SEVİNÇLİ for help in calculation of computational analysis.

To Polat BULANIK for his technical support during this study especially in most critical times.

Finally, my sincere thanks to my parents, Erdal and Aliye HARMANLI, and Chemometric Research Group and my sincerely friends, Ayten Ekin MEŞE, Başak BAŞAR and Gün Deniz AKKOÇ, also Arzu GÜZELDEREN for supporting me spiritually throughout my entire study and encouraged my activities.

ABSTRACT

3D-PRINTED MULTIPROBE ANALYSIS SYSTEM FOR SOLAR FUEL RESEARCH; DESIGN, FABRICATION AND TESTING

Methods of generating electricity with unlimited, clean and cheap energy from solar energy are tried to be investigated and developed in practical and theoretical academic fields. Especially, photocatalytic water splitting (PWS) systems have been identified as the main method in this study as well as in many studies due to the advantages provided by production of solar fuels from water. In this research, a study was carried out on the alternatives of the both used experimental set-up and used photocatalytic material for PWS systems. A study has been carried out on both the used experimental setup and the used photocatalytic material alternatives in PWS systems. As an alternative experimental setup that allows small volume analysis for PWS by Unisense gas microsensors, a mini photoreactor was designed using 3-D drawing and printing techniques and its usability was tested for PWS applications. Moreover, some characterization results for the electronic band structure and the band gap of the lead (II) trioxovanadate (V) chloride [PbVO₃Cl] crystal, which was discovered by Eanes and co-workers in 2007 at IZTECH, was introduced in this study by not only theoretical (DFT approximations; LDA, GGA and HSE06) but also experimental (XRD, Diffuse Reflectance Method- Tauc Plot, Raman Spectroscopy, Four Probe) methods. Also, its estimated theoretical price and its potential for future application in tandem solar fuel device as a photoanode in combination with Si photocathode was calculated and discussed. The results showed that the designed mini photoreactor system is an open to development apparatus that is suitable for PWS, besides, PbVO₃Cl has an "indirect transition" band structure and a band energy of ~ 2.2 eV. Although it did not give an effective result in PWS applications done by the designed mini photoreactor, it can be said that it is a semiconductor which is worth studying and developing in detail for other researches in this field due to the compatibility of its band energy amount and optical properties for PWS.

ÖZET

GÜNEŞ YAKITLARI ARAŞTIRMALARI İÇİN ÜÇ BOYUTLU PRİNER BASKILI ÇOKLU SENSÖR ANALİZ SİSTEMİ; DİZAYNI, ÜRETİMİ VE TEST EDİLMESİ

Son yıllarda dünyanın içinde bulunduğu enerji krizine alternatif olarak sunulan güneş enerjisi limitsiz olması, ücretsiz elde edilebilirliği ve çevre duyarlılığı ile alternatif enerji kaynağı araştırmaların en popüler konusu haline gelmiştir. Kullanıcılar için maliyetli olmayacak ve güneş enerjisini en verimli şekilde hayatımıza dahil edebilecek sistemleri arttırmak ve geliştirmek amacıyla birçok teknolojik ve bilimsel araştırma yapılmaktadır. Güneş enerjisinin kimyasal enerji olarak depolanmasıyla dolaylı yoldan elektrik üretimi sağlayan güneş yakıtlarını ve bu yakıtların fotokatalitik su ayrıştırması (FSA) basamağındaki sistemlerinin geliştirilmesini temel alan bu çalışmada; suyun fotokatalizi sırasında ihtiyaç duyduğu enerjiyi verimli şekilde güneşten almasına yardımcı ışığa duyarlı fotokatalitik bir malzeme ve hem bu malzemenin hem de önerilen tüm fotokatalitik malzemelerin küçük hacimlerde analiz edilebileceği bir deneysel düzenek önerilmiştir. Bu düzenek için ince uçlu gaz mikro-sensörleri kullanılmış ve 3D çizim/baskı teknikleri kullanılarak ufak bir fotoreaktör tasarlanıp bu reaktörün FSA yöntemindeki amacına uygunluğu test edilmiştir. Ayrıca, 2007’de Mehtap Emirdağ Eanes ve ekibi tarafından bulunan *kurşun (II) trioksovanadat (V) klorür [PbVO₃Cl]* kristalinin elektronik bant yapısı ve bant enerjisinin tespiti için hem teorik (DFT yaklaşımları; LDA, GGA, HSE06) hem de deneysel karakterizasyon metotları (XRD, Diffuse Reflectance Method- Tauc Plot, Raman Spectroscopy, Four Probe) uygulanmış ve güneş yakıtı cihazlarında yarı iletken madde olarak kullanılabilirliği incelenmiştir. İlaveten, ileride PbVO₃Cl’nin fotoanot, silikonun (Si) fotokatot olarak kullanıldığı çift katmanlı bir güneş yakıtı cihazının verimliliği ve PbVO₃Cl’nin tahmini fiyatı teorik olarak hesaplanmış ve tartışılmıştır. Sonuçta, dizayn edilen mini fotoreaktör sisteminin FSA’nın amacına uygun ve geliştirilmeye açık bir deneysel düzenek olduğu, PbVO₃Cl’nin ise “dolaylı geçiş” bant yapısına ve ~2.2 eV’lik bant enerjisine sahip olduğu ve FSA’da etkili bir sonuç vermese de optik özelliklerinin ve bant enerjisinin uygunluğu sebebiyle bu alanda yapılan diğer çalışmalar için daha detaylı incelenip geliştirilmeye değer bir yarı iletken olduğu söylenebilmektedir.

TABLE OF CONTENTS

LIST OF FIGURES	ix
LIST OF TABLES	xii
CHAPTER 1.INTRODUCTION	13
1.1. History of Energy	13
1.2. Global Energy Consumption	15
1.3. Solar Energy	18
1.4. Solar Fuels	22
1.5. Natural and Artificial Photosynthesis by Water Splitting	25
1.5.1. Photo catalysts and Semiconductors	29
1.5.2. Water Splitting Principles of Semiconductors	34
1.6. Aim and outline of the of thesis	39
CHAPTER 2.DESIGN OF THE MINI PHOTOREACTOR	41
2.1. Abstract	41
2.2. Why is a mini photo reactor needed to design for PWS?.....	42
2.2.1. Scientific Problems.....	42
2.2.2. The Solution by Proposing Experimental Set-up	43
2.3. Design by 3D-drawing	43
2.3.1. Limitations of the design for PWS applications.....	44
2.4. Conclusion: Achievements of the chapter.....	47
CHAPTER 3.FABRICATION AND TESTING OF THE MINI PHOTOREACTOR ..	48
3.1. Abstract	48
3.2. Introduction	49
3.3. Sensor calibration	54
3.3.1. Experimental	54
3.3.1.1. Calibration of Temperature sensor	54
3.3.1.2. Calibration of pH sensor	55
3.3.1.3. Calibration of Oxygen sensor.....	55
3.3.1.4. Calibration of Hydrogen sensor	56
3.3.2. Calibration Results and Discussion.....	58
3.4. Fabrication of the Mini Photoreactor	61

3.4.1. Encountered problem and remedial solution.....	63
3.5. Tests of the Mini Photoreactor	65
3.5.1. Hermetically sealed surrounding tests.....	65
3.5.2. The tests for the effects of the light on sensors	69
3.5.3. Working Test of The Designed System with Mini Photoreactor ...	74
3.5.3.1. Experimental	74
3.5.3.2. Results and Discussion.....	76
3.5.4. Efficiency limit of the new designed PWS system	78
3.6. Conclusion: Achievements of the chapter.....	79
CHAPTER 4. PbVO ₃ Cl AS A PHOTOCATALYST FOR PWS REACTIONS	81
4.1. Abstract	81
4.2. Introduction	82
4.3. Synthesis.....	82
4.4. Analysis of Optical Properties of PbVO ₃ Cl by Experimentally and Theoretically.....	85
4.4.1. Analysis of Optical Properties (Experimentally)	85
4.4.1.1 XRD Analysis	85
4.4.1.2. Band Gap Determination by using Diffuse Reflectance (UV-Vis Spectroscopy) and Tauc Plot Method.....	86
4.4.1.3. Four Probe	89
4.4.2. Analysis of Optical Properties (Theoretically).....	90
4.4.2.1. State-of-the-art Density Functional Theory Calculation	90
4.4.2.2. Electronic Band Structure – Plotting GGA Approximation.....	91
4.4.2.3. Drawback of DFT formalism - LDA, GGA and HSE06 Approximation.....	92
4.4.2.4. Phonon Calculations by Raman Spectroscopy and DFT	94
4.5. PbVO ₃ Cl in the new designed PWS system.....	95
4.6. The Future Speculations about PbVO ₃ Cl.....	99
4.6.1. Theoretical Solar Efficiency Calculation for Single Layer PbVO ₃ Cl.....	99
4.6.2. Theoretical Solar Efficiency of Double Layer Semiconductor	101
4.6.3. How much voltage can be produced by designed device with PbVO ₃ Cl? – The Band Position of PbVO ₃ Cl.....	103
4.6.4. Tecno-economic Analysis of PbVO ₃ Cl.....	104
4.7. Conclusion: Achievements of the chapter.....	107

CHAPTER 5.CONCLUSIONS AND FUTURE PERPECTIVES 109

REFERENCES 112



LIST OF FIGURES

<u>Figure</u>	<u>Page</u>
Figure 1.1. A basic illusion for two ways of energy generation by sun light.	22
Figure 1.2. A schematic for Natural & Artificial Photosynthesis by Water Splitting. ..	25
Figure 1.3. Gibbs energy change in photocatalytic reactions.	29
Figure 1.4. Generally, the schematized band edge positions of the materials depending on the band theory.	32
Figure 1.5. Simple diagram for the band structure of a semiconductor to show the significant parts.	32
Figure 1.6. A diagram for the Direct and Indirect band gaps.	34
Figure 1.7. The photocatalytic reaction steps while occurring with photocatalysts.	36
Figure 1.8. The photoabsorption step in the semiconductors.	36
Figure 1.9. Band edge positions of some semiconductors at pH=0.	37
Figure 1.10. The effect of the particle size on the recombination center in the photocatalysts.	38
Figure 2.1. A graphical abstract for the used experimental set-up for photocatalytic water splitting process.	41
Figure 2.2. The dimensional size of the standard UV-quartz cuvette.	44
Figure 2.3. The dimensional size of the Unisense Microsensors.	44
Figure 2.4. Solidworks drawings: the primitive parts of designed mini photoreactor; a) the container, b) the lid.	45
Figure 2.5. Solidworks drawings: a small window was opened on the container.	46
Figure 2.6. Solidworks drawings: the sensor entrance holes were placed on the lid; a) side view, b) top view.	47
Figure 3.1. A graphical abstract for the fabrication of the new designed mini photoreactor.	48
Figure 3.2. a) The Unisense Multimeter, b) a schematic of internal structure of sensors, c) a photograph of one of the physically identical three micro sensors; T, H ₂ , O ₂ , d) the pH sensor.	51
Figure 3.3. The read sensor signals and the calibration curve obtained with the samples of known values, for Temperature sensor.	58
Figure 3.4. The read sensor signals and the calibration curve obtained with the samples of known values, for pH sensor.	59
Figure 3.5. The read sensor signals and the calibration curve obtained with the samples of known values, for Oxygen sensor.	60

Figure 3.6. The read sensor signals and the calibration curve obtained with the samples of known values, for Hydrogen sensor.....	61
Figure 3.7. The Stratasys- Objet30 Prime 3D printer that used in this study.....	62
Figure 3.8. One of the tester 3D models of the mini photoreactor by opaque material (VeroWhite).	62
Figure 3.9. Numerous and different forms of the mini photoreactor test prints.	63
Figure 3.10. The test printing of the reactor (by VeroClear) and the sensor simulations (by Verowhite).....	64
Figure 3.11. The final design of the mini photoreactor.	64
Figure 3.12. Ready to be used for the airtightness test of the reactor.....	66
Figure 3.13. Airtight system experiment modified with sticky tape wrt. the amount of dissolved oxygen gas in the system.	67
Figure 3.14. Airtight system experiment modified with paraffin film wrt. the amount of dissolved oxygen gas in the system.	68
Figure 3.15. Airtight system experiment modified with gum adhesive wrt. the amount of dissolved oxygen gas in the system.	68
Figure 3.16. The whole image of the used solar simulator device with its parts and the configurable posemeter and the numerical monitoring system according to intensity of light which is read by posemeter a) long distance, b) short distance.	69
Figure 3.17. The image of the Unisense microsensors a) transparent tip, b) black tip.....	70
Figure 3.18. An image from the light impression tests during an light-on part of the experiments in the dark.	71
Figure 3.19. Response of old transparent-tipped O ₂ /H ₂ sensors to light in pure water analysis.	72
Figure 3.20. Response of new black-tipped O ₂ /H ₂ sensors to light in pure water analysis.	73
Figure 3.21. Response of all new black-tipped sensors to light in pure water analysis.	74
Figure 3.22. The hand-made magnetic stirrers; a) small:6.5*6.0*9.5, b) large:17.5*17.5*6.5.....	75
Figure 3.23. Response of Degussa p25 to green laser light in pure water, 10 min.	76
Figure 4.1. Crystal structure of PbVO ₃ Cl.....	81
Figure 4.2. The synthesized PbVO ₃ Cl crystals.....	83
Figure 4.3. Produced PbVO ₃ Cl Samples: a) Trial-1, b) Trial-2, c) Trial-3, d) Trial-4... ..	84
Figure 4.4. The snaps of the yellow needle PbVO ₃ Cl crystal by Optical Microscope “Olympus BX53”.	85

Figure 4.5. XRD results of powdered crystal PbVO_3Cl (1.540598 Å wavelength in data range 4.993° - 69.995°).	86
Figure 4.6. The absorption edge plot of 4 optical band gap predictions depending on transition type.	88
Figure 4.7. Four Probe Mechanism.	89
Figure 4.8. Electronic band structure as obtained from GGA.	92
Figure 4.9. Electronic density of states as obtained from LDA, GGA and HSE06 schemes (red, green, blue, respectively). The zero of the energy is set to the valence band edge.	93
Figure 4.10. Phonon calculation plots of PbVO_3Cl ; theoretical DFT analysis and Raman Spectroscopy.	95
Figure 4.11. The used light sources.	96
Figure 4.12. Response of PbVO_3Cl a) under sun light in pure water - 30 min. periods, b) under White led light in pure water - 5 min. periods, c) under green laser light in pure water - 5 min. periods.....	97
Figure 4.13. Response of PbVO_3Cl a) under green laser light in pure water - 30 min. periods, PbVO_3Cl with Pt powder, b) under Xenon light in pure water - 5 min. periods, PbVO_3Cl with Pt powder.	98
Figure 4.14. The Total Solar Radiation Power Spectrum was drawn with OriginPro by taking data from https://www.pvlighthouse.com.au	100
Figure 4.15. Lewis Structure in PEC cell. Reproduced with permission of the Nature Publishing Group (Nature Chemistry)(Gray 2009) 2009, Macmillan Publishers Limited.	102
Figure 4.16. Band edge positions of selected semiconductors and 4 possible band edge positions of PbVO_3Cl	104
Figure 4.17. Plotting the price of a) Vanadium and b) Lead versus years(Service 2015). The tendency refers to forecasting in average price of the matter. The sharper temporal increase in price data may be caused by global wars or global crisis.....	106

LIST OF TABLES

<u>Table</u>	<u>Page</u>
Table 1.1. The roughly consumed energy data of some countries, in TW units (2000-2013)	17
Table 1.2. Estimated global potentials of the power in energy generation per year (in TW) depending on the all of energy sources.....	19
Table 1.3. Comparison of hydrogen with other fuels that is based on their lower heating values (LHV) at 1 atm and the LHV-HHV values of these common fuels at 25 °C, 1 atm. (Parthasarathy and Narayanan 2014).	24
Table 2.1. The technical information sheet for the Unisense Microsensors.....	52
Table 4.1. Reactants of Synthesis Reaction.....	83
Table 4.2. PbVO ₃ Cl pallet Four Probe Measurement results, the thickness is 850 microns in all measurements); Conductivity = 1/ R*Thickness	90
Table 4.3. Electron energy efficiency result of PbVO ₃ Cl/Si tandem PEC device.....	102
Table 4.4 Material list with respect to their earth abundancy and price. (WebElements.com Archived from the original on 9 March 2007).....	105
Table 4.5. Comparison of hydrogen with other fuels that is based on their prices for 1 kWh, at 1 atm, at 25 °C, 1 atm.....	107

CHAPTER 1

INTRODUCTION

1.1. History of Energy

Energy has a critical role in the life cycle. Every living organism remains alive using several variations of the energy. Although the definition of energy varies depending on the source or use of living organisms, it can be identified as the source of life in the universe.

The Greek (*energeia*) produced “energy” word was entitled as the first time in Aristotle's work which was mentioned in *Nicomachean Ethics* in the 4th century-BC (Joachim and Rees 1953, Reeve 1992). In spite of the fact that the mankind was not aware of the concept of energy-in today's sense-in the first period, houses were oriented regarding the sun and wind for heating, cooling, and light.

Over centuries, humankind who need more energy from day to day, they exert more effort to find the necessary energy to be self-sufficient. At the beginning of the 13th century, coal mines and wood gained popularity in Europe (Davids and Davids 2012, Jerome 1934). Then, more coal was mined and at deeper depths when became scarce In Europe, in 1600s. For this aim, in the early 1700s, Thomas Savery (1650-1715, an English military engineer) developed the first steam engines, which could run on coal and did not need to be powered by wind or water, to pump water out of the mines (More 2002). In 1712, the engines were refined by Thomas Newcomen (1663-1729, another English engineer) More (2002). James Watt (1736-1819), who was asked to repair a Newcomen engine, improved the efficiency of these engines over several years, from 1763 to 1775 (Rider 2007, Stearns 1993). And then sold or rented his engines to mining companies, charging them for the "power" in the rate of work the engine produced. As the result of this new source of power, the Industrial Revolution that created a new world in the universe, began in Europe (Stearns 1993).

During all this time, energy had a meaning from the point of not only industry and mechanics but also science. There are many speculations about the first debut of the scientific meaning of energy. According to some historical sources questionably,

Gottfried Leibniz expressed an opinion in 17th century (1676-1689) about energy with a Latin term, “vis viva”, which was similar with the meaning of energy in modern sense (he believed the total vis viva was conserved) although Thomas Young was the first person who mentioned about “energy” as a term while he was teaching the royal society in 1802 (Smil 1994, 2000, Smith 1998, Young 1807).

In 1669, the laws of collision was published by Christian Huygens (Smil 1994). Also, many physicists likely Newton claimed that the conservation of momentum which includes the systems in the presence of friction (Smil 1994, Smith 1998). After many years, it would be determined that both kinetic energy and momentum are conserved at the suitable conditions, for example during elastic collision. In the early 19th century as firstly, the laws of energy conservation were accepted and performed some applications on isolated systems. Gustave-Gaspard Coriolis (in 1829) identified kinetic energy and in 1845, the link between the heat generation and mechanical work was discovered by James Prescott Joule (Joule 1845). In the meantime, William Rankine lexicalized the potential energy term and the phrase of the law of the conservation energy with respect to principle was used firstly by him in 1850 (Macquorn Rankine 1853, Smith 1998). Also, William Thomson merged all of these terms and the laws of these term under the name of “thermodynamics” by virtue of the well-developed explanations of chemical processes which were based on the usage of the energy concept by Josiah Willard Gibbs, Walther Nernst and Rudolf Clausius (Qasim 2014, Smil 1994, Smith 1998). Moreover, this mergence played a role in not only development of the mathematical formulation of the entropy concept (by Clausius) but also investigation of laws of radiant energy (by Jožef Stefan). Furthermore, in 1844, William Robert Grove brought together- heat, electricity, mechanics, magnetism and light- under the same roof as a single word: “force” by asserting the relationship between them and his theories were published in his book (The Correlation of Physical Forces) in 1847 (Grove 1874).

In addition to these, energy concept began to be investigated in more detail at the molecular level. In 1911, when it was discovered that the beta decay is not part of a continuous radiation, energy conservation was considered to be a contradictory phenomenon by the reason that at it was believed that an electron beam of beta radiation from the atomic nucleus at that time (Jensen 1999, Brown 1978). In 1933, Enriko Fermi resolved this problem by explanation of the source of missing energy as the correct

approximation of beta decay; emission of not only an electron but also an antineutrino were possible (Wilson 1968, Griffiths 2009).

1.2. Global Energy Consumption

For all we do as individuals and as societies, the energy needs have not changed since ancient times and still, the energy consumption is essential in our lives. By the reason of our energy consumption, humanity need to investigate and develop new energy sources and technologies. In a short time, electricity and liquid fuels have reformed our life standards.

Generally, consuming the total produced energy by human civilization is called *global energy consumption* and it is measured in every year by some specific information agencies statistically to realize the current situation and to make predictions about the growth of the circumstances. According to the agency that is one of the most popular one, International Energy Agency (IEA)-USA, the consumed energy was almost 12.3 TW that was consumed as fuel (~70%) and as electricity (~30) by humanity, in 2013 (Sinha and Chattopadhyay 2015).

On the other hand, in 21th century, humanity have a serious problem in energy consumption that is directly related to famine of energy sources, globally. Currently, the primary energy source is supplied from fossil fuels, which accounts for ~81% of all energy supplies in 2011 and 2012. According to a report, which was published 2009 by Richard and Marc Perez, the world (~7 billion people) consumed 16 TW and 17 TW energy in 2009 and 2013, respectively (Perez and Perez 2009). It is estimated that the number of people will increase to ~9 billion (or upper) and this population will consume 30 TW energy in 2050 and when that time comes, the fossil fuel reserves will be depleted. Depending on the current and estimated global energy consumption rate, coal, oil and natural gas can be sufficient for more 150-350, 45-70 and 65-170 years, respectively. However, they are in a short supply because the speed of discovering the attainable new fossil fuel reserves is impossible to keep up with the speed of the global energy consumption. On the other side, the fossil fuels are really detrimental energy source for environment due to the fact that their contribution to global warming and the emission of greenhouse gases via CO₂ production (Allison et al. 2011, Oppenheim and Beinbocker 2009). For these reasons, many researchers, scientists and also politicians

show interest to find a large scale, sustainable, clean (carbon- neutral) and economic alternative energy sources. Wind, water (hydrolic power), geothermal water and sun are the biggest candidates as a new energy source to be alternative to fossil fuels due to be a limitless sources (renewable), although lots of energy source reserves are found and investigated for energy generation (especially electricity) from nuclear to the hybrid technology.

As it mentioned before, electricity is the essential and easy form of energy to use it for our daily-technological lives. According to IEA data, the statistical predictions shows that the global energy consumption as electricity will increase 30% (Blok and Nieuwlaar 2016) in 2040. Furthermore, this consumption need will be supplied by ~80% growth of renewable energy. Likely this, the Bridge Scenario (the special prediction cycle for energy consumption in time) claims that the role of electricity generation by renewable -primary- energy sources will scale from 14% (2013) up to 20% (2030) (SourceOECD 2006). However, the utilization of oil, natural gas and coal went on to increase much more than renewable energy even though the renewable energy concept had jumped rapidly to higher utilization rate between 2000 and 2012. The utilization of renewable energy data, which belong to some countries between 2000-2013, are placed in Table 1.1 (Sidén et al. 2016). As it can be seen from the table, the total energy consumption by renewable energy source increased from 2000 to 2013 as ~6,500 TW, globally.

Table 1.1. The roughly consumed energy data of some countries, in TW units (2000-2013)

Countries	2000	2010	2013
Asia (-China)	4,147	4,996	5,361
Africa	2,966	3,930	4,304
China	2,613	3,374	3,847
North-America	1,973	2,237	2,443
Latin America	1,502	2,127	2,242
EU	1,204	2,093	2,428
Russia	245	239	271
Others	567	670	738
Total energy	116,958	148,736	157,485
Total non-renewable	101,721	129,025	135,800
Total renewable	15,237	19,711	21,685

Briefly, if it is needed to explain the most common renewable energy utilizations in general;

The geothermal- power plants use the heat energy extraction of the hot-underground water to convert the thermal energy to the electrical power by helping of mechanical systems such as heat pumps. Geothermal energy is used for electricity generation (~56 TWh, in 2004) and to use it directly for heating (~75 TWh, in 2004) in almost 70 countries of the world (Thorsteinsson et al. 2008).

The hydroelectric- power plants use the kinetic energy of flowing or falling water to generate electricity. Hydropower is used in over 150 countries and now there are three large capacity (~10 GW) power plants which are used the hydropower to generate electricity. Hydroelectric power plants generated 16.5% of the total electricity and 71% of the total renewable electricity of the world in 2015 (Breyer et al. 2016).

The marine energy is depended on the tidal and wave power in oceans and it uses to generate electricity by hydrokinetic energy, likely hydroelectric power plants. Although the marine power utilization is placed at beginner level, the theoretical

numbers shows that the electricity generation potential of marine power is equivalent to 4-15 million toe (tone of oil equivalent) (Castellucci, Eriksson, and Waters 2016).

The biomass energy generates electric power and heating power for direct use by chemical reactions. Biomass energy was capable to compete with fuel at the beginning of 19th century but now it is just a little part of the overall energy supply. In 2005, ~44 GW of electricity production was by biomass and also in 2005, the bioethanol production in the world increased by 7.9% (Martinot and Sawin 2012).

The wind power is one of the most developed types of renewable energy sources. The kinetic energy that it comes with wind naturally is converted to electricity or it is used for as a mechanical power source to transport the water, to grind the legume, likely in ancient times. According to 2011 data, all over the world, 84 countries have used the wind power for electricity generation and common other uses. ~3,5% of the total electricity production of the world was supplied by wind power, in 2013. In 2015, the worldwide installed capacity of wind power was ~450 MW by developing rate of 17% (Aguilar and Mabee 2014, Pullen 2007).

The solar energy is the greatest hope of the world for future. Since ancient times, it has been used for heating and it has been also used for electricity generation in modern life. The solar energy can be stored not only by exposing the conductive materials to sun directly (domestic water storage tanks), due to get thermal-heat energy but also by using some modern- material technologies due to generate electricity (photovoltaics). Even though the number of countries in which it is used is not known precisely, the recent statistical energy data are known to show that the world economy in energy is getting better by helps of solar technologies. Currently, water heating is more favorable application than generating electricity by solar power, approximately 1% of the world's energy in electricity (in 2007, 154000 MW) (Green et al. 2015).

1.3. Solar Energy

Confirming the effort to find alternative energy sources, when the energy consumption profile of the world is examined, it is seen that the use of needed energy of world is much more than the promise of dominant fossil fuels. Therefore, among the alternative energy sources such as wind energy, hydrokinetic energy or geothermal energy, solar energy is the most striking. Obviously, sun is the natural heat and light

source for the earth and the heat and light of sun can be harnessed to produce electricity and heat energy as long as the world exists.

Global primary energy consumption in 2009 was 16 TW, in 2013 was 17 TW and is predicted to at least double by 2050. It can be seen from Table 1.2 that the most powerful type is solar sources to cope up with the energy needs of the world (Perez and Perez 2009).

Table 1.2. Estimated global potentials of the power in energy generation per year (in TW) depending on the all of energy sources.

Source	Power per year(TW-year)
Tides	0.3
Geothermal	0.3-2
Hydro	3-4
Biomass	2-6
Ocean Thermal Energy	3-11
Wind	25-70
Uranium	90-300
Natural Gas	215
Petroleum	240
Coal	900
Sun	23000
<i>World energy use (estimated)</i>	<i>16</i>

Among the various energy sources, sun is an energy source available on our planet (solar energy received by emerged continents only, assuming 65% losses by atmosphere and clouds). When the world consumes 16 TW energy, sun provides 23,000 TW (~500,000 billion barrels of oil or 800,000 billion metric tons of coal) energy to earth in a year (Perez and Perez 2009). It is estimated that around 0.01% of the energy of one second of sunlight irradiation is sufficient for the annual energy consumption of human society. That is to say, we are really lucky due to use it in the energy conversion for our lives.

On the average, the sun delivers ~1400 W/m² to the earth and also, at the upper levels of atmosphere in 24-hours, the collected energy amount reaches to 14 million calories. Furthermore, cloud cover reflects back the 1/3 of it into the space as the other portion 2/3 is traveled along with atmosphere by powerful wind and water cycles thus

and so the Earth's climate is derived by sun. To give concrete support, when the sun is at the highest point on a sunny day and cloudy day in the northern part, it can be between 1000 W/m^2 and 200 W/m^2 , respectively (Painuly 2001). Nevertheless, using this power directly to produce utilizable energy - especially for electricity- is more difficult than to use it directly for heating homes or water.

Currently, the scientists' main problem with solar energy for high levels of use comes from the fact that it is so diffuse and spread out, and must be collected over large areas. Scientifically, the solar energy generation techniques had been built by collection methods. In general, we can gain favor from sun via two fundamental collections; as *passive solar power collection*: warming and lightening of houses and buildings – naturally, no need external intervention- by sun, as *active solar power collection*: using extra materials –chemicals, collectors, reflectors etc.- by sun to collect the sunlight for energy generation. The active solar collection depends on energy generation using thermal or photonic properties of the sun light to produce energy for directly use as electricity –conversion with direct electron transfer-and to produce energy for indirectly use as fuels -collect the energy through artificial/natural chemicals (in the form of biomass or in water or in chemicals).

The oldest studies were about electricity generation for directly use of solar light with collectors which are called as photovoltaic devices/solar cells- now it is known as solar panels. These cells are placed into modules which are made by a sandwich-between a plate and glass- with semiconducting materials and then their arrangements in arrays are used on rooftops or over acres to convert the sunlight into electricity, directly. Actually, the world's first solar collector was designed by Horace de Saussure in 1767. And then, the phenomenon of photoelectricity, which was discovered by George May in the late 1800's- light can discharge electrons from used materials that they can be converted to electricity directly - is the main point of photovoltaic cells (Blok and Nieuwlaar 2016, Breyer et al. 2016). Although the first photoelectric cell- using the selenium (the photoconductivity of selenium was discovered by Willoughby Smith in 1873)- was produced by Rudolf Hertz soon thereafter the physics of photoelectricity was explained by Albert Einstein in 1905, the first practical and commercial solar cells were developed by the Bell Telephone Company in the 1950's. In recent years, the production of solar cells and photovoltaic arrays has been developed because of the raised require for renewable energy sources. Whereas the early cells contained

selenium, the later cells contain especially silicon derivatives- (Malhotra et al. 2010) which is commonly used today since 1940s-1950s (monocrystalline silicon, polycrystalline silicon, amorphous silicon), cadmium telluride, and copper indium gallium selenide/sulfide etc. By using indium, gallium and deselenide, the latest development in PV has been performed as the thin film solar panel (Walsh 2008). Photovoltaic solar cells were used on satellites firstly but now they are used for signaling and telecommunications and alarm systems all over the world. In 2012, the installed capacity of PV cells achieved to 100 GW (Nelson and Starcher 2015). Although the largest photoelectric cells still have a conversion efficiency under 20%, now in sense of globally installed capacity, solar PVs are the third (after hydro-power and wind-power) useful renewable energy source which are used in more than 100 countries.

As you can see from Figure 1.1, the most basic difference between two methods is the used device system in order to convert the sun light. The characteristics of the operating device in the process of operation affect the usability of the resulting energy product. As a consequence of this, direct generation of electricity has some obstacles. PVs have a fixed place where optimizes for the most efficient conversion in power plants although the sun light can change its direction, intensity or position associated with day/night and summer/winter times. In spite of that the place of PV systems- in a large scale (such as power plants) cannot transport whenever want to depend on the sun. Additionally, PV systems are expensive devices when considering the material benefit of saving energy over time even though the cost of them has been reduced steadily by developing solar technology- since the first solar cells were developed. Furthermore, all we know that electricity is not a storable energy form and it should be used when it produces to protect the electric network.

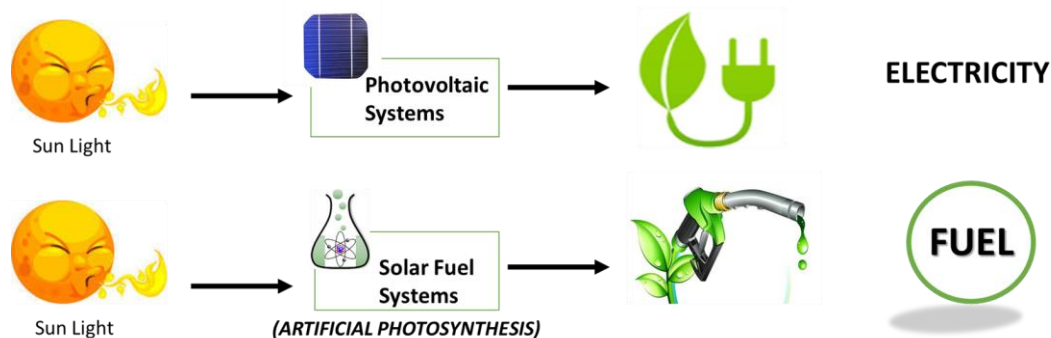


Figure 1.1. A basic illustration for two ways of energy generation by sun light.

On the other hand, solar fuels are energy rich chemical compounds made from sunlight, such as methanol or methane or CO. Unlike PV systems, solar fuel devices covenant the energy storage in a vessel (Kalyanasundaram and Graetzel 2010) and also, this storage capability allows easy transportation for energy in daily life. Besides of these advantages, hydrogen generation by using water (water splitting) and products of carbon dioxide reduction are the most widely researched solar fuels as roofing under artificial photosynthesis works (as the artificial photosynthesis, photon properties, semiconductors, hydrogen as an energy carrier and other significant concepts that should be known will be covered in summarily in the next chapter). The scientists try to find the cheapest way of producing energy from the sun light with solar fuel devices and the recent studies show that it will be a cheaper way than PVs for solar energy conversion (Navarro Yerga et al. 2009). Under these considerations, within the photon collection methods by sun, the most popular and hopeful one in academical researches and the technique that motivates this work is *solar fuel applications*.

1.4. Solar Fuels

Solar fuels are the alternative chemical fuels- can be produced directly or indirectly from solar light by thermochemical, electrochemical, photochemical or photobiological reactions- which are capable of storing and transporting the energy that comes from sun. Means that they can be stored or produced for later usage when the sunlight is inefficient or unavailable also that is the reason why solar fuels are the powerful alternative choices to fossil fuels.

In addition to that photons are the milestones of the sun/light which allow us to feel warmth of the air molecules and to comprehend the shapes/ colors of materials. The

reason of this, photons can be absorbed by nucleus- atoms-molecules. Just after the absorption, photons push their energetic particles (e.g. electrons) for transitions between their energy levels. On the basis of this, sun light has an ability (energy) to break chemical bonds and it can be used for transduction of absorbed and reduced photon energy into chemical energy.

For this transitional stage (from sun to fuel), there is a significant progress, which is developed by scientists, about using an intermediate energy (as an energy carrier) while producing energy from sun to be consumed by the final users as a fuel. Fundamentally, it is based on benefiting from materials that containing hydrogen and carbon (e.g. water, ethanol, methanol, etc.) to re-produce them as energy carriers (Van de Krol and Grätzel 2012b). But, the production of carbon derivatives (especially, CO₂ release) not welcomed by environmentalist views even if it helps to get rid of fossil fuels- cause to release in amount of carbon dioxide more than 3 times. Also, because of the electrochemical conversion of CO₂ to such as methane (8 electrons) needs more half reaction steps so that the direct photo/electrochemical conversion of CO₂ to solar fuels is more complicated than hydrogen (Lehn and Ziessel 1982, Rakowski Dubois and Dubois 2009). Thus, hydrogen (as a transport fuel) generation becomes more preferred method for solar fuel applications. Additionally, hydrogen has the highest energy content by weight of all the fuels but the lowest energy content by volume (Moriarty and Honnery 2009) thus, it must be condensed in order to make its use more practical.

In order to determine the amount of energy, every fuel has been tested, experimentally. The results of these tests are reported as the higher (HHV) and lower (LHV) heating value of fuels. Table 1.3 shows the comparison of hydrogen with other fuels that is based on their lower heating values (LHV) at 1atm and also it shows the LHV- HHV values of these common fuels. The heating values are based on the water phase in the reaction products. For instance, if water vapor is formed in the reaction, the LHV would be favorable. It can be possible that water is formed as in liquid form, then for this time, the HHV would be appropriate. In fact, likely in a combustion reaction, the production of water occurs in vapor form in a fuel cell, by this way, these numbers come into prominence with a discrimination: particularly the LHV values. It represents the amount of energy available to do work by the used fuel (Parthasarathy and Narayanan 2014).

Liquid hydrogen is used as a rocket fuel, and condensed hydrogen is used to generate electricity through the use of fuel cells. In both processes, the only and efficiently used product is water (it will mention as more detailed in next section) for making it the cleanest one of all fuels. However, there is one difficulty with hydrogen as a fuel is in its production. Hydrogen production requires a large amount of power or electricity and unless only carbon-free energy is used.

Table 1.3. Comparison of hydrogen with other fuels that is based on their lower heating values (LHV) at 1 atm and the LHV-HHV values of these common fuels at 25 °C, 1 atm. (Parthasarathy and Narayanan 2014).

FUELS	Density, kg/m³	Energy density, MJ/m³	Energy density, kWh/m³	Energy, kWh/kg	HHV*, kJ/g	LHV*, kJ/g
Hydrogen	0.0838	10.8	3.0	33.3	141.9	119.9
Methane	0.71	32.6	9.1	12.8	55.5	50.0
Gasoline	702	31,240	8,680	12.4	47.5	44.5
Diesel	855	36,340	10,090	11.8	44.8	42.5
Methanol	799	14,500	4,030	5.0	20.0	25.0

**Energy density = LHV * density, and the conversion factor is 1 kWh = 3.6 MJ.*

On the other hand, the sunlight is the best power source for hydrogen production. Solar hydrogen can be obtained by many ways such as; photobiological applications, photo electrochemical and photocatalytic methods, thermochemical conversion, coupled photovoltaic- electrolysis systems, plasma- chemical conversion, magnetolysis methods and radiolysis methods etc. However, this work is predominantly based on the principles of photo electrochemical and photocatalytic methods of solar hydrogen fuel production.

Up to now, the production possibilities, efficiencies and different methods of solar- hydrogen fuel production have been pursued by lots of scientists in laboratories all over the world. Currently, they agree on the existence of three approaches; solar thermochemical path (thermochemical conversion), solar electrochemical path (PVs) and solar photochemical path (natural photosynthesis and artificial photosynthesis) (Purchase et al. 2015, Steinfeld and Meier 2004). In a brief explanation, firstly, solar electrochemical approach is depended on made electricity by sunlight from photovoltaic systems or solar thermal systems- followed by an electrolytic process. Both natural and artificial photosynthesis directly use the photon energy; as examples for solar photochemical approach. As known that natural photosynthesis is a chemical process

which uses sunlight by plants, algae and certain bacteria to turn CO_2 into sugars that the cell can use as energy. Similarly, artificial photosynthesis is also a chemical process but it replicates the natural process of natural photosynthesis. Unlike these two processes, the sunlight is used due to its heat-richness instead of its photonic property. Namely, the thermochemical conversions are independent from photosynthesis principles. They are just based on heating materials to very high temperatures via using sunlight in order to produce H_2 or CO by reaction with steam or carbon dioxide at high temperatures.

1.5. Natural and Artificial Photosynthesis by Water Splitting

In nature, the green plants, bacteria and algae store energy from the sun in the diverse form of carbon hydrates by consuming water and CO_2 to producing them into oxygen and sugar. As a consequence of this production, the produced sugar (carbon hydrates) is used to grow and maintain the plants, or to make the plants be a food source for animals, or to reform living organisms that photosynthesize at the underground as a fossil fuels after their deaths by nature (Figure 1.2).

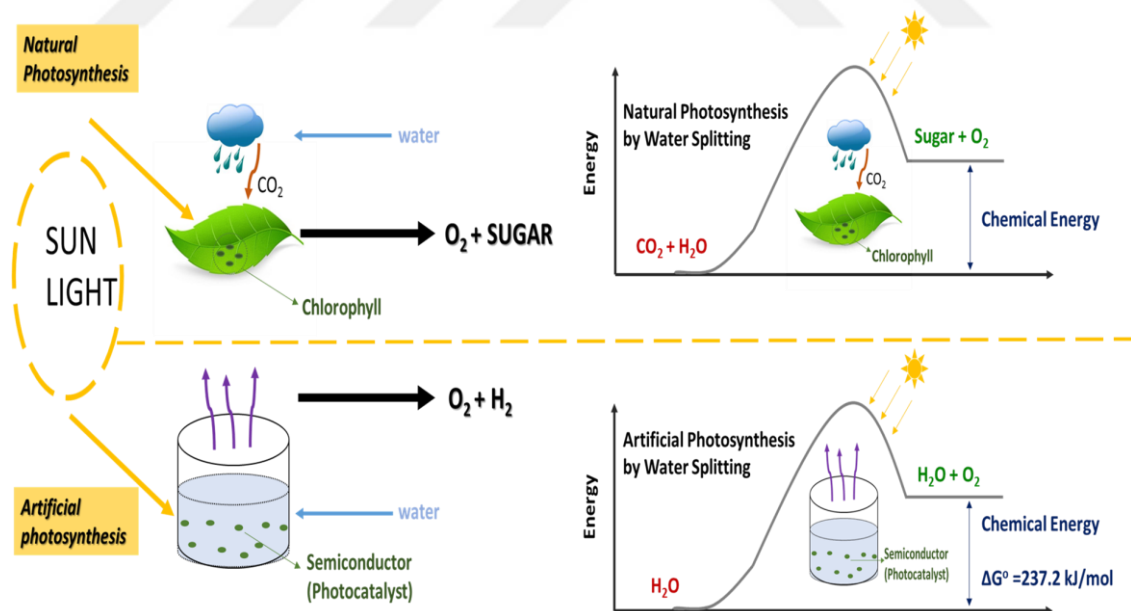


Figure 1.2. A schematic for Natural & Artificial Photosynthesis by Water Splitting.

Moreover, the formation of fossil fuels by living organisms' deaths has a slow conversion process at high pressures and high temperatures under the ground with containing high energy densities. Because of this, fossil fuels are favorable energy

sources of currently used fuels. By *natural photosynthesis*, the efficiency is relatively low though these high densities. Even if the plants, algae/ bacteria with the highest ability to perform photosynthesis are used, the conversion yield is only max. 2% and 5-10% in terms of solar energy, respectively (Purchase et al. 2015). One of the most possible causes is related with the inefficient usage of the sunlight by plants or others. In the violet and some in the red region- a narrow part- of the solar spectrum is used for NP but the sunlight has a significant energy potential in the green and yellow regions thus most of this energy is reflected by green leaves. On the contrary, the inspiration of natural photosynthesis- *artificial photosynthesis*- has an efficiency in practice as max. 18-20% and in theory as max. 40%. Natural photosynthesis is performed by four processes in nature; harvesting of light, charge separation, water splitting and production of fuel (Cogdell et al. 2010). Basically;

1. Chlorophyll is a vital piece for the first step. It captures the energy of sunlight and allow it to be used for the complex chemical reactions inside the plant to create various forms of carbohydrate. Light harvesting occurs with absorption of electromagnetic radiation (photons) by help of chlorophyll (antenna molecules). Protein complexes/ organelles pack these molecules together and deliver them to reaction centers to concentrate the captured energy.
2. In the charge separation step, a negatively charged electron is rejected by a chlorophyll molecule, at the same time, it leaves as a positively charged hole. In this way, the incoming sunlight energy has been used to degrade the positive and negative charges.
3. The third step is water splitting process that is the most important stage of energy production of the system. Contrary to wrong belief, most of the energy storage in photosynthesis is occurred in water splitting step, not CO₂ fixation. Lots of positive charges are huddled to split water molecules hydrogen ions and oxygen.
4. At this stage, small mobile electron carriers transfer the electrons (came from charge separation step) to another protein complex and then by addition of more energy from sunlight photons, a needed chemical reactions occur to provide ultimately producing of carbon hydrates (Barber and Tran 2013).

(Water splits into electrons, oxygen and hydrogen ions)



(Carbon dioxide is fixed)



(Overall fuel production reaction of NP)



Academically, the artificial photosynthesis is the most worked part of the solar fuel system studies, because of being a carbon neutral renewable green alternative source to fossil fuels. Also, unlike most methods of generating alternative energy, AP has the potential to produce more than one type of fuel. Although the plants use photosynthesis as a food/energy source in nature, for an artificial system the output has to change to work for human needs. Likely natural photosynthesis, but with some differences about molecules and procedures, the artificial photosynthesis is performed by four processes; harvesting of light, charge separation, water splitting and production of fuel. Basically;

1. The photons are collected together in reaction center to absorb the solar radiation by help of antenna molecules (photo catalysts/ semiconductors, a material which can be act as a chlorophyll).
2. The collected sunlight is separated as holes (positive charges) and electrons (negative charges).
3. Positive charges attack into catalytic centers to take a part for separation of hydrogen ions and oxygen by water splitting.
4. By new photons, more energy is given to the electrons -which came from charge separation. Then they come together with hydrogen ions to produce either a carbon based fuel or hydrogen fuel (Ball 1999).



Water is an abundant, cheap and convenient source for hydrogen production. Van de Krol and Grätzel (2012b) claim that $\sim 3.5 \times 10^{13}$ L of water is sufficient to supply the 1 year-needed energy (in hydrogen energy form) of the world. It equals that 0.01% of the annual rain or 0.000002% of the water amount of oceans all over the world.

Because of the ease of the application of water, this technique is regarded as one of the most important scientific development in solar fuel-energy technology researches for recent century.

Most generally, the photocatalytic water splitting can be described as an artificial photosynthesis method that can decompose (H_2O is split by 2:1 the stoichiometric ratio into H_2 and O_2) oxygen and hydrogen as components of water in a photochemical cell using natural sunlight and artificial sunlight by photo catalysis. In theory, photons which come from sunlight, water and a photo catalyst are sufficient for water splitting to happen.

As a basic mention for water splitting process, the light hits the photo catalyst and the energy transfer is done by step wise -electron transfer in electrolyte. The required energy for water splitting as a result of this flow of electrons is obtained (Kudo and Miseki 2009). According to the state of the electron flow to occur in the photo catalyst can classify in three basic systems, although this electron flow principle is common to use for solar fuel device that allows us to obtain fuel by using solar light to achieve an efficient solar energy conversion; electrode systems, nanoparticle systems and molecular systems.

Obviously, each one of them has advantages and disadvantages in sense of their practicality. Electrode systems, such as Si-electrode, need an external bias potential to complete the electron cycle between the counter electrode and electrolyte (Van de Krol and Grätzel 2012b). Although this system has a good stability, its cost is not cheap. Unlike electrode system, nanoparticle systems (as TiO_2 nanoparticle system) are quite cheap but might be dangerous in large scale studies, because electron flow cannot be controlled while O_2 and H_2 produced in the same medium. Moreover, the molecular systems are known as natural and artificial photosynthetic system could easily provide the electron flow when used with a suitable catalyst as it has mentioned many times in this study.

A promising family of thermochemical cycles is the two-step water-splitting cycle using redox systems. During the first step of this cycle (water splitting step) the reduced and activated material is oxidized by abstracting oxygen from water and producing hydrogen. In the next step (the reduction step) the material is reduced again, setting some of its lattice oxygen free (Roeb et al. 2009). The main idea is that the photon energy is converted to chemical energy accompanied with a largely positive

change in Gibbs free energy through water splitting (a highly endothermic process, $\Delta H > 0$). In general, the change in Gibbs free energy gives an idea about the tendency of reaction energetically; if ΔG is positive or negative, the reaction absorbs or releases energy, respectively. Fundamentally, at the standard ambient temperature and pressure, the change in Gibbs free energy (ΔG) for the water splitting reaction is the positive and non-spontaneous. As it can be seen from Figure 1.3, depending on the Gibbs free energy change, both photocatalytic water splitting and natural photosynthesis give similar uphill reactions in sense of thermodynamics (Kudo and Miseki 2009). Therefore, photocatalytic water splitting is regarded as an artificial photosynthesis and it is an attractive and challenging theme in chemistry of energy researches.

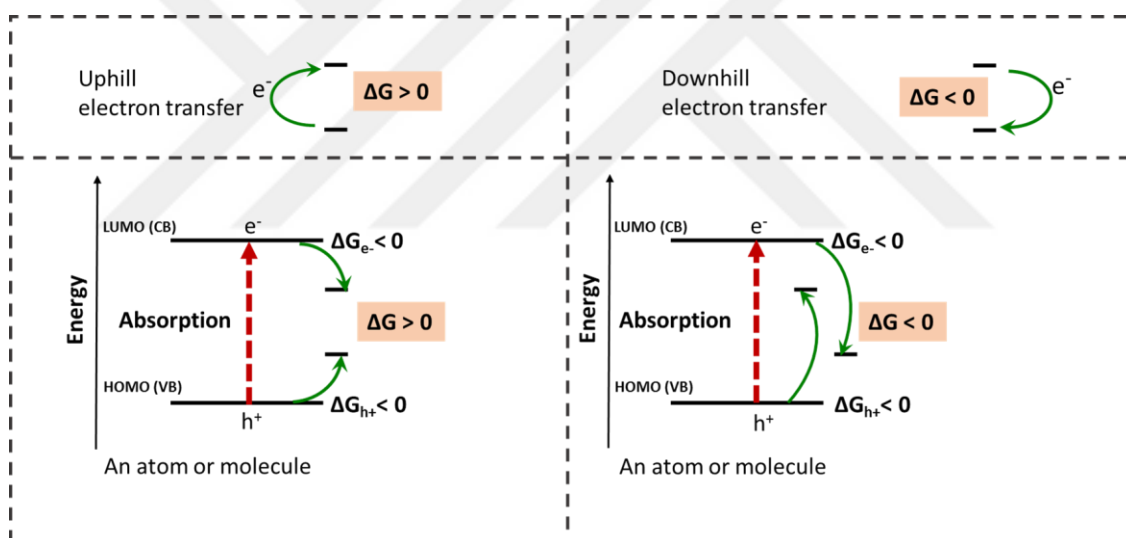


Figure 1.3. Gibbs energy change in photocatalytic reactions.

1.5.1. Photo catalysts and Semiconductors

Thermodynamically, it should be mentioned that there is a subtle but significant difference between the concepts of catalyst and photo catalyst, which are constantly intermingled with each other. The catalysts are used to accelerate a chemical reaction (which occurs spontaneously, $\Delta G < 0$) by reducing its activation energy while the photo catalysts are used to drive the energy-storing reactions (which occurs non-spontaneously, $\Delta G > 0$) (Ohtani 2010). Hence, it should be noted that the catalysts are

quite different terms from the term photo catalyst mentioned in this study and all other water splitting/artificial photosynthesis studies because of the difference in their functional purposes.

Since the decelerated work (Fujishima 1972) of Honda and Fujishima (1972)- a spearheading study on construction of a photo electrochemical cell, the using sunlight on semiconductor photo catalysts for water splitting has attracted intensive attention in researches. In addition to Honda and Fujishima's work, the reports about the stoichiometric evolution of hydrogen and oxygen- which were written by Lehn et al. (Lehn, Sauvage, and Ziesel 1980), Sato and White (Sato and White 1980), and Domen et al. (K. Domen 1980) in 1980- have accumulated the research for overall water splitting reaction using semiconductor photo catalysts. By these and following similar studies to improve, it has been clearly demonstrated that the energy conversion efficiency of splitting can be determined by the characteristics of the semiconductors used as photo catalysts (Navarro Yerga et al. 2009).

Primarily, the photo catalysts used in water splitting process must be able to fulfill the task of chlorophyll (absorbs the sun light then the absorbed light is involved in the chemical transformation of the reaction partners) that performs in the natural photosynthesis process, so that the natural photosynthesis process can be artificially imitated. Simply, the used photo catalyst for water splitting should be able to provide oxygen-hydrogen production. However, many semiconductors may be become inactive or degraded photo catalysts by corrosion for water splitting due to the aqueous environment of the reaction medium, even if they have the ability to produce oxygen and hydrogen. On the contrary, some semiconductors may be unresponsive to behave as photocatalysts in an aqueous environment although they may not have the ability to produce hydrogen and oxygen. Depending on the principle of mimicking chlorophyll, a semiconducting photocatalyst should provide other several requirements (*will be mentioned in next section*) to be useful for water splitting process. Thereby, the examination and development studies on determination of the most appropriate photocatalysts (semiconductors) for photocatalytic water splitting process can be defined as the major challenge of today's researches.

Although they are not proven exact numbers, it is generally aimed to find a semiconductor which provides a low price (160\$/m²), a high efficiency (10%) and a good stability (5 years) in solar fuels applications by several private and government-

sponsored institutes, research centers and companies that focus on finding, investigating and developing semiconductor photocatalyst materials for use in water splitting process; such as “Catalysis for Sustainable Energy” (DTU-CASE) in Denmark, “Artificial Photosynthesis Consortium” (APC) in Sweden, “Joint Center for Artificial Photosynthesis” (JCAP) in USA and “Japan Core Research for Evolutionary Science and Technology Agency” (JST-CREST) in Japan are the most famous ones. As a final note, the exploration, investigation or development of photocatalyst materials for artificial photosynthesis applications are the focus of much research, but thus far no technology has been commercialized.

Most of the heterogeneous photocatalysts have similar characteristics with semiconductors. Therefore, the material features of the semiconductor is distinctive to pass successfully from the main processes of photocatalytic water splitting.

The behaviors of semiconducting materials can be explained by *the band theory* of solids materials. The band structure of the general materials, which is schematized simply by sticking to the band theory with respect to band edge positions, can be seen from Figure 1.4. According to band theory, every semiconductor has its own characteristic energy band structure. In order for a material to be conductive, both free electrons and empty states must be available. For this reason, the materials called *metal* have free electrons and partially filled valence bands, therefore they are highly conductive. If the materials have filled valence bands and empty conduction bands, they are called as *insulators*. Insulators are separated by a large band gap (> 4 eV) and they have high resistivity. The materials that have gap between the energy bands, as less as metals and not as much as insulators, are called as *semiconductors*. Occasionally, the semiconductors may be on the metallic or on the insulating side depending on the energy density of its bands or the severity of the excitation factor- some electrons can jump to the empty conduction band by thermal or optical excitation.

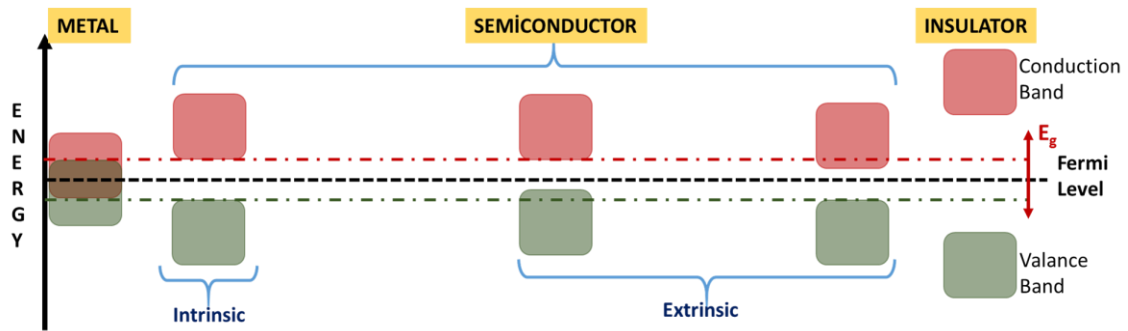


Figure 1.4. Generally, the schematized band edge positions of the materials depending on the band theory.

When a large number of atoms are linked to form a solid, their external orbitals begin to overlap, and then a large number of levels are formed with a close spacing, as in semiconductors (Hernández-Ramírez and Medina-Ramírez 2014). Therefore, it can be considered as a continuous band of energy levels and the semiconductors are referred to their band structures. The band structure of a semiconductor consists of fundamental four parts; conduction band, valance band, band gap and Fermi level (Figure 1.5).

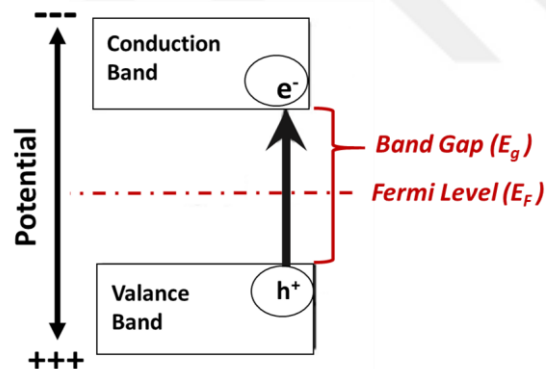


Figure 1.5. Simple diagram for the band structure of a semiconductor to show the significant parts.

The upper band of the structure is called as *the conduction band* (CB) of a semiconductor. CB is the more negative band of semiconductor due to hosting a large number of electrons. At this band, energetically similar energy levels lie at higher energy level. And this band also forms the part of the macromolecular crystal associated with conductivity. Contrary to this, the lower band of the structure, which is called *the valance band* (VB), is associated with covalent bonding between atoms composing the crystallite. In addition to that the energetically closed spaced energy levels occur at the

VB. The electrons breaking from the valence band create some spaces and these created spaces are called “holes”. Due to the fact that these holes behave as positively charge carriers when they get rid of the negative value and enter into a new electron request, the VB shows a more positive feature in the semiconductor structure (Jewett and Serway 2008). The difference in energy between these two bands, which differ in terms of energy, is defined as *the band gap* (BG or E_g) of a semiconductor. Although the gap word recalls the distance- when it is thought that the bands are arranged according to the increasing energy level though the concept of distance is not so wrong, it is an energy term and it can be defined as the self-energy of the semiconductor. The dashed lines shown in Figure 1.5 refer to *the Fermi Level* (FL or E_F) of the semiconductor. Simply, the Fermi level can be defined as the highest occupied energy level in a semiconductor- at absolute zero temperature.

In general, semiconductors are grouped under two headlines (Figure 1.4); intrinsic and extrinsic semiconductors (Serpone and Pelizzetti 1989b). Whenever an *intrinsic* semiconductor is mentioned, a pure crystalline material- containing only one element or one compound- should come to mind. Moreover, their Fermi level is located at the middle and they behave as insulators due to having the same number of electrons and holes. Differently from an intrinsic semiconductor, an *extrinsic* semiconductor conjures up the impurity and the number of their electrons and holes are varied depending on the type of impurity they have. Also, when impurities are added to semiconductors, the band structure is modified; this process is called *doping*. The modified structure causes to some characteristic changes in the extrinsic semiconductor depending on the added doping material.

If a semiconductor is doped with acceptor atoms, it is called *p-type* semiconductor. These acceptor atoms can be reduced taking electrons from the valence band and increasing the density of holes. Hence, the p-type semiconductors are hole-rich; the number of their positive charges are larger than negative charges. The excess amount holes make the Fermi level shift closer to the valance band. Additionally, they act as a photocathode in a photocatalysis reaction via reduction reaction. Cu_2O , FeO , FeS and etc. can be given as examples for p- type semiconductors (Atkins 2010).

Using a donor impurity as a doping material for semiconductor makes the extrinsic semiconductor as a *n-type*. Donor atoms provide a large number of electrons to the conduction band. Therefore, they are enriched in number of electrons by doping.

Consequently, their Fermi levels shift near to the conduction band. The n-type semiconductors have photoanode properties in photocatalysis processes via oxidation reactions. Several d-metal oxides, including ZnO, TiO₂, and Fe₂O₃ etc. act like a n-type semiconductor (Atkins 2010).

On the other hand, when the lowest energy excitation of an electron from the valence band to the conduction band involves no change in momentum, k (Figure 1.6), the semiconductor has a *direct band gap*, and the absorption probability is high for these transitions (i.e., GaS, ZnO, and CdTe), direct band gap materials provide more efficient absorption and emission of light (Jacobsson and Edvinsson 2012). An *indirect band gap* is presented in a material where the k at the valence band maximum is different from the k at the conduction band minimum. Gap, TiO₂, and CdS are examples of semiconductors with an indirect band gap (Hernández-Ramírez and Medina-Ramírez 2014, Serpone and Pelizzetti 1989b).

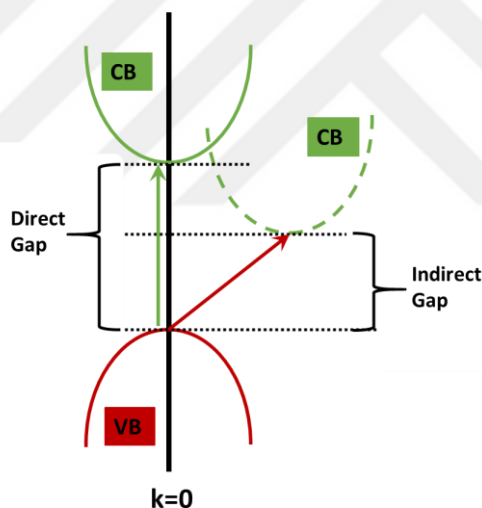


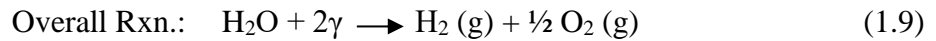
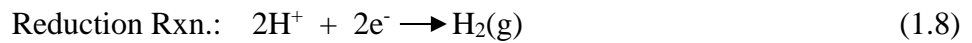
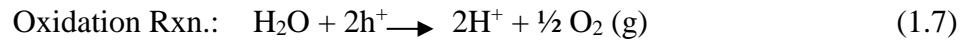
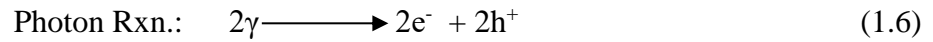
Figure 1.6. A diagram for the Direct and Indirect band gaps.

1.5.2. Water Splitting Principles of Semiconductors

Basically, when the energy of incident light is suitable that of a band gap, electrons and holes are generated in the conduction and valence bands, respectively. The photogenerated electrons and holes cause redox reactions similarly to electrolysis. Water molecules are reduced by the electrons to form H₂ and are oxidized by the holes to form O₂ for overall water splitting. The needed photon energy calculates from “Plank’s equation” by using wavelength of incoming photon. Planck's energy formula is

(1.11) often used both to compute the change in energy resulting from a photon absorption and to determine the frequency of the light emitted from a given photon emission.

As it known that the overall reaction of water splitting is,



$$\text{Nerst's Equation: } \Delta G^{\circ} = +237.18 \text{ kJ.mol}^{-1} \text{ (for PWS)} \quad (1.10)$$

$$V_{\text{rev}}^{\circ} = \Delta G^{\circ} / nF = 1.23 \text{ eV}$$

$$\text{Plank's Equation: } E = h\nu \quad (1.11)$$

$$\text{Band gap (eV)} = 1240/\lambda(\text{nm})$$

The Gibbs free energy is $237.18 \text{ kJ/mol}^{-1}$ for overall photocatalytic water splitting process (PWS). Hence, the needed energy (derived by Nerst equation, 1.10) for PWS corresponds to $\Delta E^{\circ} = 1.23 \text{ V}$ per electron under standard conditions. The semiconductor must absorb radiant light with photon energies of $>1.23 \text{ eV}$ ($\sim 1100 \text{ nm}$ and shorter) in order to convert the photon energy to chemical energy (H_2 and O_2) and to use it in water splitting applications. Up to now, the required semiconductor band gap (energy) has been reported as $1.6\text{-}2.4 \text{ eV}$ per electron in order to make it be suitable for use in PWS (Bak et al. 2002, Bolton, Strickler, and Connolly 1985, Currao 2007, Fujishima 1972, Heller 1981, 1984, Lewis 2001, Turner 1999, Walter et al. 2010).

The photocatalytic water splitting occurs by three fundamental photocatalytic reactions occurring on the photocatalyst/semiconductor (Figure 1.7).

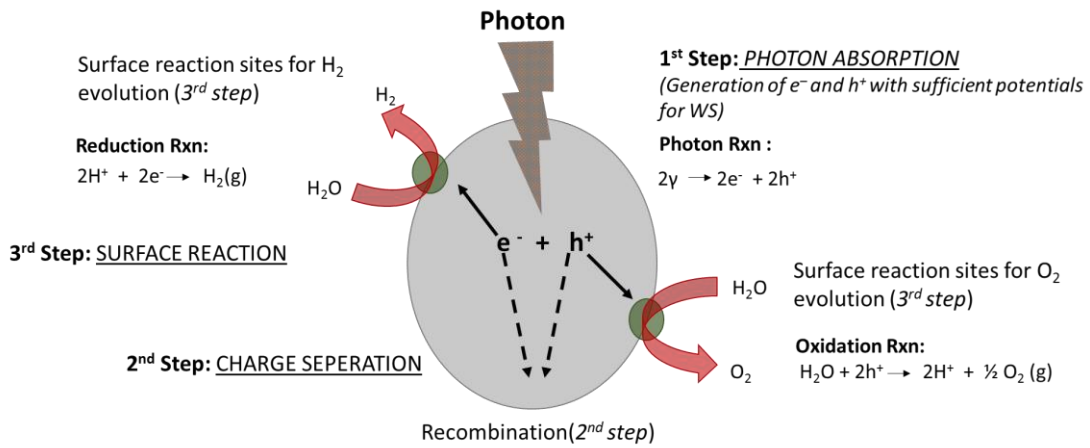


Figure 1.7. The photocatalytic reaction steps while occurring with photocatalysts.

The first step is the photoabsorption that is formed electron hole pairs by absorption of photons. The main point of photoabsorption step is that the semiconductor and the photon should meet together with sufficient energy. If the energy of the incoming photon energy larger than the band gap energy, the photoabsorption is introduced by electron generation in the conduction band and hole generation in the valance band of the semiconductor.

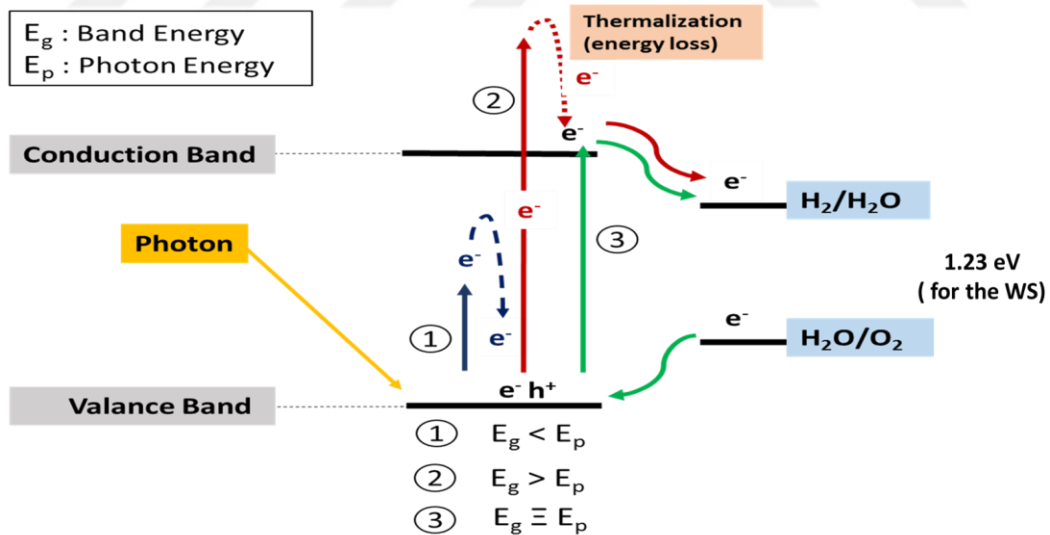


Figure 1.8. The photoabsorption step in the semiconductors.

To explain through the Figure 1.8, if the photon energy is smaller than the E_g of the semiconductor, the excited electrons cannot jump to the CB, in other words, the photoabsorption step cannot be occurred (the blue path). For example, silicon (Si) is not sufficient semiconductor for PWS studies because of its E_g (~1.1 eV) value. Besides, if

the photon energy is larger than the E_g of the semiconductor, the photoabsorption is introduced by electron generation but the residual energy- the energy difference between the band gap and photon energy is wasted by thermalization (the red path). Obviously, the target is to get maximum efficiency from the incoming photon, thus it is not desirable, too. Consequently, the green path is the ideal situation for the photoabsorption step of PWS. The closest energy values make the photoabsorption be easier and more efficient.

To remind again, when the photon hits the semiconductor, the redox reactions occur in the system by photo generation of electrons and holes. Electrons reduce water molecules to form H_2 while holes oxidize the water molecules to form O_2 . The redox potentials of H^+/H_2 and O_2/H_2O are 0 V and 1.23 V (V vs. NHE), respectively (Walter et al. 2010). As it mentioned, the minimum band gap of semiconductor should be 1.23 eV (~ 1100 nm) for water splitting. This theoretical number is effective just to decide whether if semiconductor has enough energy to water separation. For the main purpose of water splitting, producing both O_2 and H_2 , the band position of the semiconductor has an important role. To produce O_2 and H_2 by using semiconductor, the bottom level of conduction band should be more negative than H^+/H_2 level and the upper level of valance band should be more positive than O_2/H_2O level. This level difference creates a charge-potential difference to make the electron/hole migration be easy in the system (Figure 1.9).

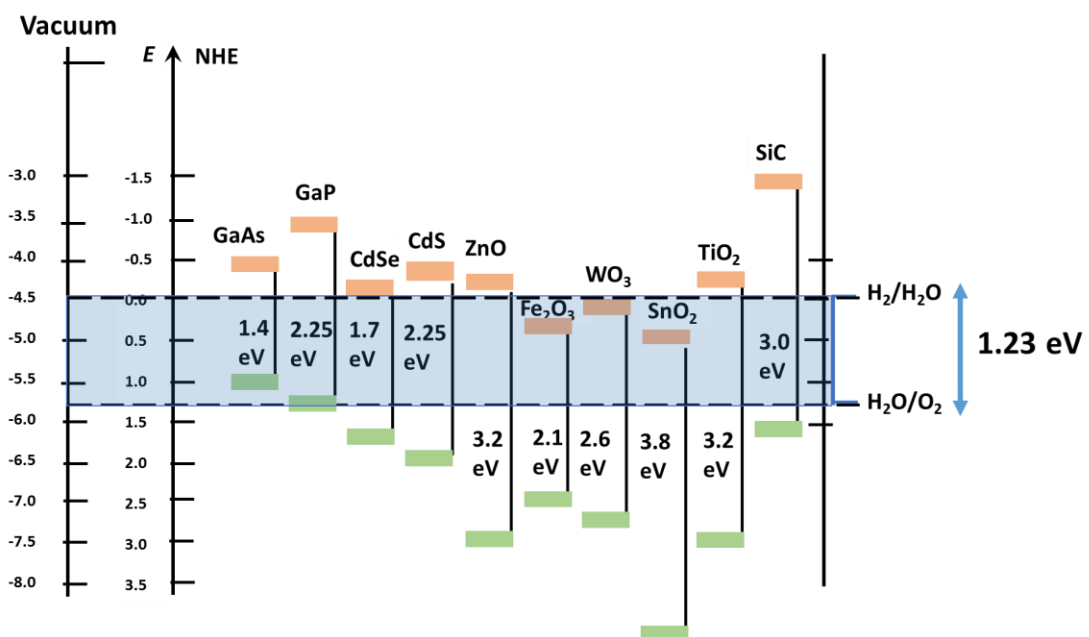


Figure 1.9. Band edge positions of some semiconductors at pH=0.

The second step is the charge separation that is occurred by separation and migration of photogenerated electron/ hole carriers. The distinctive points of this step are crystallinity, crystal structure and particle size of the material (Lewis 2001). Defects that naturally stay inside of material are big enemies of recombination route and electron/hole migration in charge separation step. Since, increase in the amount of defects causes a reduction in photocatalytic activity. In order to get rid of defects, the crystalline quality should be high. Additionally, the particle size is important as the crystal structure of semiconductor. Small particle size causes to make the migration path of electrons/ holes be shorter and consequently the recombination probability decreases (Figure 1.10).

The last step is the surface reaction in which the chemical reactions occur between the semiconductor and the electrolyte. Surface area of the crystal and the active sites of the crystal are the important criteria for the surface reactions (Bak et al. 2002). The photogenerated electrons and holes will have to recombine with each other if the active sites for redox reactions do not exist on the surface although they have a sufficient potential in thermodynamics for photocatalytic water splitting. In some cases, the conduction band levels of many oxide photocatalysts are not high enough to reduce water to produce H_2 . In order to establish active sites for H_2 generation, some additional materials used are generally called as co-catalysts such as Pt, NiO and RuO_2 . Generally, despite the use of a suitable semiconductor for the first two stages it may not be the result in the final stage.

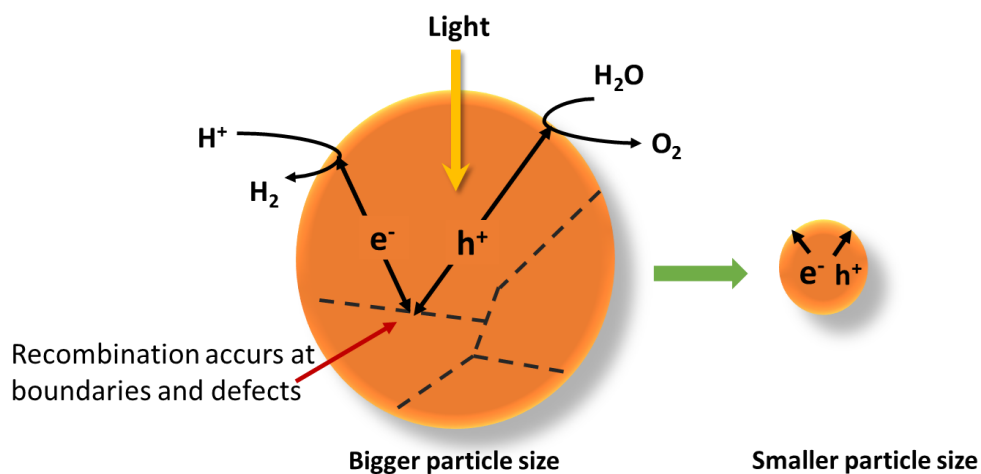


Figure 1.10. The effect of the particle size on the recombination center in the photocatalysts.

1.6. Aim and outline of the of thesis

Due to the fact that the most of the generated energy is derived from the decomposition step of the water and it is used to survive by organisms capable of photosynthesis in nature, the water splitting process is the one of the most worked study to follow the natural energy production routes artificially in laboratories. Numerous experimental apparatus are used for the observability of these systems (Kudo and Miseki 2009).

In this thesis, an experimental apparatus which was idealized associated with the gas closed system principles by co-operation of two gas (H_2 - O_2 evolution) sensors, a temperature sensor, a pH sensor, one solar simulator device and a new designed mini photoreactor that covers a reaction cell (including a photocatalyst) air-freely, was proposed to use for applications of photocatalytic water splitting process. Additionally, an underrecognized semiconductor ($PbVO_3Cl$) was analyzed to be informed about its optical properties and then it was tested by the proposed experimental set-up in order to try to observe its ability in O_2/H_2 production.

Chapter 2: Design of the mini photoreactor

In this chapter, the commonly used gas sensing methods and the sensor system, which is recommended as an alternative to them, are introduced in general by their positive-negative aspects. Besides this, a new mini photoreactor design which is suitable for the proposed experimental PWS apparatus is described and the limitations which were considered during this design are discussed. Then, the final design for the shape and functions of the reactor is illustrated by “Solidworks” 3D-drawing.

Chapter 3: Fabrication and testing of the mini photoreactor

In Chapter 3, the fabrication method (3D printing) of the design described in Chapter 2 is introduced by some difficulties encountered during fabrication of the mini photoreactor and our solutions for these problems. Additionally, the calibration instructions and results of the microsensors are presented. Besides, the tests performed to ensure that the modelled mini photoreactor provides the necessary criteria for PWS reaction and that it works in compatibility with the microsensors are discussed. After all, the final image of two-piece mini photoreactor, which matches the used sensors, that proposed as an efficient alternative experimental apparatus for photocatalytic reactions is shown.

Chapter 4: PbVO₃Cl as a photocatalyst for PWS reactions

In 4th Chapter, it is aimed to test the proposed experimental setup with a semiconducting material. Lead(II) trioxovanadate(V) chloride, [PbVO₃Cl], which was discovered in 2007 (IYTE, Eanes et.al) was chosen as the subject material. On account of the fact that there is little information about PbVO₃Cl in literature, some theoretical and experimental analysis were performed to identify its unknown optical properties and their results are presented in this chapter. After these identifications, the results obtained from its photocatalytic reaction tests in the new designed experimental setup are introduced. Although PbVO₃Cl did not show any efficient response in the PWS applications by using new designed experimental set-up, the theoretical efficiencies of solar fuel devices, which can be illustrated with PbVO₃Cl, were calculated. Depending on these theoretical results, the future potential of PbVO₃Cl in solar fuel systems as a photocatalyst/semiconductor is discussed.

Chapter 5: Conclusion

In Chapter 5, a summary of the works which were described in the previous chapters is proposed as a conclusion of the potential use of the new designed experimental set-up for PWS reactions and the potential contribution of the new material studied to future solar fuel device designs.

CHAPTER 2

DESIGN OF THE MINI PHOTOREACTOR

2.1. Abstract

This chapter presents an alternative experimental set-up for PWS applications which is defined as a combination of one light source, four microsensors as the gas sensing method and one mini photoreactor (Figure 2.1). Owing to the fact that it provides more advantages over commonly used methods, a microsensor system is selected in which four sensors can be used together as a gas selective method. Since the concept is solar fuels, which are focused on this thesis, the light source is chosen as a solar simulator and the stages of the design of a mini photoreactor that allows direct measurement of dissolved gas in small volumes are highlighted by its limitations on design.

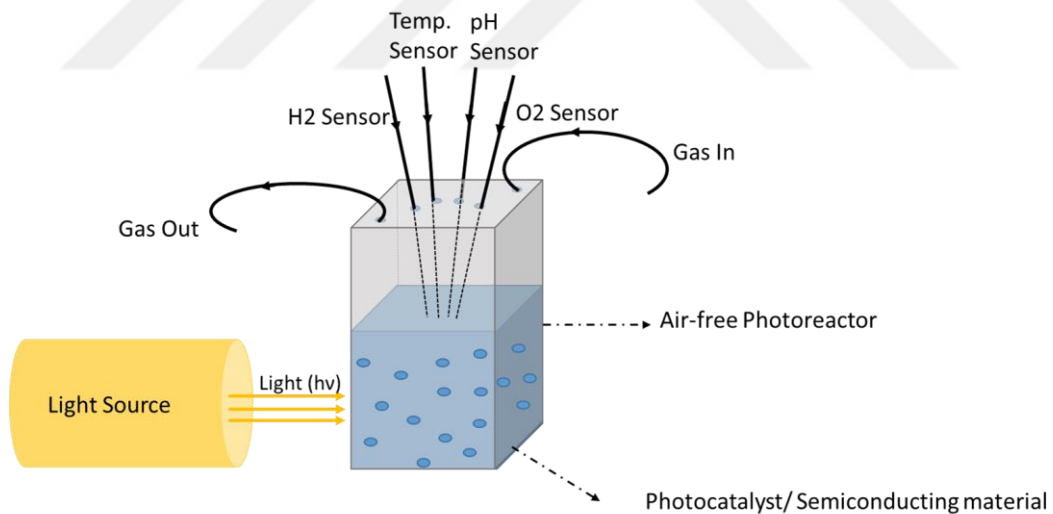


Figure 2.1. A graphical abstract for the used experimental set-up for photocatalytic water splitting process.

A manuscript based on parts of this chapter is in preparation: İ. Harmanlı, E. Karabudak*, *3D-Printed Multiprobe Analysis System for Solar Fuel Research; Design, Fabrication and Testing*.

2.2. Why is a mini photo reactor needed to design for PWS?

2.2.1. Scientific Problems

Time-consuming, inflexible for working and expensive gas sensing methods:

Recent researches have shown that the scientists mostly prefer to use a gas-closed system for water splitting process applications (Kudo and Miseki 2009). Primarily, the gas sensing methods can be classified in two methods; the methods which are based on electrical variation with different material (carbon nanotubes, moisture absorbing materials, metal oxide semiconductors and etc.) and other kinds of variations (calorimetric methods, acoustic methods, gas chromatography and etc.) (Liu et al. 2012). Actually, the most common method of gas detection is using Gas Chromatography (GC) because of its excellent separation performance, high sensitivity and selectivity (Kim 2005). However, the cost of GC is high and the time that is needed to respond is very long, it may take a day to get the results of the analyzes made with GC. Moreover, working with GC (Catalan, Liang, and Jia 2006) has some limitations such as its non-concurrence response to materials that have high photocatalytic activity. Because of this, the volumetric methods can be operated in systems with excess photocatalytic activity rather to use gas chromatography for evolved gas determination. Also, the miniaturization of GC for portable application needs more technological breakthroughs. Therefore, GC does not quite satisfy the device and material constraints for unattended, flexible basic sensors. Even if it is rare, the usage of Infrared (IR)spectroscopy may be observed in literature as a gas sensing method (Werle et al. 2002). However, the IR measurements are not cost effective and not suitable to work easily, likely GC.

Bigger volumes:

In general, the PWS applications need repeated experiments depending on the photocatalyst type or the separation yield of the used photocatalyst. Studying in smaller volumes allows for the least loss of material due to these repeated experiments. It is a bit of a challenge to make an experiment with high volumes of materials such as quantum dots, which are scientifically proven to be tried, difficult and expensive to synthesize, are the new look of science and technology. Besides this, working in small

volumes makes the experiments more secure when considering the possibility of hydrogen and oxygen gases being produced in the same environment and at high rates in water splitting. Considering that most of the reactions that can be observed in small volumes are easier to carry to large volumes, the establishment and development of experimental laboratory set-ups in as possible as small volumes can be considered as a good scientific goal.

2.2.2. The Solution by Proposing Experimental Set-up

Considering the problems which were mentioned above, working with a flexible, sensitive and time-saver gas sensing method is proposed in this study- *the microsensors (Unisense A/S Microsensors, Denmark)*. Furthermore, the common gas sensing methods such as GC can be used to interpret only the amount of gas generated in the system, but it is possible to directly measure the amount of dissolved gas in the water by a microsensor method, as well as a common interpretation of the change of different parameters at the same time; temperature, pH and concentration. Additionally, the new mini photoreactor is designed to take advantage of the fact that the selected micro sensors have small tips and the minimum volume that can be worked on is targeted and included in the analysis system. Thus, the proposed new experimental set-up prevents the loss of material in large volumes, as well as creating a safe working environment and avoids negative aspects of common gas sensing methods.

2.3. Design by 3D-drawing

The main objective of study is to design a new mini photo reactor that facilitates ease during experimental analysis, allows all sensors to take measurements directly from the base container, and keeps the mains surround away from the changing physical conditions of the surrounding environment. In accordance with this, the selection of the base container to be used in the base part of the design was the first action to be taken. Therefore, quartz UV cuvette (~ 3mL, Figure 2.2) has been identified as the base sample vessel (the reaction cell) due to its easy availability, efficiency in working under light and volumetric suitability for experimental purposes.

Based on dimensional measurements of the selected standard UV cuvette and the sizes of the microsensors tips (Figure 2.3), a mini photoreactor has been launched that incorporates the cuvette and allows all sensors to remain in the system in a steady state.

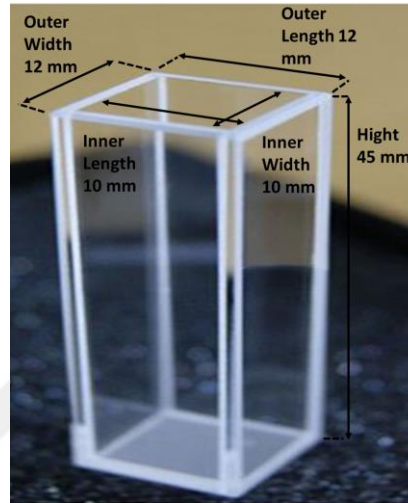


Figure 2.2. The dimensional size of the standard UV-quartz cuvette.



Figure 2.3. The dimensional size of the Unisense Microsensors.

2.3.1. Limitations of the design for PWS applications

At the beginning of the drawings, some criteria which are considered simultaneously must be identified due to design of a reactor for an efficient experimental set-up;

- The vessel must be placed at hermetically sealed environment (because of the importance of O₂ evaluation),
- Meanwhile this environment must allow the sun light to pass through the cuvette,
- The microsensors must be stable position and they must be in the inner side of cuvette with all together and also the environment must have an entrance for external gas (in) and an exit for internal gas (out).

Therefore, it was decided that this aim could be achieved with a design consisting of two parts- *container* (enclose the cuvette) and *lid* (hold the sensors), after many drawings (all 3D-drawings were performed by using “Solidworks” software) made for the most efficient appropriate reactor (Figure 2.4).

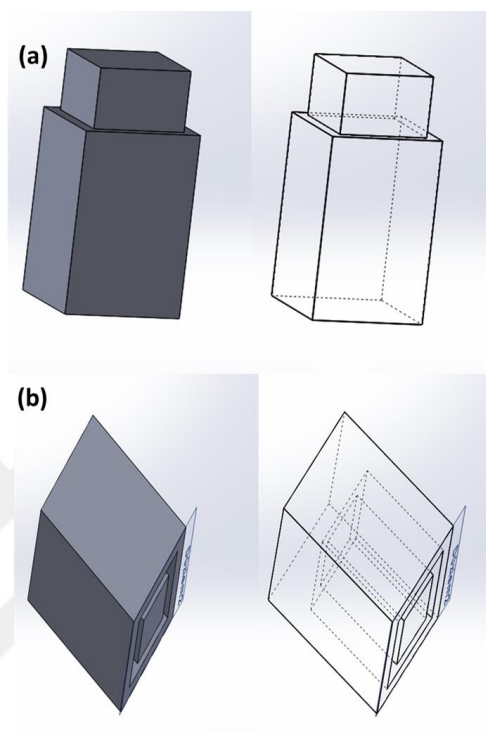


Figure 2.4. Solidworks drawings: the primitive parts of designed mini photoreactor; a) the container, b) the lid.

Additionally, it should not be forgotten that the designed reactor must allow the light to pass through to the reaction cell which is surrounded by it. So, a small window (Figure 2.5) was opened in the container part of the reactor- equivalent to the size of the outgoing end of the light source- so that the reactor could fulfill this task.

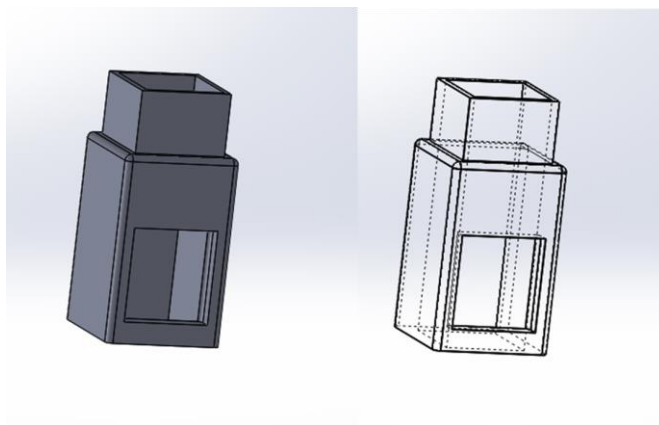


Figure 2.5. Solidworks drawings: a small window was opened on the container.

Subsequently, the holes on the lid were opened so that the sensors could be measured from inside the reactor by standing still on the hanger. But in this step, the important obstacle was to locate the all sensors in the inner side of cuvette by cap. Due to the fact that each sensor alone occupies at least 11 mm of space while the top surface area of the main cuvette is 10*10 mm and also all of them must be placed together on the lid (Figure 2.6). Finally, the most possible entry angles and locations, as all sensors and gas inlet and outlet can be positioned at the same time in the reactor lid, were ready to print out it to use it efficiently for the minimalized photocatalytic water splitting applications.

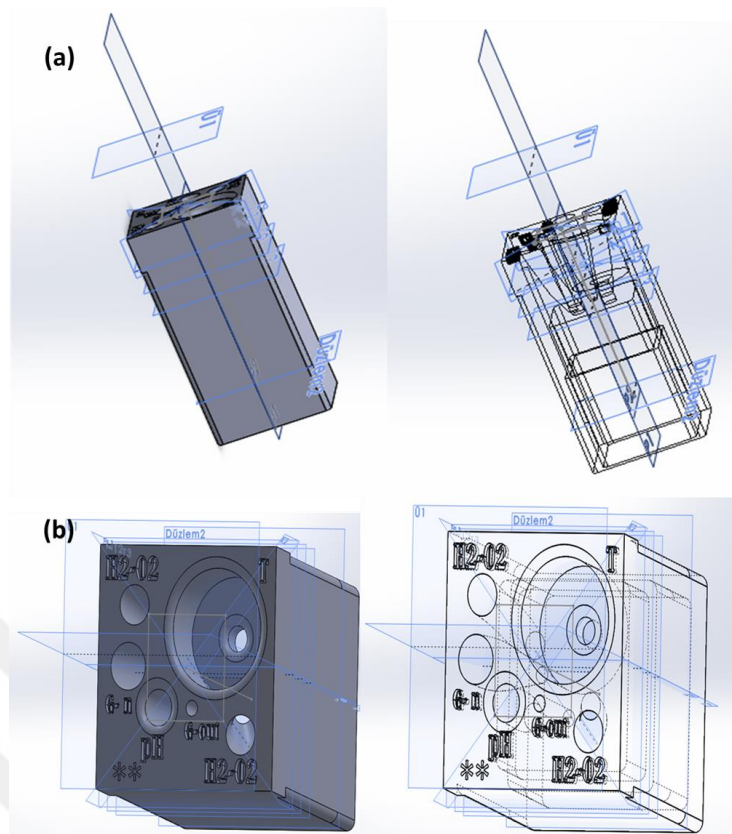


Figure 2.6. Solidworks drawings: the sensor entrance holes were placed on the lid; a) side view, b) top view.

2.4. Conclusion: Achievements of the chapter

The concept of the design a mini photoreactor for PWS applications has been presented in this chapter. The design of the new experimental set-up with the newly designed mini photoreactor overcomes some problems of macroscale experiments and instrumental analysis method during PWS applications. The method- *Unisense* microsensors, which allows to work with smaller volumes in less time, were chosen as a gas sensing method. By considering the sizes of the all four microsensors (T, pH, O₂, H₂), a mini photoreactor consisting of two parts, on which the sensors are stationary and which receives light directly into the solution in airtight environment, is designed by *Solidworks* and its design phases are presented by plenty of 3D-drawings.

Finally, the difficulties encountered in as fitting the sensors into the lid of the mini photoreactor, fitting and placing at the right angles have been solved and a basic design model drawing that meets all the constraints of PWS applications was achieved in this chapter.

CHAPTER 3

FABRICATION AND TESTING OF THE MINI PHOTOREACTOR

3.1. Abstract

As mentioned in the previous section, microsensors that one of the limitations of the 3D design of the mini photoreactor are also effective in its fabrication process because of an important criterion to be able to receive a proper signal when they are positioned on the photoreactor. That is why this chapter primarily presents the properties of the selected microsensors and their calibration results in order to check the fabricated mini photoreactor by 3D printing technology. In addition, the problems encountered during fabrication and the solutions for these problems are introduced before the final version of the mini photoreactor is presented. Ultimately, tests are performed to verify the production so that the bare responses to the light and air-tight feature, which are the other limitations of the photoreactor, are ensured to provide the main settlement and measurement criteria for the microsensors on the designed system.



Figure 3.1. A graphical abstract for the fabrication of the new designed mini photoreactor.

A manuscript based on parts of this chapter is in preparation: İ. Harmanlı, E. Karabudak*, *3D-Printed Multiprobe Analysis System for Solar Fuel Research; Design, Fabrication and Testing*.

3.2. Introduction

Generally, sensor can be defined as an analytical device that transforms chemical information -may originate from a chemical reaction of the analyte or from a physical property of the system investigated-, ranging from the concentration of a specific sample component to total composition analysis, into an analytically useful signal (Hulanicki, Glab, and Ingman 1991). Chemical sensors are made by two basic functional units; a receptor part and a transducer part but also Some sensors may contain a separator which is called membrane. Mainly, the receptor part is needed to transform the chemical information into a measurable (by transducer) form of energy. After this energy formation, the transducer (a device) is used to transport this energy (includes the chemical information) into a useful analytical signal.

Besides the design of a sensor, the chemical/analytical sensors are classified according to the operating principle of the transducer or the electrochemical interaction of analyte - electrode into a useful signal or the application to detect and determine a given analyte such as; pH sensors, for metal ions or for determining oxygen or other gases (Arnold and Meyerhoff 1988, Nylander 1985).

In general, the performance of a gas sensor is evaluated by some criteria;

- Sensitivity: the minimum value of target gases' volume concentration when they could be detected;
- Selectivity: the ability of gas sensors to identify a specific gas among a gas mixture;
- Response time: the period from the time when gas concentration reaches a specific value to that when sensor generates a warning signal;
- Energy consumption;
- Reversibility: whether the sensing materials could return to its original state after detection;
- Adsorptive capacity (also affects sensitivity and selectivity) (Liu et al. 2012).

Commonly, the first two criteria are the most effective ones on the productive usage of the gas sensors. In order to make the utilization of a gas sensor be significant, the sensors should be designed consistent with the operation of sensor under well-defined conditions for specified analytes in the certain sample types- called as “specificity/ selectivity”. Furthermore, “sensitivity” of the sensor that the ratio between the output signal and measured property is the other criterion for utilization of the sensors in specific experimental analyses. Thus, these design criteria of sensors bring about “the resolution” term which is related to the precision (the smallest changes during sensor reading) with which the measurement is made. In other words, higher sensitivity and selectivity of a sensor makes the read values be more precise by high resolution impact for the experimental analyses.

Unisense A/S Microsensors

Unisense A/S microsensors can be used for many scientific applications such as Microbiology, Photosynthetic Biofilms, Measuring in Rhizosphere, Benthic Microbial Mats, Oxygen Profiles In Salty Crust, Microrespiration, Nanorespiration, Photosynthesis Of Corals and etc. (Kampschreur et al. 2008, Masamoto et al. 2009, Oharazawa et al. 2010, Ulstrup, Hill, and Ralph 2005)

The microsensors can be used for sediment, biofilm, cheese, intact tissue and much more materials. They can not only detect any changes at micrometer scale in the chemical systems but also make the diffusion processes that govern the signal really fast. Some of the general advantages of the microsensors are listed below;

- Non-destructive measurements,
- High spatial resolution,
- Fast response,
- Low analyte consumption,
- Low stirring sensitivity,
- No temperature hysteresis,
- High pressure resistance.

This study was depend on using of four different microsensors- Temperature, Oxygen, Hydrogen, pH- and (Figure 3.2.c, d,) one compatible multimeter (Figure 3.2.a) with the sensors that allows us to read the results from all sensors, simultaneously. The microsensor multimeter has a OLED screen and “plug and play” automatization for four separated channels-two channels for amperometric sensors (O_2 , NO, H_2 , H_2S , N_2O , NO_x^-), one for potentiometric sensors (pH and Redox) and one channel for a temperature sensor- to measure multiple parameters at once. Another good point of working with this microsensors and multimeter system is that it has a software (Sensor Trace PC program) which transfers the sensors readings directly to a computer. In addition, this program has the ability to perform complex mathematical operations on its own, thus reducing instantaneous calculation errors and time loss to a minimum level during the experiments.

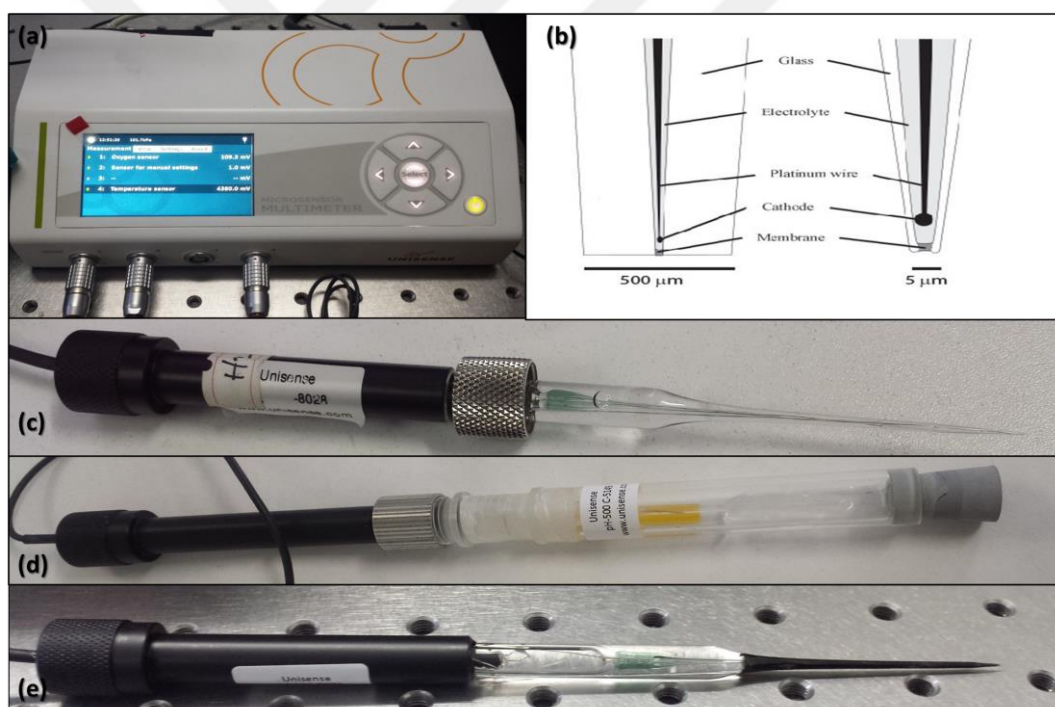


Figure 3.2. a) The Unisense Multimeter, b) a schematic of internal structure of sensors, c) a photograph of one of the physically identical three micro sensors; T, H_2 , O_2 , d) the pH sensor.

For selectivities and specificities of Unisense micro sensors, the Unisense Company guarantees that each of the sensors is unique and cannot detect any characteristics that are different from their classifications. Physically, all microsensors have sensitive tiny glass tip ($\sim 500 \mu m$, except for pH sensor $\sim 2 mm$ - Figure 3.2.b).

Hence, the sensors are suitable to work in small volumes. Particularly, the gas sensors (H₂ and O₂), which are capable to detect the dissolved gas molecules even in a small solution system, come into prominence for this study.

Furthermore, the microsensors take point measurements (as surface area of tip on solution molecules) from the sample solution. Because of this, stirring might be needed as a procedure by working with them. According to the promise of the manufacturer company, for general purpose use the sensors with a stirring sensitivity of <2% and a response time of <3 sec, which is a good compromise for most users. Therefore, the error rate in the readings is extremely small even if they are instantly affected by physical or magnetic factors (stirring).

To sum up, all of used sensors in this work have high selectivity and sensitivity with good a resolution range. Additionally, you can look through Table 2.1 that includes the physical and other detailed technical information of Unisense microsensors (*see for more information: the website of Unisense Microsensors: http://www.unisense.com/sensors_and_electrodes/, for each sensor*)

Table 2.1. The technical information sheet for the Unisense Microsensors.

Technical Information	Hydrogen Micro Sensor	Oxygen Micro Sensor	Temperature Micro Sensor	pH Electrode
Code	H2-500 (standard)	OX-500 (standard)	TP-500 (standard)	PH-500C
Type	Glass- Black Tip	Glass- Black Tip	Glass- Black Tip Thermocouple, copper/constant an (type T)	Glass- Black Tip Combine Electrode
Internal Reference	Yes	Yes	Yes	Yes
Shaft Protection Diameter	11 mm	11 mm	11 mm	11 mm
Glass Shaft Diameter	8 mm	8 mm	8 mm	8 mm

(cont. on next page)

Table 2.1. (cont.)

Technical Information	Hydrogen Micro Sensor	Oxygen Micro Sensor	Temperature Micro Sensor	pH Electrode
Total Sensor Length	150-200 mm	150-200 mm	150-200 mm	150-200 mm
Temperature Range	-10 -60°	-10 -60°	-10 -70°	-10 -60°
Tip Tolerance Temp. Range	-10 -90°	-10 -60°	-20 -100°	-10 -90°
Temperature Coefficient	2-3 % per °C	2-3 % per °C	-	
Range by Resolution	0-800 µM dissolved H ₂ (0-1 atm pH ₂) Low Range Sensors: 0-80µM (approx. 0-10%)	About 0-1 atm pO ₂	0.1 °C	pH 2-10 (linear 4-9) about 100-250µm (PH-500 about 500µm)
Detection limit	0.3µM in water <50nM for Low Range Sensor	0.3µM<50nM for Low Range Sensor	40µV per °C	0.1 pH unit
Stirring sensitive**	Low	1.5 %	Low	Low
Response time (80%)	≤ 30 sec	≤ 15 sec	≤ 3sec	≤ 10 sec (from pH 7 to pH 4)
Response	Linear	Linear	Linear	Log Linear

**Due to the nature of the sensor function, it is however not possible to optimize sensitivity (high signal) and low stirring sensitivity simultaneously, so there will always be a trade of between these parameters. Sensors that is made stirring insensitive will have all lower signal as a function of hydrogen partial pressure and thereby a lower sensitivity (about 0.5µM H₂ in water).

3.3. Sensor calibration

3.3.1. Experimental

Primarily, the calibration steps of the sensors recommended by the manufacturer were applied for each sensor calibration by using the logger software of Unisense-*SensorTrace Suite v2.8.0*. The computer program, which is specific to the sensors used for measurements, provides both an automatic and easy calibration with instant data entry and automatical calculations for the graphs and equations of the calibration curve. And then, it gives the results directly as final screen for user. Additionally, the program provides an opportunity to users with an excel file where the data is stored and saved for use when requested, as well as displaying the test results directly on the screen. The device reads the signals in microvolts (mV) and turns the signals to an intended unit of material by calibration such as; in °C, in $\mu\text{mol/L}$, in pH unit.

Generally, to calibrate all four sensors, a small amount of ultra-pure water was used in 25 mL beaker by covering with the paraffin film to protect the system from instant environmental changes. The applied calibration procedures of Unisense user program are listed below for each sensor.

3.3.1.1. Calibration of Temperature sensor

Materials:

1. Approximately, 10 mL ultra-pure water.
2. 25 mL glass beaker.
3. 1 external thermometer to get actual results from the sample as in °C unit by instant temperature values.

Procedure: At least three data entries are recommended for a precise calibration.

1. An ultra-pure water sample is known for its temperature is measured by T sensor in mV units, as the 1st sample.
2. Live measurement graph on the screen will be fluctuating until the temperature in the solution is up to the equilibrium (a few seconds).
3. At the point where the anchoring is observed, the temperature (in °C) is entered and recorded to the software.

4. Other samples, which are desired to be used at different temperature values, are prepared and recorded individually by the same procedure.
5. After the temperature data are added as desired numbers, the calibration is recorded by pressing the “Save and Apply Calibration” button shown on the calibration sheet on the screen.
6. The calibration curve, slope and intercept will be shown by program on the calibration screen.

3.3.1.2. Calibration of pH sensor

Materials:

1. Approximately, 10 mL buffer solutions; pH 4, pH 7 and pH 10.
2. 25 mL glass beaker.

Procedure: At least three data entries are recommended for a precise calibration.

1. One by one, the pH buffers are measured by program.
2. For each, at the point where the anchoring is observed, the known pH value is entered and recorded to the software.
3. After the three pH data are added, the calibration is recorded by pressing the “Save and Apply Calibration” button shown on the calibration sheet on the screen.
4. The calibration curve, slope and intercept will be shown by program on the calibration screen.

3.3.1.3. Calibration of Oxygen sensor

Materials:

1. Approximately, 10 mL ultra-pure water.
2. 25 mL glass beaker.
3. External O₂ and N₂ gases.

Procedure: Two data entries, minimum and maximum, are recommended for a precise calibration.

1. The beaker in which the solution is contained is closed with paraffin film by including the oxygen sensor and also two gas entrances (for O₂ and N₂).
2. The calibration is started by program when the system is ready.
3. Firstly, the nitrogen (N₂) gas is purged into the system to observe the minimum oxygen concentration in the sample, it is called as “zero reading”.
4. At the point where the anchoring is observed, the known concentration value (for water is not actual 0, almost 0.001 μmol/L) is entered and recorded to the software.
5. The N₂ gas purge is closed and immediately after O₂ purge is started in order to observe the maximum concentration of oxygen in the sample.
6. The solution is saturated with oxygen gas until at a point where no further increase in oxygen concentration is observed in sample solution.
7. The solubility of oxygen in water is directly dependent on the salinity of the water and its temperature and these solubility values are tabulated in the literature (Garcia and Gordon 1992, Millero and Poisson 1981). Unisense calibration tab has an automatic solubility calculation engine for oxygen associated with these tabulated numbers. (When you manually enter the instantaneous temperature and salinity ratio of the solution- 0.0‰ for ultra-pure water-, the maximum oxygen concentration is automatically calculated by program via those values.)
8. Then, the known (calculated) O₂ concentration value is entered and recorded to software.
9. After the minimum and maximum concentration/ O₂ solubility data are added, the calibration is recorded by pressing the “Save and Apply Calibration” button shown on the calibration sheet on the screen.
10. The calibration curve, slope and intercept will be shown by program on the calibration screen.

3.3.1.4. Calibration of Hydrogen sensor

Materials:

1. Approximately, 10 mL ultra-pure water.
2. 25 mL glass beaker.

3. External H₂ gas (a tank of gas mixture by containing %1.5 H₂ gas).

Procedure: Two data entries, minimum and maximum, are recommended for a precise calibration.

1. The beaker in which the solution is contained is closed with paraffin film by including the hydrogen sensor and H₂ gas entrance.
2. The calibration is started by program when the system is ready.
3. Firstly, there is no need to purge the nitrogen (N₂) gas into the system because ultra pure water does not contain any dissolved hydrogen molecules as naturally. Thus, it is possible to assume that the point at which the sensor is immersed in the solution is the point of “zero reading”.
4. At the point where the anchoring is observed, the known concentration value (0.00 μmol/L) is entered and recorded to the software.
5. And then, H₂ purge is started in order to observe the maximum concentration of hydrogen in the sample.
6. The solution is saturated with hydrogen gas until at a point where no further increase in hydrogen concentration is observed in sample solution.
7. The solubility of hydrogen in water is directly dependent on the salinity of the water and its temperature. There are some tabulated values in the literature for identification of hydrogen concentration in water associated with its salinity and temperature (Wiesenburg and Guinasso Jr 1979).
8. By using this table with instantaneous temperature and salinity ratio of the solution- 0.0‰ for ultra pure water-, the maximum hydrogen concentration of the sample can be manually calculated.
9. Then, the known (calculated) H₂ concentration value is entered and recorded to software.
10. After the minimum and maximum concentration/ H₂ solubility data are added, the calibration is recorded by pressing the “Save and Apply Calibration” button shown on the calibration sheet on the screen.
11. The calibration curve, slope and intercept will be shown by program on the calibration screen.

3.3.2. Calibration Results and Discussion

The Unisense microsensors respond in microvolt unit to read all introduced samples. Therefore, the sensor readings made regarding the known values make it easy to see the correspondence of all the samples introduced during the analysis on the known units according to the sensor type. As it mentioned before, the user software automatically records all the data taken during the calibration (used to redraw by Origin Pro.9) and calculates the calibration curve and calibrates the equation- which it guarantees as a linear response.

For temperature sensor calibration, 7 samples with known temperature were read. The calculated R^2 , slope and intercepts are 0.99976, 9.7925, 9.4863 and 0.99971, 9.7925, 9.4863 by Unisense logger program and the Origin Pro., respectively. As the number of introduced values increases, the reliability of the calibration increases (low std. error), so that the calibration curve drawn with the origin is also very similar to the linear curve (Figure 3.3).

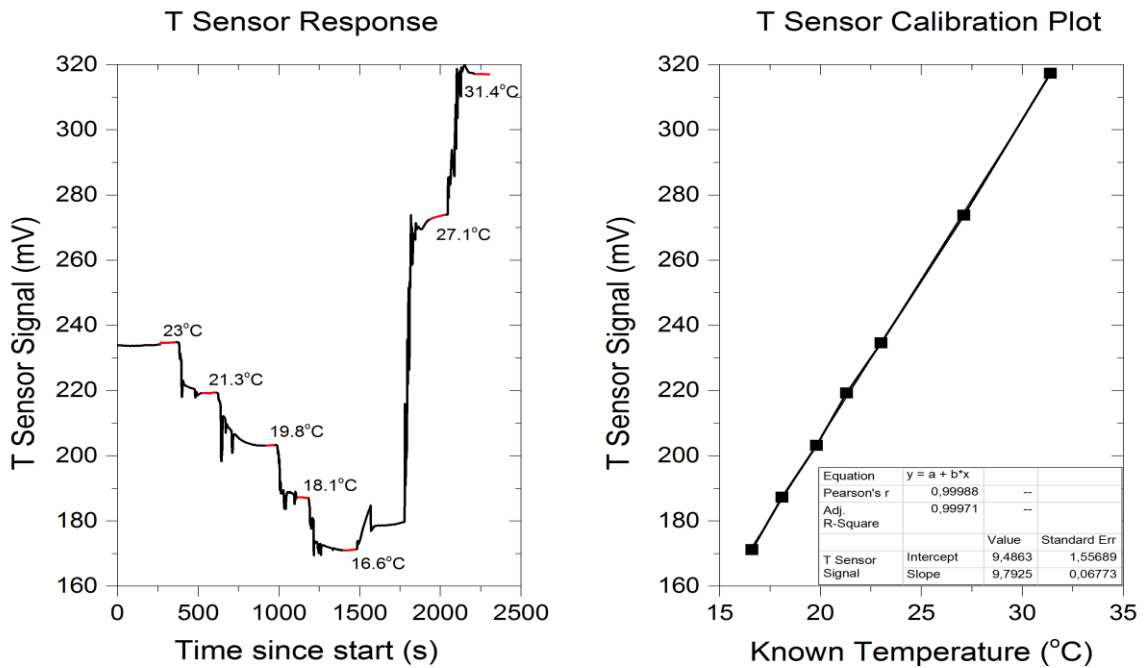


Figure 3.3. The read sensor signals and the calibration curve obtained with the samples of known values, for Temperature sensor.

The calibration graph obtained by reading the samples at 3 different pH values (pH 4, 7, 10) is shown in Figure 3.4. The pH sensor is also in the reliable measurement range when the analytical and automatic calibration values are compared. The calculated R^2 , slope and intercepts are 0.99762, -55.3949, 491.6307 and 0.99524, -55.3949, 491.630 by Unisense logger program and the Origin Pro., respectively. Due to the small difference between the R^2 values, there is a margin of error (std. error ~2.70) for the pH sensor. In order to determine the reflection of this error rate to the measurements, pH 4, 7 and 10 were repeatedly measured and the results showed that 0.80 high readings were detected in all cases- when pH 4 was introduced to sensor, program gave a calibrated result as pH 4.80.

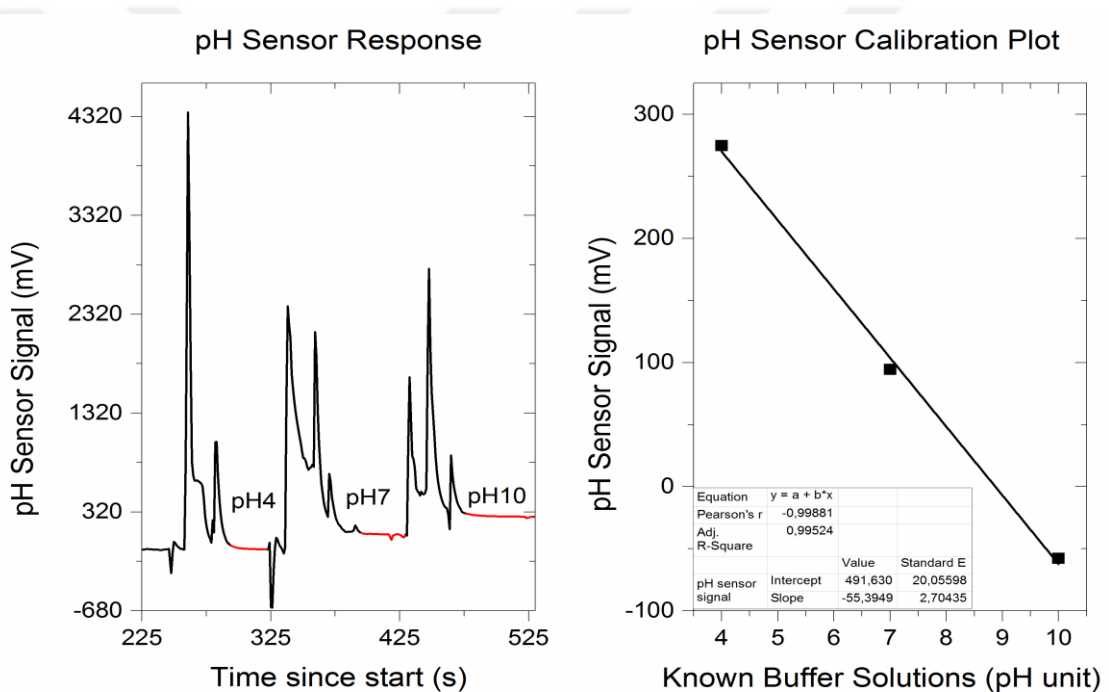


Figure 3.4. The read sensor signals and the calibration curve obtained with the samples of known values, for pH sensor.

Additionally, known values for minimum and maximum solubility of gases in water (at known salinity and temperature) were used to calibrate the oxygen and hydrogen sensors. Using only 2 values in the calibration of course makes think about causing an increase in the error margin although it cannot compute analytically. But, it should not be forgotten at this stage that the respect of the sensors to the linearity. Therefore, the calculated R^2 's, slopes and intercepts (by Origin- curve fitting) which belong to gas sensors are same with the calculated values of user program. Besides of

that, the sudden signal drops seen with Figure 3.5 show the time of nitrogen gas addition applied to draw the dissolved oxygen gas concentration in the sample to a minimum, ie zero. However, this step was not performed for hydrogen sensor calibration. The dissolved hydrogen value in the pure water was assumed to be zero depending on the calibration steps that recommended by company for the hydrogen sensor calibration. Therefore, this leads to a reading of the concentration value which goes down in the nitrogen environment of the water sample (as can be seen from airtightness test graphs of the designed mini photoreactor, in the next section). Indeed, this problem caused by the small value of the calibrated signal readings can be ignored since the focus of the experiment is on the signal change interval from the start to the end.

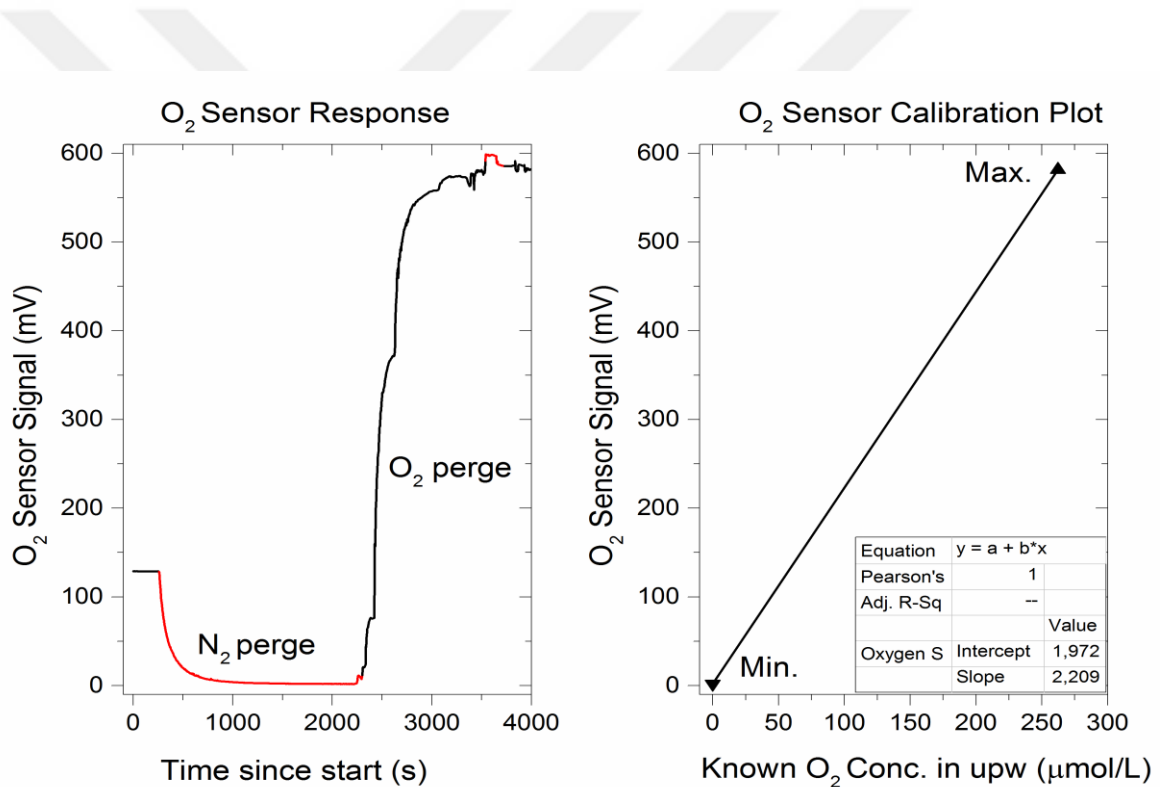


Figure 3.5. The read sensor signals and the calibration curve obtained with the samples of known values, for Oxygen sensor.

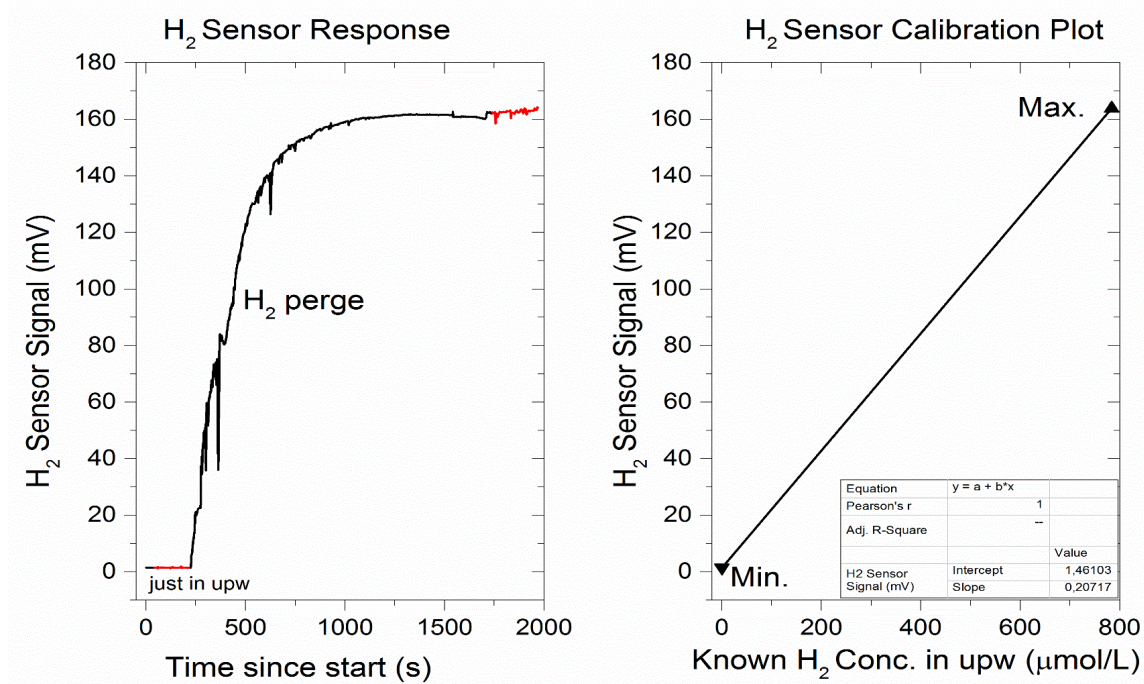


Figure 3.6. The read sensor signals and the calibration curve obtained with the samples of known values, for Hydrogen sensor.

3.4. Fabrication of the Mini Photoreactor

Currently, 3D printers are widely used in the industry and many specialized productions. 3D designs drawn with a computer software are modeled in real way by these instruments. In this study, 3D printing technology, “*Stratasy- Objet30 Prime*” 3D printer (Figure 3.7), assisted for a mini photoreactor design in order to use it in a new designed experimental set-up for photocatalytic water splitting applications. Objet30 Prime offers the broadest range of materials from elastic to transparent ones. In the Figure 3.8, an example of a test model with opaque material selected for this study is given.



Figure 3.7. The Stratasys- Objet30 Prime 3D printer that used in this study.

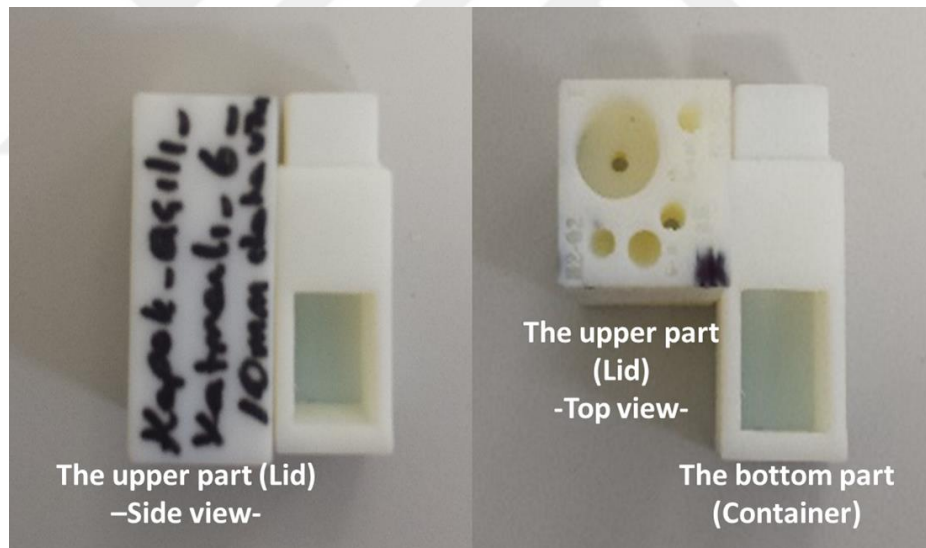


Figure 3.8. One of the tester 3D models of the mini photoreactor by opaque material (*VeroWhite*).

Actually, the fabrication progressed parallel with the design process made with 3D drawing. Every time the dimensions of the designed models were changed and each time the positions of the placed holes were modified, the newly designed model was fabricated by Objet30 Prime and physically tested. As shown in Figure 3.9, the shapes, lengths, hole positions or thicknesses of the container and lid had been changed many times.



Figure 3.9. Numerous and different forms of the mini photoreactor test prints.

3.4.1. Encountered problem and remedial solution

However, some mishaps were occurred during model tests such as breakage and cracking of two gas sensors. Due to these breaking problems, it was decided to make some changes in the material type of printings in order to protect the health of the sensors and to prevent delays in testing because of the waiting for new sensors orders. Prior to these problems, a 3D-printing polymer called as *VeroWhite*, resulting in an opaque white print, was used for test prints of reactor parts in many times (Figure 3.9). The method developed as a solution was to replace the used opaque material with a transparent polymer- *VeroClear*- for the printings of the test pieces of the reactor, whereas the opaque material was used for simulating the sensors. The sensor simulations were printed by *VeroWhite* and the tips of simulations were painted in different colors associated with the sensor type in order to make it easier to see through the outer surface of the reactor which was printed with *VeroClear* (Figure 3.10) and to be more clear about the observation of the direction of tips inside of the cuvette. Finally, a design has been achieved to print out for proposing a new designed mini photoreactor in which the container fully encloses the UV cuvette, the lid closes with the container, and the sensors can smoothly enter the cuvette (Figure 3.11).

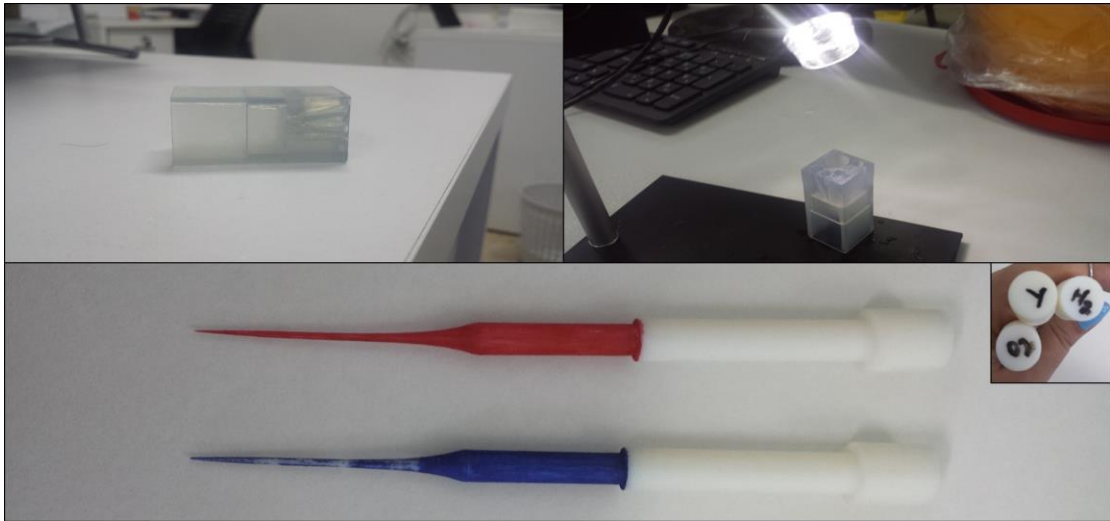


Figure 3.10. The test printing of the reactor (by VeroClear) and the sensor simulations (by Verowhite)

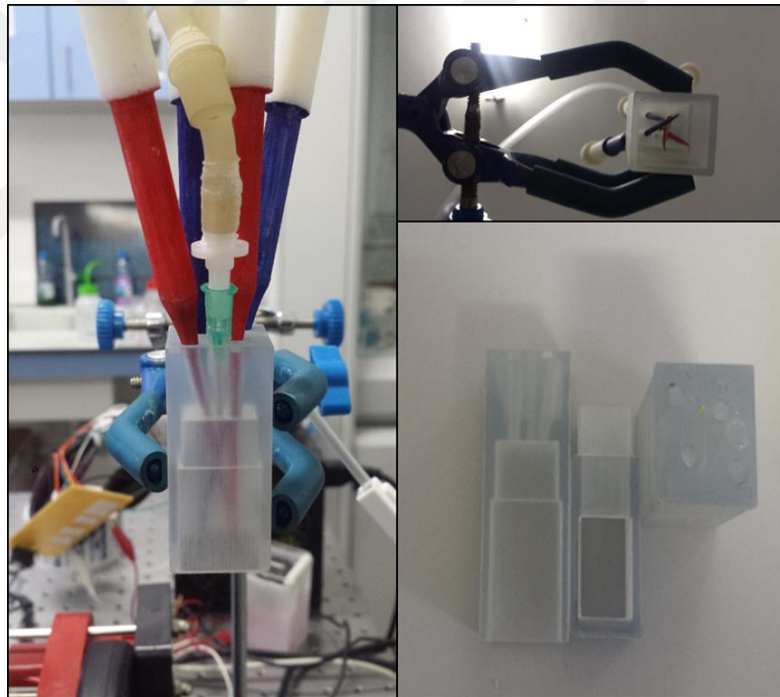


Figure 3.11. The final design of the mini photoreactor.

3.5. Tests of the Mini Photoreactor

3.5.1. Hermetically sealed surrounding tests

As it was mentioned previously, the design of the reactor must provide hermetically sealed surroundings during the photocatalytic water splitting experiments due to detection of O₂ evaluation is important. In other words, the air intake of the system can cause errors or even major faults in the experimental results. Therefore, it is necessary to determine that the system is stable and to ensure that the gas values read during this time are completely in situ. Indeed, the air-tightness could be provided by the design of the modeled mini photoreactor. The reasons why it cannot be provided by design that not only the 3D printing material is quite stiff, but also the studied micro sensors are quite fragile. When the hole designs- on the lid for the sensors to enter the system- are made at exact size of the sensors, the experiments always resulted in the breakage of the sensors because of the difficulty encountered at the time inserting the sensors into the system or removing from the system. Consequently, the reactor design was preferred that the sensors could be easily inserted into and removed from the system for the continuity and health of the measurements made with the sensors. Thereby, an external intervention was required so that the designed reactor could be airtight. For this aim, several closure methods had been tried to find the method by which the system can maintain its airtightness for the longest time. Additional gaps of the holes were covered with paraffin film, sticky tape and gum adhesive then the amount of dissolved oxygen in system was measured with the help of oxygen sensor.

To analyze how long the system can remain airtight, the same airtightness test procedure was applied in 3 different closure methods; by using sticky tape, paraffin film and gum adhesive (the validated application). The procedure used in these airtightness test measurements, which was reduced for using gum adhesive due to the fact that this method was the only working method to create an airtight environment, is listed below. The use of oxygen (not need to the hydrogen sensor as an air determinator) sensor with a gas inlet (nitrogen) and a gas outlet (to get out of the air inside) were considered sufficient for these tests only ultra-pure water was used as the sample solution.

1. Firstly, the outer top of the reactor lid was covered with a thick layer of gum adhesive for better protection from air.

2. For the sensors to enter through the reactor lid, the positions of the holes covered with gum were identified and drilled with the help of a thin needle.
3. Then, sensors were placed on the lid and the parts of the sensors entering the holes were wrapped with gum again in a conical shape corresponding to the sensor shape.
4. In addition to these, all of the edges and corners of- the portion joined to the lid and the portion cut as the window- the container (the bottom part of the reactor) were closed. (Figure 3.12)
5. When the analysis was started, the general trend of the system was observed for 3-5 minutes and then N_2 gas was started to be purged in the system.
6. It was observed that the amount of oxygen in the system remained at a value close to zero for a certain period of time, then the gas outlet hole and the nitrogen gas were shut off at the same time
7. After that, it was checked how long the system remained constant without changing the amount of oxygen.

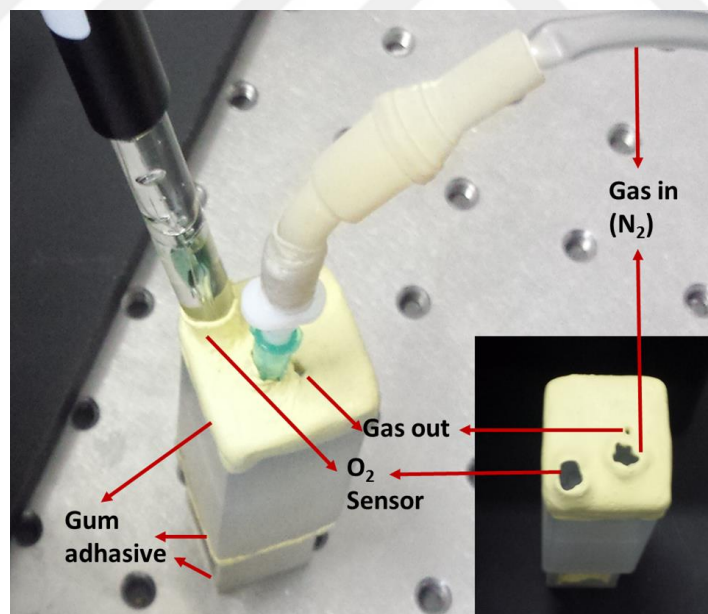


Figure 3.12. Ready to be used for the airtightness test of the reactor.

As it can be seen from Figures (3.13, 3.14, 3.15), when the nitrogen gas was supplied to the system, the signals fluctuate and when the nitrogen gas was turned off to wait for the system stability, smoother signals were obtained. It can be said that due to these fluctuations, the force at the rate of purging the nitrogen gas created noise points

in the small volume system. On the other hand, a stability of only ~2 minutes and ~3 minutes was obtained from the closure method applied using the sticky tape and paraffin film, respectively. In contrast to them, the stability obtained after the closure procedure with gum adhesive was about 30 minutes which means that the procedure to be performed for all analysis to be applied in accordance with the hermetic environmental conditions must extend for a max. of 30 minutes or more.

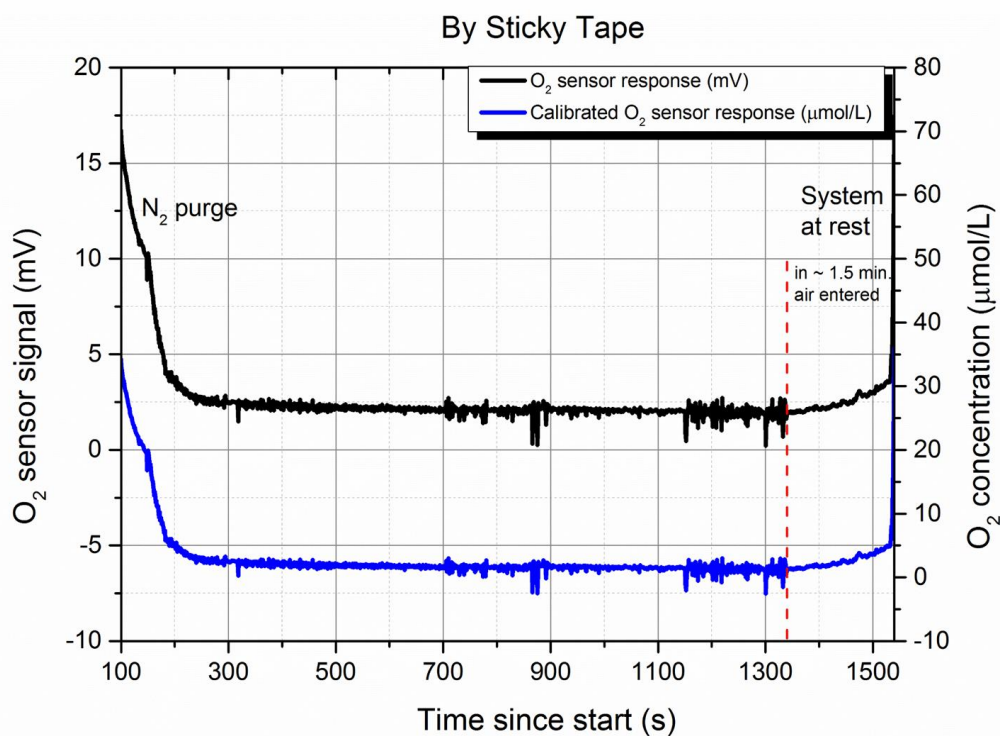


Figure 3.13. Airtight system experiment modified with sticky tape wrt. the amount of dissolved oxygen gas in the system.

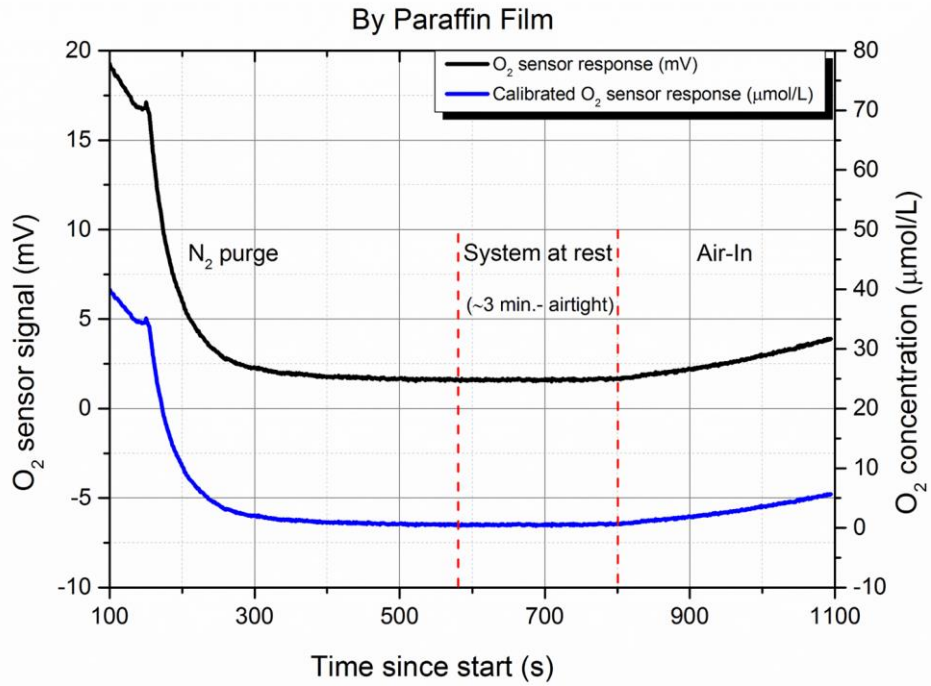


Figure 3.14. Airtight system experiment modified with paraffin film wrt. the amount of dissolved oxygen gas in the system.

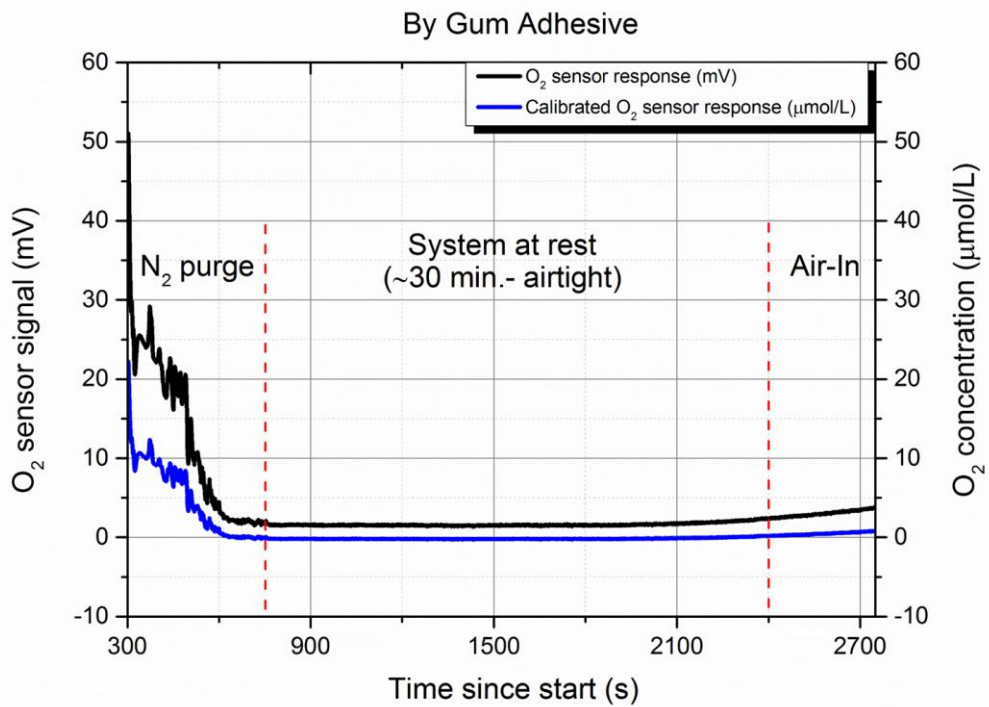


Figure 3.15. Airtight system experiment modified with gum adhesive wrt. the amount of dissolved oxygen gas in the system.

3.5.2. The tests for the effects of the light on sensors

In order to provide a high intensity light which is similar with the sun light, a solar simulator was used as the main light source of the experiments for photon collection onto reaction cell. As can be seen from Figure 3.16, the used solar simulator, which was produced by Prof. Dr. Fahrettin Yakuphanoglu (Firat University, Elazığ-Turkey), consists of three basic parts. The first part is the power supply part to which the main beam is sent out, the second part is the configurable part of the solar simulator, posemeter (exposure meter) which measures the intensity of the light hitting it over the distance, and the third part is the monitor where the light intensity that adjusted according to the distance is displayed with the numbers in different light intensity units.

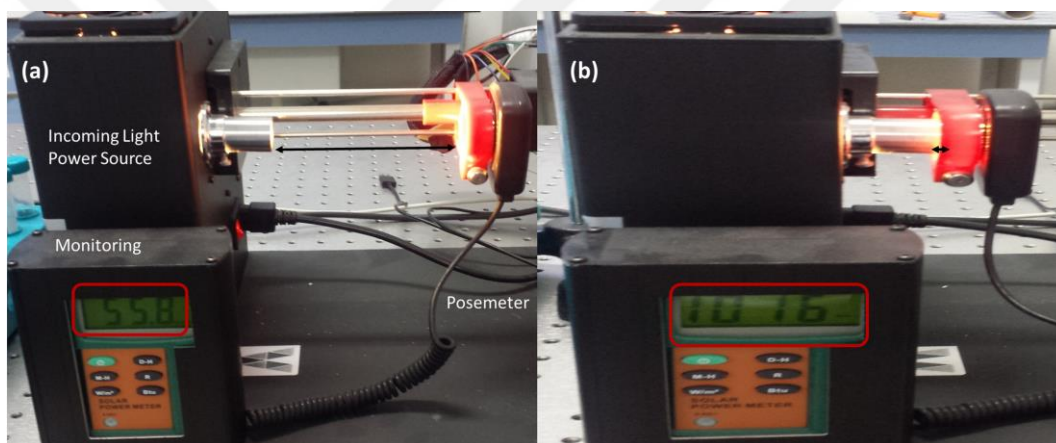


Figure 3.16. The whole image of the used solar simulator device with its parts and the configurable posemeter and the numerical monitoring system according to intensity of light which is read by posemeter a) long distance, b) short distance.

Sunlight simulation for small systems reflects the light directly into the sensor or causes the temperature of the solution in the system to increase because it directly hits the sample. Although the temperature increase is expected naturally, the false signal response that may be caused by the light reflections in the sensors may lead to unexpected interpretation errors and incorrect test results.

Therefore, before using the designed reactor in the proposed PWS experimental setup, the response of the sensors to the light should be measured only when the sensors are in water without any photocatalyst effect. In other words, it helps to understand

whether the signals read in the presence of the photocatalyst are due to the photocatalytic reaction or the response of the sensors to the direct light.

In the first light tests made with transparent sensors, it was observed that the sensors were influenced from the direct incoming light even inside the reactor. For this reason, new black-tip sensors have been ordered for use in all experiments. Technically, these black-tipped sensors (Figure 3.17b), which have the same characteristics as transparent-tipped sensors, were less influenced by direct light and helped to reduce the error margin in the observation of changes in the system.

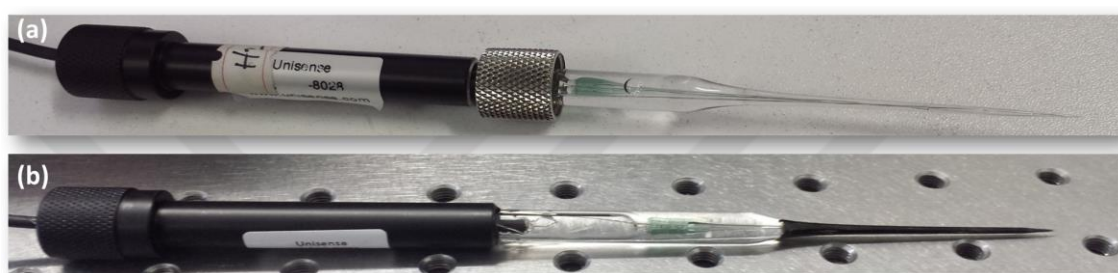


Figure 3.17. The image of the Unisense microsensors a) transparent tip, b) black tip.

In summary, the main target in these tests is to measure the responses of the sensors to light only during the interaction with pure water, without being affected by any photocatalytic agent. These responses of the sensors will help to determine whether a certain base measurement will occur and whether the reactivity of the sensors is compared during the effects under the photocatalytic substance, due to the photocatalytic reaction occurring in the system or due to the encounter with the light. Furthermore, they will create a base measurement and allow a comparison during measurements in the presence of photocatalytic material. In other words, they will help to understand that the response of the sensors is due to the photocatalytic reaction occurring in the system or due to the encounter with the light.

As the procedure of the light effect tests (in the darkness),

1. All sensors were placed in the airtight reactor system.
2. All sensors were placed in the airtight reactor system and were positioned in front of the solar simulator (position determined by measuring with a posemeter, $\sim 1000\text{W}/\text{m}^2$).
3. Every 5 minutes, the light was turned on and off (Figure 3.18) to measure the response of the sensors to the light in ultra-pure water.

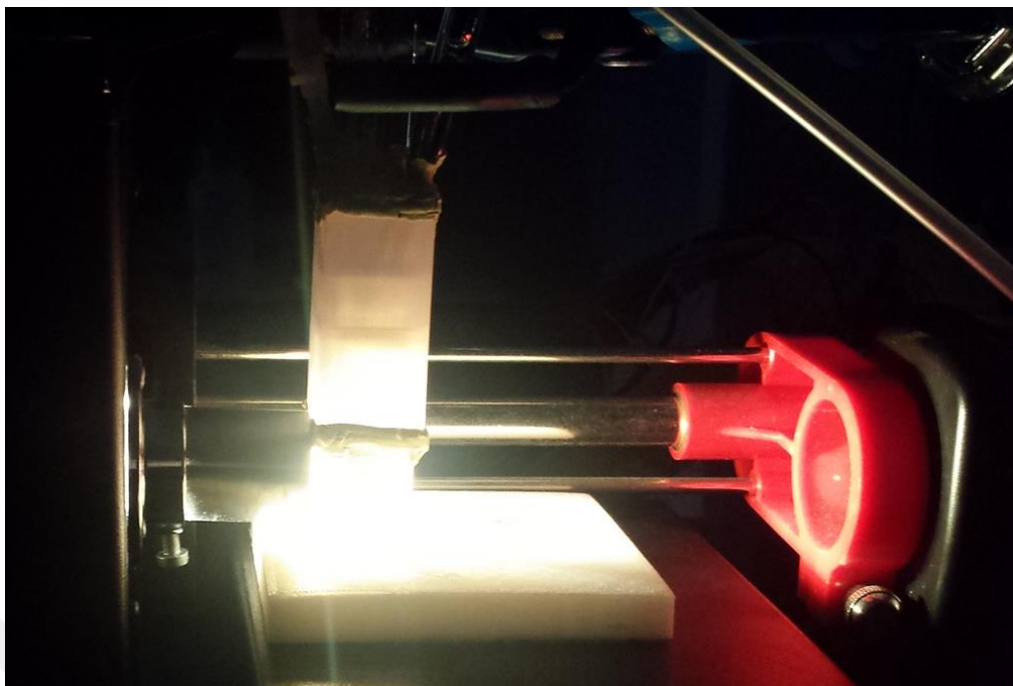


Figure 3.18. An image from the light impression tests during an light-on part of the experiments in the dark.

The responses of the transparent tipped sensors used at the beginning of this study to the light test is seen from the Figure 3.19. The sensors gave a meaningless signal every time (5 min. off/ 5 min. on) photons hit the system, especially hydrogen sensor. In addition to that, contrary to the expectation of this test made with the photocatalyst-free water sample, increases in oxygen and hydrogen concentrations were observed. Although the start of the fall in gas concentrations had been observed due to the reduction of the direct light effect at the time when the light was off, the signals had not return to the initial signal values they had before the light was turned on. For this reason, the sensors could be very specious in measuring the photocatalytic reactions and also, they could mislead the results of the experiment.

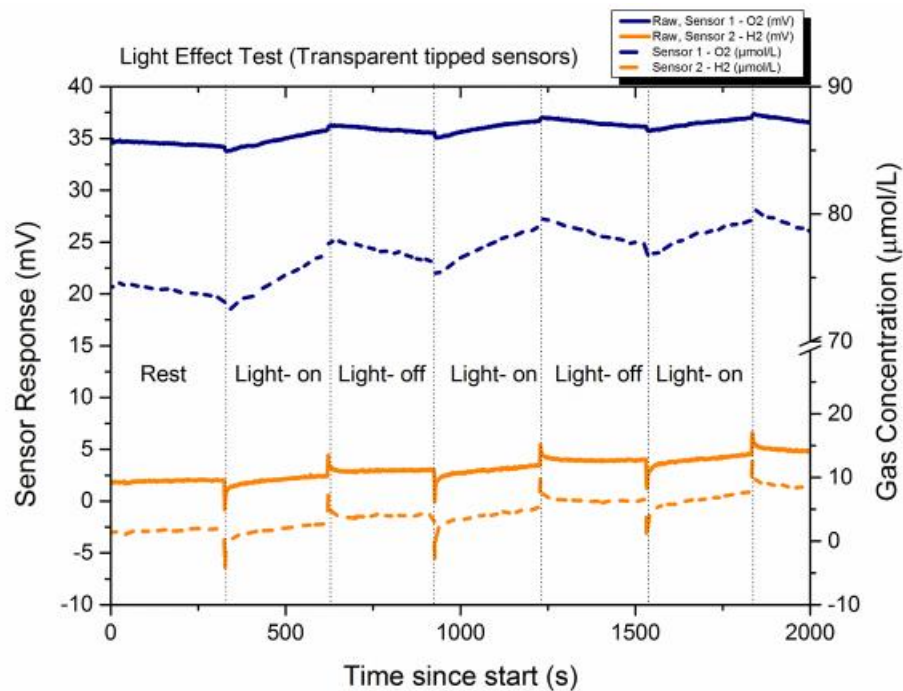


Figure 3.19. Response of old transparent-tipped O₂/H₂ sensors to light in pure water analysis.

To avoid these situations, it was useful to test the use of black-tipped sensors, whose sensors are identical but whose ends are covered with black paint. The black painted tips promise to prevent scattering of photons directly on the sensor and to remove the misleading sensor signals generated by these scatterings. As can be seen from the Figure 3.20, the responses of the new black-tipped sensors to the light was much less than the transparent ones. The reason why the signals in the Figure 3.20 seem to be more fluctuating than the Figure 3.19 is that the range of signal or/ and concentration values read against the light over time is much smaller, which is already expected to achieve by using of black sensors. Another point that is noteworthy in the Figure 3.20 is that the hydrogen sensor has increased about $\sim 1 \mu\text{mol/L}$ from the initial concentration value (from $\sim -3.5 \mu\text{mol/L}$ to $\sim -2.5 \mu\text{mol/L}$). It is beneficial to remind that the procedure of the light tests and the point-contact measurement principle of the sensors- to make the reason of this be clearer. An airtightness test is firstly applied to the prepared reactor system before each light test. The duration of the light on/ off tests, which are performed by the same reactor system, is determined in direct proportion to the duration of the airtightness test (system stability). As mentioned earlier, since the calibration of the hydrogen sensors used in the system is carried out without nitrogen while the nitrogen gas is pressed for the airtightness tests, a series of fluctuations are

observed in the signals of the hydrogen sensor by the emission of nitrogen gas in the system during the airtightness test. When the effect of the point contact principle is included, it is observed that the hydrogen concentration during the light test increases for a short time and then stabilizes.

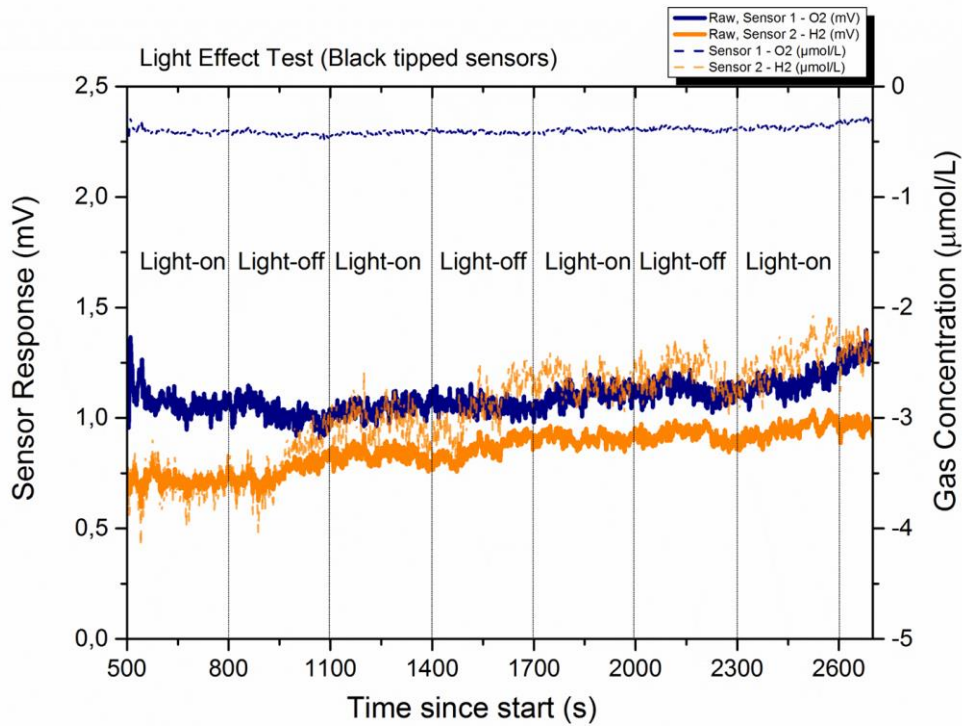


Figure 3.20. Response of new black-tipped O₂/H₂ sensors to light in pure water analysis.

In addition, a light test was carried out where all the sensors were placed in the system together and their responses against the light is shown in Figure 3.21. During the light on/ off tests for ~ 2100 seconds, there was a corresponding decreasing rate of increase in the temperature sensor and it was observed as ~ 2.5 degrees over the total time. This total degree difference, which is caused by the fact that the heat difference due to light continues to disperse in the water molecules even when the light is off, has been recorded for future photocatalytic reaction analysis. To mention about the pH sensor, it has been observed that it is not significantly affected by light and it gives stable signals while light is on unless the ion balance in the sample changes.

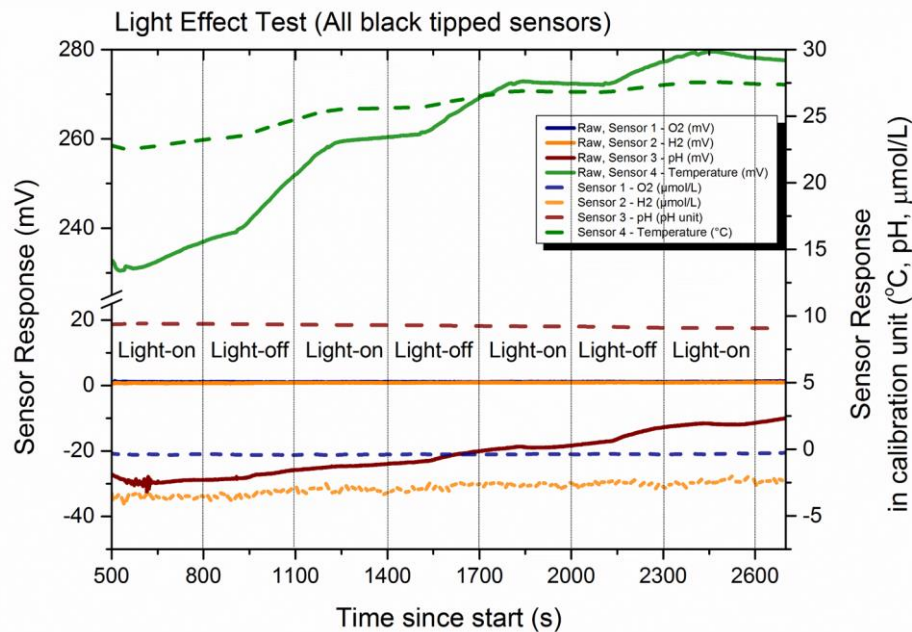


Figure 3.21. Response of all new black-tipped sensors to light in pure water analysis.

3.5.3. Working Test of The Designed System with Mini Photoreactor

3.5.3.1. Experimental

After the production of the photoreactor, which has been successfully completed in design and printed in three dimensions, it is desired to test whether the reactor is working correctly in accordance with the sensors and lights in the reaction environment. For this test, titanium dioxide (TiO₂- Degussa p25) powder was used as the photocatalyst material which is known that used in many photocatalytic applications as a water-insoluble, odorless photocatalyst that has a bandwidth of ~3.2 eV and absorbs UV light (Fujishima 1972). Moreover, a handmade magnetic stirrer designed in two different sizes (Figure 3.22) was added to the experimental test assembly because of the insolubility of titanium in water, although it was not preferred to use due to make some electrical noises in the sensor responses. The Unisense microsensors take point measurements and a homogeneous solution in the reactor is required to ensure correct reading. In conjunction with magnetic stirring, a glass coated milli-magnetic bar was used in the solution as a precaution against teflon or plastic coated magnetic bar absorbing the produced oxygen and affecting the results.

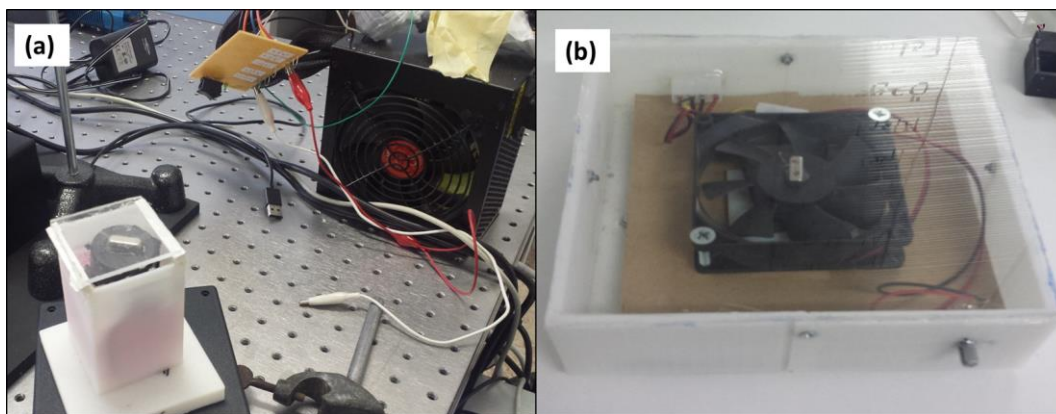


Figure 3.22. The hand-made magnetic stirrers; a) small:6.5*6.0*9.5, b) large:17.5*17.5*6.5.

Primarily, two experimental procedures had been identified for the control of the system via positive-negative expectations on the results. In other words, these two experimental procedures were intended to show the situations in which the newly designed system did produce or did not produce any results in the photocatalytic reactions. As mentioned before, the presented final mini photoreactor design can be modified to work with different light source. Therefore, the light source of the first test procedure was identified as the green laser light ($\sim 2200 \text{ W/m}^2$, $532 \pm 10 \text{ nm}$), although it is known that TiO_2 only works in the UV region. Obviously, the expectation from this experiment was that there is no H_2/O_2 production at all.

For the second test procedure, a xenon lamp ($\sim 2800 \text{ W/m}^2$, 185-2000 nm) was used as the light source of the system. As can be seen from the band position of TiO_2 under the right conditions, it can produce both oxygen and hydrogen. However, its band structure is more susceptible to hydrogen production. In order to facilitate H_2 production and support the reaction, one more material was added to the photo-reaction system as a co-catalyst, platinum (Pt, Sigma Aldrich, Platinum powder, 99.995% trace metals basis). Accordingly, it is expected that when the xenon light hits the molecules in the mini photoreactor (Pt- TiO_2 solution), the sensors will show an increase in the hydrogen concentration. Also, it should be noted that all experimental observations were made during the time that the airtightness procedure was applied and the system remained stable.

3.5.3.2. Results and Discussion

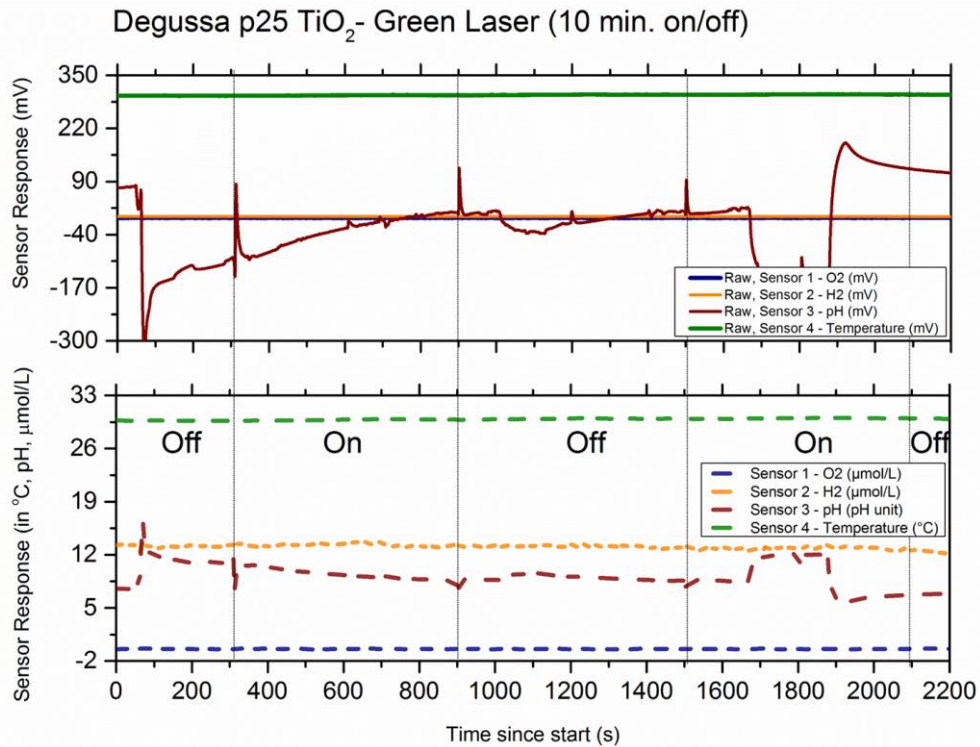


Figure 3.23. Response of Degussa p25 to green laser light in pure water, 10 min.

The Figure 3.23 shows the PWS analysis results of the first experiment which was performed by green laser light. The response of the degussa p25 in water to the green laser light was measured under open light and closed light for ~600 seconds (~10 min.) intervals for 2200 seconds. If we look at the results, no change in dissolved hydrogen and oxygen concentration was observed due to the effect of the light on and off during this time, as expected. The photons from the green laser light can not be absorbed by TiO_2 due to the fact that they do not have sufficient wavelengths similar to in the UV range also these photons are insufficient to excite the electrons in the valance band so that the electromagnetical cycle which is necessary for the oxygen and hydrogen evaluation can not be achieved. Moreover, according to Figure 3.23, it can be said that there is a slight increase in temperature at intervals where the light is on, and the solution is cooled down to thermal equilibrium, when the light is off. Furthermore, the response of the pH sensor by the sharp peaks are clearly observed when the light is turned on and off, as well as the pH increase that is thought to be caused by these mobilizations in the solution temperature. Nevertheless, there is no expectation of a significant change in the acidity of the solution unless there is a difference in ion

concentration that would normally change the environment acidity significantly. The change, which is the effect of these sharp responses from the pH sensor, is lost due to the experiment's stabilization of the system during the last 200 seconds under closed light, and the pH value at the beginning and at the end of the system is in balance. Apart from these probable factors thought to effect on the pH measurement, an incoherent pH increase was observed for 200 seconds between the 1700th and 1900th minutes of the experiment.

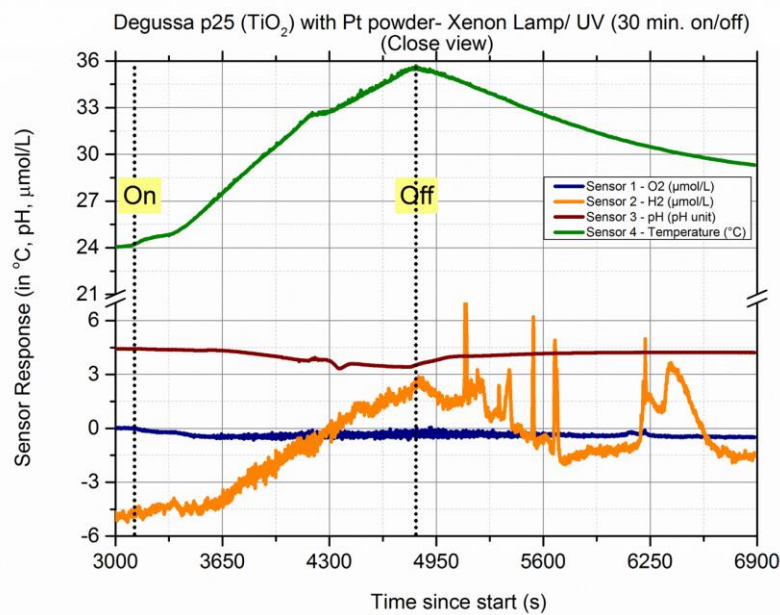


Figure 3.24. Response of Degussa p25 with Pt powder under Xenon lamp in pure water.

The test results of the second experimental procedure, which was performed by xenon lamp, is shown in Figure 3.24 with close view to make it more clear. Light exposure was measured as closed and opened at 1800 second (~30 min.) intervals for approximately 3900 seconds.

In the rough view, it appears that as the light exposure time progresses over the first 30 minutes of light on, the temperature sensor and H₂ sensor tended to increase while a slight decrease in the pH sensor and O₂ sensor was observed during this time. Primarily, the increase in temperature can be assumed that is directly caused by the power of the light source. But depending on the results, since a significant change is observed in the dissolved gas concentrations in the system, the ion balance of the solution must also be considered before correlating pH change directly to the temperature change.

As it known that the pH value depends on the ratio of H^+ and OH^- ions in the solution, and in cases where the H^+ ion concentration is higher than the OH^- ion concentration, the solution is called acidic ($pH < 7$). If the system is producing hydrogen, then it means that the proportion of H^+ ions is decreasing by reduction reaction. On account of decreasing H^+ ions, the observed pH value decreases although an increase in pH should have observed. Depending on this observation, TiO_2 may have found another H^+ molecule source that will reduce without oxidation in water. Additionally, observing a decreasing trend rather than an increase in oxygen concentration to prove water splitting can be considered as supporter inference. Namely, Pt and TiO_2 have produced H_2 by photon activation in water but have done this in a different path than water splitting. On the other hand, when the light is turned off, the temperature and the hydrogen sensors show a decreasing trend by direct proportion to the decreasing photons, the oxygen and pH sensors indicate that a balance has been established within the system during this period. Ultimately the hydrogen production, which was expected of the TiO_2 to be achieved with Pt support under UV light, was dedected and it was observed successfully by the newly designed mini photoreactor system, which can measure four different parameters at the same time, allows the interpretation of the effects of the changes in the system by altogether parameters.

3.5.4. Efficiency limit of the new designed PWS system

Theoretically, the efficiency limit of the proposed experimental set-up for PWS was calculated. The system is mainly depended on solar applications; therefore, the starting power was indicated as 1000 W/m^2 . When this light comes to the designed mini photoreactor, which has a $2.25E-4 \text{ m}^2$ light exposure area (the window on the bottom part, $15 \text{ mm} \times 15 \text{ mm}$), the designed mini photoreactor can absorb 0.225 W of the total power. Considering that the minimum light exposure time in the applied test procedures is 5 minutes, 0.225 W corresponds to 67.5 J of energy for 5 minutes.

According to H_2 energy values in kJ/g (Table 1.3), 67.5 J energy is obtained by $\sim 4.7569E-4 \text{ gram}$ ($\sim 2.3597E-4 \text{ mol}$) H_2 . Hence, the system can detect max. $\sim 0.07866 \text{ M}$ H_2 with 100% efficiency because of 3 mL of the max. solution (water) capacity of reactor. Therefore, due to the fact that the detection limit of the hydrogen sensor in the system, which determines the amount of dissolved hydrogen in the water, is $0.3 \mu\text{M}$

(Table 2.1), the efficiency limit of the proposed system is calculated as **0.0003814%**. Besides, when the same calculation steps are followed, the efficiency limit of the proposed system is calculated as **0.000063567%** for the maximum light exposure time in the applied test procedures is 30 minutes.

As a result, the system can measure as low a efficiency as $6.3567\text{E-}5\%$ - $3.814\text{E-}4\%$ interval, since the experiments made within 5min. and 30 min. experimental periods are theoretically approached. Normally it is difficult to design a system that can correctly read low-efficiency reactions (a system which is sensitive for detection of the low efficiencies). Therefore, it can be thought that another advantage of the presented system that can detect such a low yield. Namely in theory, a reaction with the ability to produce hydrogen with such a small yield can be easily observed and measured by the proposed PWS system.

3.6. Conclusion: Achievements of the chapter

A new two-piece mini photoreactor design, which allows four different microsensors (O_2 , H_2 , pH, T) for measurement to be housed in the system at the same time, allowing the sensors to remain and fixed on the lid, has been proposed by 3D-printing models.

As a result of the successful simulation of the sensor, which prevents the physical damage to the sensors that caused by modelling with the errors that made during the design, the physical modeling of the mini photoreactor (3 ml max. solution capacity) was printed out successfully.

Independently of the designed mini photoreactor and following to the procedure recommended by the manufacturer, the calibrations of glass-tipped microsensors, which have a high selectivity, a high sensitivity and a wide detection range, used as gas sensing method in this mini photoreactor system that allows measurement (T, pH and O_2/H_2 dissolved gas concentration) at the same time, are uneventfully performed to prepare for general analysis.

After the calibration process, two important factors that must be met by the modeled system- the airtightness time of the mini photoreactor and responses of the sensors during light exposure- were tested to verify the convenience of the system in PWS experiments. According to the results obtained, it was decided that the mini

photoreactor was needed to modify with the gum adhesive so that the system could be hermetically sealed for a minimum of 30 minutes as well as replacing the glass tips with the black dyed ones to minimize the effect of the sensors on the light. At the final stage, the design and manufacture of a portable mini photo-reactor, which is affected by a minimum level of direct light exposure, airtight for min. 30 minutes, and where the sensors are permanently located on the lid, for PWS applications has been successfully completed.

In addition, the proposed experimental set-up, which involves a light source, four calibrated microsensors, a gas inlet-outlet (N_2 for safety) and a new designed mini photoreactor, is constructed. Then, the system was tested by a common semiconductor; TiO_2 -Degussa p25 and demonstrated by results of tests that the expected change over time in temperature, in pH and in dissolved hydrogen/oxygen concentration can be observed by cooperation of the proposed microsensors and the new designed mini photoreactor.

CHAPTER 4

PbVO₃Cl AS A PHOTOCATALYST FOR PWS REACTIONS

4.1. Abstract

This chapter aims to test the experimental PWS set-up, which was proposed in previous chapters, with a semiconductor as a photocatalyst. The lead(II) trioxovanadate(V) chloride crystal, [PbVO₃Cl], which is thought to be suitable for this purpose, has been investigated as a photocatalyst for PWS applications. However, there is a limited literature on the characteristic features of this material which was discovered in 2007 at IZTECH by M. Eanes and her research group. For this reason, some theoretical and experimental analysis about PbVO₃Cl, which were performed to identify some unknown optical properties, are described and then the results are presented in this chapter. Furthermore, the results of the photocatalytic applications made with the new designed set-up are shown, however, no observation has been recorded that PbVO₃Cl can be used as a photocatalyst in PWS. In the light of the detected properties such as band transition type, band energy and conductivity, it has been foreseen that PbVO₃Cl crystal may be an efficient semiconductor for solar fuel researches. By this prediction, a solar fuel device, which is imaginarily designed, is introduced. Consequently, the theoretical yield of this device is calculated and the price analysis of PbVO₃Cl is performed to present a prediction about the future potential of PbVO₃Cl.

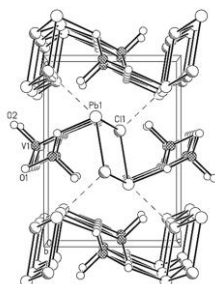


Figure 4.1. Crystal structure of PbVO₃Cl.

A manuscript based on parts of this chapter has been submitted as: İ. Harmanlı, M. Koç, U. Soğukkuyu, E. Tarhan, V. Cecen, H. Sevinçli, M. Emirdağ, E. Karabudak*, *Discovery of a New Semiconductor, PbVO₃Cl*, *Advanced Energy Materials*, 2016.

4.2. Introduction

Research is required for new cost effective, stable and efficient semiconductors on the path of global solar fuel energy dream. GaAs(Serpone and Pelizzetti 1989a), CdTe(Hernández-Ramírez and Medina-Ramírez 2014, Pellizzetti and Serpone 1989), Si(Cody, Brooks, and Abeles 1982, Tauc 1966), GaP(Spitzer et al. 1959), CdS(Giribabu et al. 2012, Yu et al. 2010) and various non-oxide semiconductors have good absorbivity in solar spectrum, but their surface is not stable in water oxidation environment. On the other hand, oxide semiconductors (e.g., TiO₂(Pelaez et al. 2012, Rehman et al. 2009), ZnO(Bamwenda and Arakawa 2001, Phuruangrat et al. 2014), WO₃(Takeuchi et al. 2011, Tang et al. 2003), Bi₂WO₄(Shang et al. 2010) an etc.) are stable, but their visible light absorption is low. There are also various semiconductors in field, but still we need to discover new semiconductors on the pathway of building stable, efficient and cost effective devices.

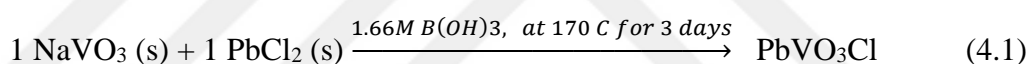
Vanadium oxides have large application area, especially including catalysis; so P-V-O compounds systems have been studied many times(Luca et al. 1995, Vannier et al. 1992, WITTMER and BUCHANAN 1981). On the purpose lots of vanadium compounds were synthesized. However a few chlorovanadates are present. In 2007, Iztech Inorganic Lab. (Mehtap Eanes et.all) using hydrothermal synthesis method, a new P-V-O-Cl compound (PbVO₃Cl) was synthesized(Borel et al. 1999, Jo et al. 2009, Mentré, Huvé, and Abraham 1999, Sahin and Emirdag-Eanes 2007).

4.3. Synthesis

PbVO₃Cl sample (Figure 4.2) was synthesized by routing from the research of Şahin A., and Emirdağ M.(Sahin and Emirdag-Eanes 2007). The following reagents were used as obtained: NaVO₃ (Fluka, 98%) and PbCl₂ (Riedel-de Haen, 98%). PbVO₃Cl was obtained from the reaction of NaVO₃ (460.5 mg, 3.3 mmol) and PbCl₂ (992 mg, 3.56 mmol).



Figure 4.2. The synthesized PbVO₃Cl crystals.



Four trials tried to synthesize PbVO₃Cl crystal by bomb synthesis method which is a basic method for crystal synthesis via heating and cooling. Table 4.1 shows amount of reactants for the trials. Samples were prepared according to table values in teflon on-lined autoclave. They were heated in an oven at 170⁰C for 3 days and then cooled slowly to room temperature. Cooling must be done slowly, because the crystallization occurs in the cooling part of the procedure (Jo et al. 2009, Mentré, Huvé, and Abraham 1999, Sahin and Emirdag-Eanes 2007). After 3 days; PbVO₃Cl crystals were obtained (Figure 4.3).

Table 4.1. Reactants of Synthesis Reaction

Trials	NaVO ₃ , gram	PbCl ₂ , gram	B(OH) ₃ , gram	Water, mL	B(OH) _{3(aq)} , M
1	0,4877	1,1124	1,8549	12,5	2,4
2	0,2438	0,5562	0,9274	22	1,66
3	0,1219	0,2781	0,4637	12,5	1,66
4	0,4877	1,1124	10mL (aq)	-	1,66

The four trials of PbVO_3Cl synthesis are shown Figure 4.3, Trial 1 and Trial 4 have better crystals and yields than the others and Trial 4 is the best yield and also has the least B(OH)_3 crystals (white needles) in these trials. In trial 4, B(OH)_3 is used as aqueous solution but in the others, it is not used as aqueous solution. It can be said that $\text{B(OH)}_3(\text{aq})$ may cause better yield and less white needles formation.

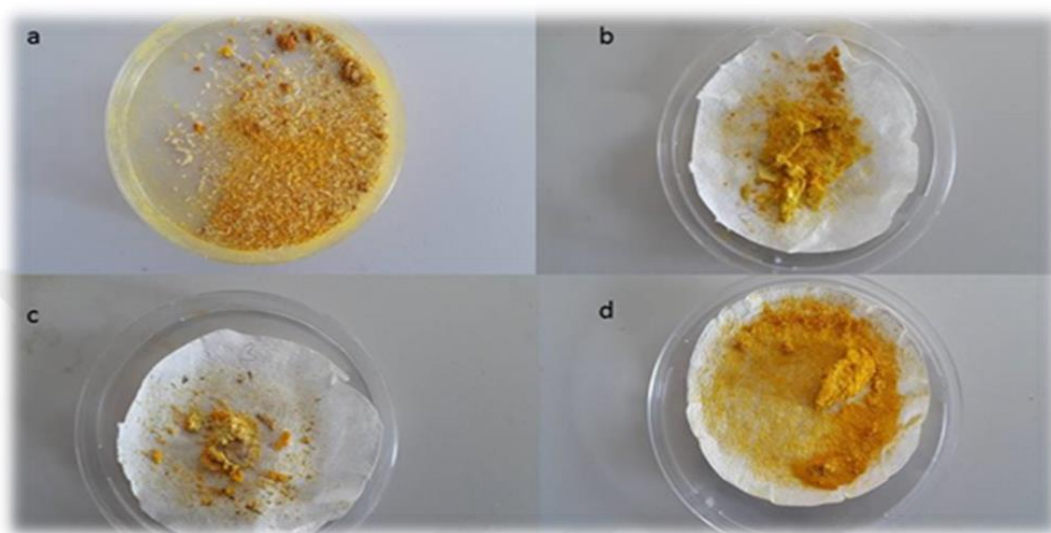


Figure 4.3. Produced PbVO_3Cl Samples: a) Trial-1, b) Trial-2, c) Trial-3, d) Trial-4.

The product was a mixture of yellow needle crystals in millimetric size and white powder (PbCl_2)- it can be seen by naked eyes and be held by a tweezer to sever the needle crystals from each other if it needs. Yellow needles of PbVO_3Cl were obtained in approximately 60% yield and white powder was analyzed as side-product (PbCl_2) by using XRD.

Synthesis in millimetric size is not easy for some materials (Figure 4.4). Due to the fact that, the applications of semiconductors in device design as a single crystal is easier and more significant, this size specialty can be called an advantage of PbVO_3Cl . For instance, the nanoparticle semiconductors are being researched by scientists for years. Due to synthesize in bigger size the application area of the nanoparticle semiconductors. The further researches should include the synthesis of PbVO_3Cl in bigger size to get benefits in determination of its band position. In addition to that synthesis in bigger size might be promising for application studies of PbVO_3Cl in solar fuel devices or photovoltaic devices, directly.

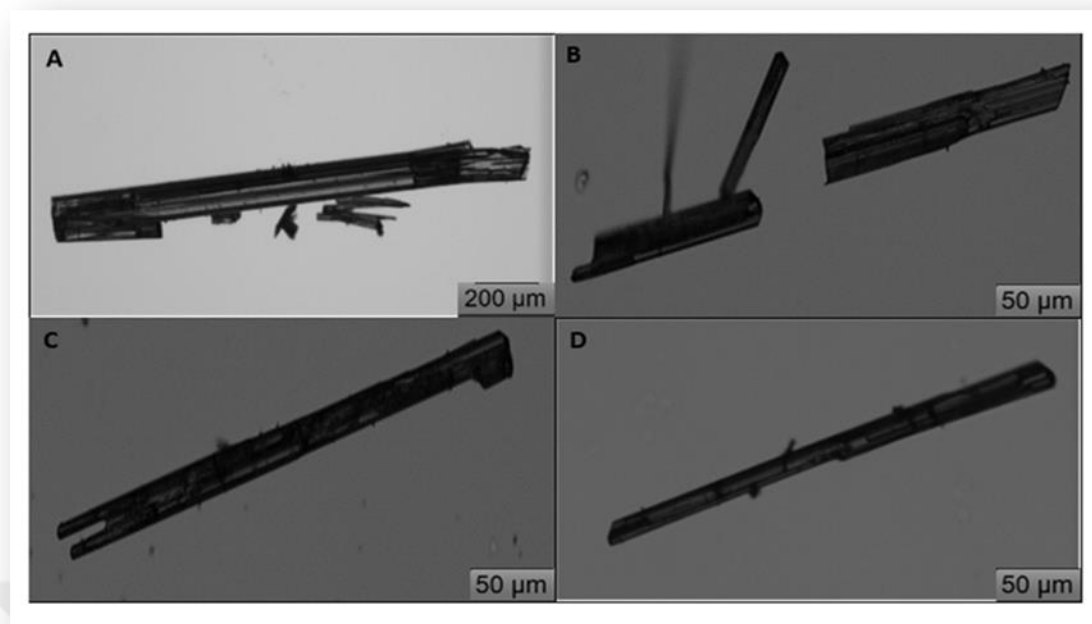


Figure 4.4. The snaps of the yellow needle PbVO_3Cl crystal by Optical Microscope “Olympus BX53”.

4.4. Analysis of Optical Properties of PbVO_3Cl by Experimentally and Theoretically

4.4.1. Analysis of Optical Properties (Experimentally)

4.4.1.1 XRD Analysis

Primarily, XRD (X-Ray Diffractometer) analysis was applied to synthesized PbVO_3Cl crystals to make a validation with the its original (published) structure. X-Ray diffraction, which investigates the material structure, atomic arrangements and imperfections, is a characterization technique which helps to be sure about similar lattice constants/phase in materials. For this analysis, PbVO_3Cl yellow needle shape crystals are grounded uniformly using a mortar and pestle. Powder material was analyzed by using XRD (X-Ray Diffractometer) Philips X’Pert Pro with 1.540598 \AA wavelength in data range $4.993^\circ - 69.995^\circ$.

Standard data of XRD patterns of different crystals have been compiled and stored in large database so that an experimental sample can be compared to a standard

on order to identify the material and/or phase(Bank). Conventional X-ray diffraction patterns for the PbVO_3Cl are plotted in Figure 4.5 with 1.540598 \AA wavelengths in data range between 4.993° and 69.995° . In this study, a standard for PbVO_3Cl was obtained and plotted along with the experimentally collected data by helping of High Score program. The report of the data comparison shows that there was 100% similarity between experimental and standard PbVO_3Cl .

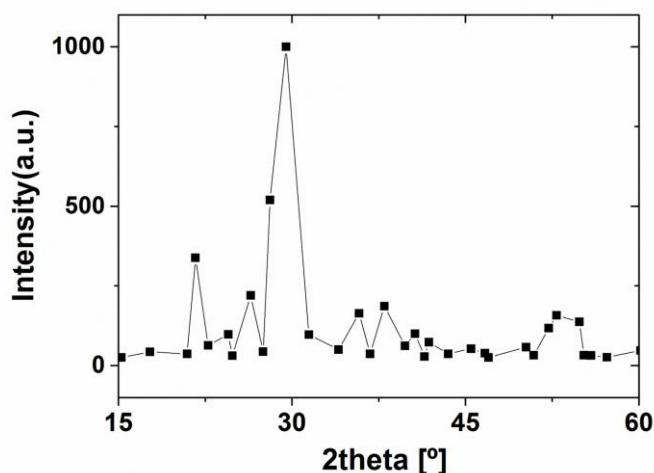


Figure 4.5. XRD results of powdered crystal PbVO_3Cl (1.540598 \AA wavelength in data range $4.993^\circ - 69.995^\circ$).

4.4.1.2. Band Gap Determination by using Diffuse Reflectance (UV-Vis Spectroscopy) and Tauc Plot Method

It is clear that the band gap energy is one of the criteria to make a claim about PbVO_3Cl , whether it is an applicable semiconductor for the applications of energy conversion devices. Although the transmission techniques are the main effective methods which are used for determination of the band gap energy of solid materials, we could not make it beneficial for this study by the reason of the small single crystalline size. Thus, it was decided that the best method to adopt for this research was to use Diffuse Reflectance Method since the PbVO_3Cl samples were analyzed in powder form. On the contrary, diffuse reflectance gave us just reflective results in the absence of reference material. Since the reference material has an effect on just reflection data, we should apply Tauc plot calculation methods for determination of the band gap energy of the PbVO_3Cl .

Tauc *et al.* (Tauc, Grigorovici, and Vancu 1966) proposed and substantiated a method for determining the band gap using optical absorbance data plotted appropriately with respect to energy. This was further developed in Davis and Mott's more general work on amorphous semiconductors. (Davis and Mott 1970, Mott and Davis 1979) Their study demonstrated that the optical absorption strength depends on the difference between the photon energy and the band gap as follows:

$$(\alpha h \nu)^{1/n} = A (h \nu - E_g), \quad (4.2)$$

where h is Planck's constant, ν is the photon's frequency, α is the absorption coefficient, E_g is the band gap, and A is a proportionality constant. The value of the exponent denotes the nature of the electronic transition, whether allowed or forbidden and whether direct or indirect:

- for direct allowed transitions: $n = 1/2$,
- for direct forbidden transitions: $n = 3/2$,
- for indirect allowed transitions: $n = 2$,
- for indirect forbidden transitions: $n = 3$. (Viezbicke et al. 2015)

The UV-Vis Spectroscopy was applied by using Shimadzu UV-2550, reflectance of PbVO₃Cl crystal was scanned between 800-200nm. In this method, BaSO₄ was used as a reference. Sample was prepared in mineral oil as mud and was applied between two thin glass plates. Also, reflectance of one thin glass plate; with mineral oil, was measured for effects of glass and oil.

The study described in this research demonstrated, for the first time, the optical properties of the recommended PbVO₃Cl semiconductor. For this reason, any information was found for the first time in the literature on the question of the transition type of PbVO₃Cl. Therefore, all four transition possibilities of PbVO₃Cl should be calculated by Tauc plot. Figure 4.6 presents the intercorrelations among the optical absorption data and Tauc plot application by using "edge plotting method" for absorption spectra (Bashouti et al. 2012, Bencina et al. 2014).

$$F(R) \quad \alpha \rightarrow \quad (4.3)$$

$$F(R) = (1 - R)^2 / (2.R) \quad (4.4)$$

R: Reflectance data /100

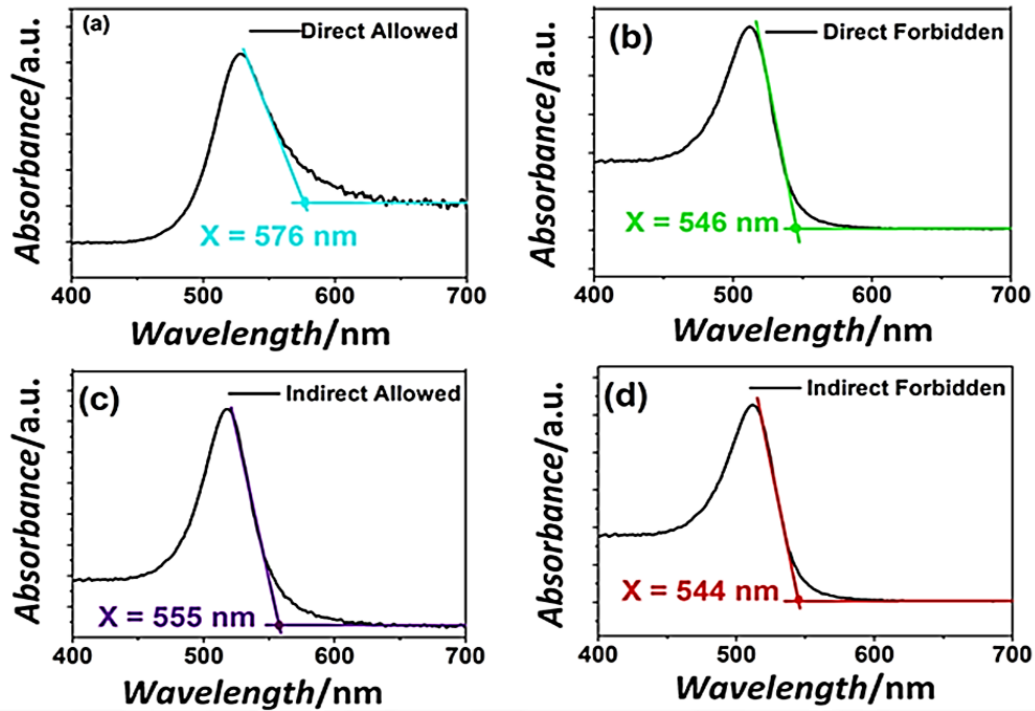


Figure 4.6. The absorption edge plot of 4 optical band gap predictions depending on transition type.

The peak point as in wavelength leads the “edge plotting” to calculate the maximum and minimum absorbance difference as eV. To define the common wavelength data point, offset lines and onset lines were drawn on the absorbance graph for each transition types (Boris et al. 2012, Ivill et al. 2008, Kannammal et al. 2014).

According to the defined point, the optical band gap of promising single crystal semiconductor was calculated for direct allowed, direct forbidden, indirect allowed and indirect forbidden transitions as 2.15 eV, 2.27 eV, 2.23 eV and 2.28 eV, respectively. Overall, four band gap energies, which were depended on transition types, were obtained by Tauc plot method but it was not known which one is the correct result for the PbVO₃Cl.

4.4.1.3. Four Probe

The “4 probe” is a measurement method that measure resistivity of matters (semiconductors) with its four probe. Each probe has a equal distance next to the other side probe. Working mechanism of 4 probe is shown in Figure 4.7. Between 1. and 4. probes; there is a constant current so that voltage change is measurable. Then resistivity is calculated by the light of these information.

To make “4 probe” measurement, PbVO_3Cl film or pallet was needed. PbVO_3Cl was more convenient to make pallet. Firstly, sample was grinded in a muller. Then grinded PbVO_3Cl was put into pellet machine and 5000 bars was applied with KNF-N-022-AN-18 vacuum pump for 10 minutes. After that it was gently taken out from the holder. Produced pellet had a thickness about 850 microns.

Four probe measurements were made by using Lucas-Signatone Pro4-440N. At the beginning; 0.1, 0.2, 0.5, and 0.8 mA constant currents were given to the pallet at different trials and taken 5 measurement from 5 different XY positions, however these measurements was not good enough to calculate resistivity. At last, 1 mA constant current was given and taken 5 measurement from 5 different XY positions again. Results were good to calculate resistivity.

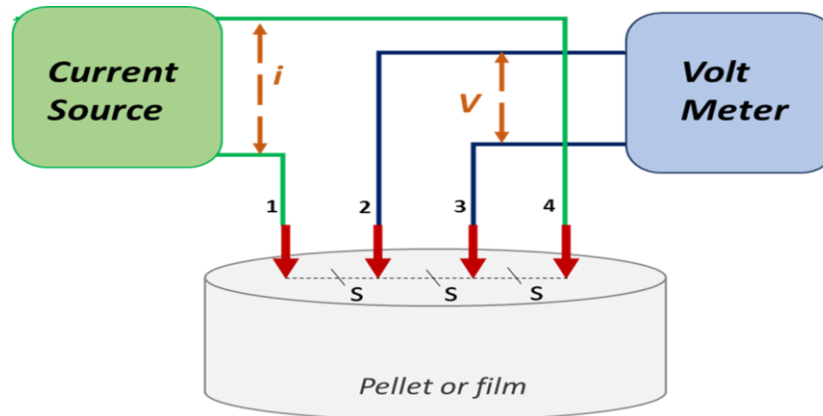


Figure 4.7. Four Probe Mechanism.

The results of the 5 measurements from 5 different XY positions by “4 Probe” are shown in Table 4.2 and the used formulations to calculate the resistivity and conductivity of PbVO_3Cl are listed below. According to the results PbVO_3Cl has a value of $\sim 2.97564\text{E-}4$ (ohm-cm)⁻¹ conductivity. Besides the evaluated conductivity

result, another deduction from this analysis can be made that we can form pellets for PbVO_3Cl by pressure and this pellet has some conductivity properties even though it is form of multiple crystals and there is no binding material or something.

$$\text{Resistivity: } \rho = 2\pi S \frac{V}{I} (\Omega.\text{cm}) \quad (4.5)$$

$$\text{Conductivity: } \sigma = \frac{1}{\rho} (\Omega.\text{cm})^{-1} \quad (4.6)$$

Table 4.2. PbVO_3Cl pallet Four Probe Measurement results, the thickness is 850 microns in all measurements); Conductivity = $1/ R*\text{Thickness}$

Trial	X (mm)	Y (mm)	R (Ohm/sq)	Res (Ohm.cm)	V/I	Thickness (μ)	Conductivity (ohm-cm) ⁻¹
1	0	0	44690.640625	3646.438477	18203.3632	850	2.7424E-4
2	7.5	0	33771.128906	2755.483887	18238.7656	850	3.62913E-4
3	0	7.5	45259.648438	3692.865479	18252.3222	850	2.70792E-4
4	-7.5	0	43413.261719	3542.213623	18255.4238	850	2.82309E-4
5	0	-7.5	0	0	0	0	0

4.4.2. Analysis of Optical Properties (Theoretically)

4.4.2.1. State-of-the-art Density Functional Theory Calculation

Before working on the determination of the transition type of PbVO_3Cl , we wanted to be satisfied at lattice constants of the proposed semiconductor by computationally. The state-of-the-art density functional theory (DFT) (Hohenberg and Kohn 1964, Kohn and Sham 1965) calculations using plane wave basis sets.(Furthmüller, Hafner, and Kresse 1996, Kresse and Furthmüller 1996, Kresse and Hafner 1993, 1994) The projector augmented-wave method(Blöchl 1994) was used as implemented with local density (LDA)(Perdew and Zunger 1981) and generalized gradient (GGA)(Perdew, Burke, and Ernzerhof 1996) approximations. Also, the XRD was used deduced crystal structure(Sahin and Emirdag-Eanes 2007) as the starting point of our calculations. Structural optimization was performed by allowing all atomic positions and all cell parameters to vary. The upper limit for the Hellman–Feynman forces was set to be $10 \text{ meV}^\circ\text{A}^{-1}$. A Monkhorst–Pack scheme(Monkhorst and Pack 1976) was performed with a $11 \times 11 \times 11$ mesh for Brillouin zone integrations. The

kinetic energy cut-off for the plane wave basis set was chosen as 600 eV and the convergence criterion for electronic relaxation had been set to 10^{-5} eV.

The lattice constants were found to be 5.2, 7.0, 9.9 °Å using LDA, and 5.3, 7.3, 10.5 °Å using GGA, where the experimental lattice constants were 5.3, 7.2 and 10.0 °Å, respectively. Both LDA and GGA results were in good agreement with the experiment with deviations from experiment ranging between 0% to 5% in the different directions.

4.4.2.2. Electronic Band Structure – Plotting GGA Approximation

When the question arises: which value of 4 calculated optical band gap is the anticipated transition type of PbVO_3Cl in theory? To get an answer for this question by identification of the transition type of PbVO_3Cl , the electronic band structure was plotted as obtained from HSE06 approach.

As it can be seen from Figure 4.8, the valance band edge places at vertical S direction, although the conduction band edge places at vertical Y direction. The difference between the valance band edge and conduction band edge level directions indicates that PbVO_3Cl has indirect transition specialty. In Figure 4.8, the high symmetry points of the orthorhombic (ORC) lattice are given as $\Gamma - X - S - Y - \Gamma - Z - U - R - T - Z|Y - T|U - X|S - R$ (Setyawan and Curtarolo 2010).

The indirect materials have lower ability in excitation of the photon than direct materials. The reason for this fundamental difference in difficulty of excitation between the indirect and the direct materials related with momentum. Unlike direct transition, indirect transition needs to momentum to excite the photon. It means that the absorption coefficients of indirect materials are smaller than direct materials. Therefore, the decrease in absorption coefficient causes to increase in the thickness of material to design of device. This is because these materials require a large thickness to absorb all the incident light, which means that photogenerated electrons and holes have to travel large distances before reaching the interface (Van de Krol and Grätzel 2012a). This is why direct semiconductors, such as amorphous Si or $\text{CuIn}_x\text{Ga}_{1-x}\text{Se}_2$ (CIGS) can absorb all incident light in just a few micrometers, whereas crystalline (indirect) Si solar cells typically have a thickness of ~300 mm (Van de Krol and Grätzel 2012a). It seems that PbVO_3Cl is an indirect material and further device design studies with PbVO_3Cl should be considered that PbVO_3Cl needs to design with thick layer-single crystal for a device.

(The all expressions for the thickness of the inversion and accumulation layers are seldom necessary in photoelectrochemical water splitting – they can be found in the literature)(Morrison 1980, Sze 1981).

Consequently, 2 optical band gap (indirect allowed and indirect forbidden) results can be called the significant optical band gap results of the study, when the other 2 values concerning the direct transition type were eliminated by depending on the theoretical (computational) calculations.

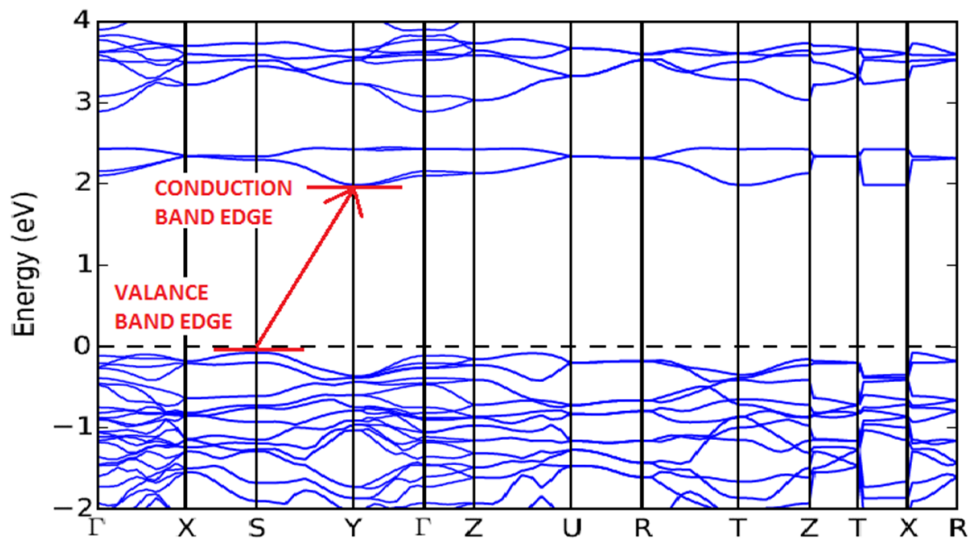


Figure 4.8. Electronic band structure as obtained from GGA.

4.4.2.3. Drawback of DFT formalism - LDA, GGA and HSE06 Approximation

A screened hybrid functional (HSE06) was also used to amend the band gap estimation (Monkhorst and Pack 1976, Sahin and Emirdag-Eanes 2007). We investigated the electronic density of states. It is a known drawback of DFT formalism that the energy band gaps are underestimated within the standard LDA and GGA frameworks. Nevertheless, it is possible to give better estimations with hybrid approaches which compose GGA results with that of Hartree-Fock approximation. In this work, we followed HSE06 approximation.

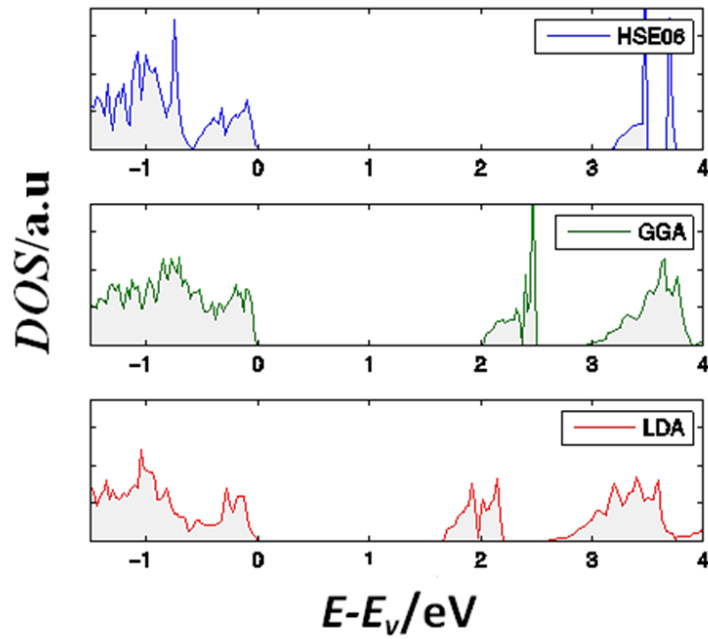


Figure 4.9. Electronic density of states as obtained from LDA, GGA and HSE06 schemes (red, green, blue, respectively). The zero of the energy is set to the valence band edge.

In this study, 4 optical band gap energies were determined by experimental analysis and 3 theoretical band gap energies were calculated by computational analysis for PbVO_3Cl . According to quantum mechanics calculations, PbVO_3Cl has 3 possible band gap energies (Figure 4.9). The corresponding theoretical energy band gap estimations were 1.65 eV, 2.05 and 3.18 eV, respectively. One observes a clear increase in the estimated energy gap using the hybrid approach.

As mentioned in computational method calculations, the theoretical results are not precise and the most reliable result belongs to HSE06 method. Therefore, we assumed the theoretical band gap of PbVO_3Cl as 3.18 eV. In addition to that we calculated 4 probable optical band gap energies for PbVO_3Cl and 2 of these 4 values were eliminated by GGA framework because of determination of “indirect transition” specialty in PbVO_3Cl . Unlike theoretical band gap results, 2 optical band gap results, which belong to indirect transition, were precise results. Because of the precision of optical results, the optical band gap of PbVO_3Cl was assumed as ~ 2.2 eV. However, there is no evidence to make a decision for which one is the accurate band gap. Also, 2 band gap predictions are not close to each other. Probably, this remarkable difference comes from the contexture of material. We have a suspicion that material can be doped or defected. It means that the actual band gap can be ~ 3 eV but the optical-experimental

results could be misled by doping factor. If PbVO_3Cl is doped, experimental results must have pointed the lower band gap energy than accurate band gap.

On the other hand, the theoretical methods might stumble in approximation of band gap energy. To abolish this uncertainty, the PbVO_3Cl results need to be supported with other unique experimental synthesizes and analyses.

4.4.2.4. Phonon Calculations by Raman Spectroscopy and DFT

The DFT method and the Raman Spectroscopy were applied for phonon calculations of PbVO_3Cl . The phonon density of states is calculated using DFT within the same framework as in the electronic structure calculations. In order to obtain the force constants, we perform a calculation in which an atom is displaced from its equilibrium position by 0.01 Ang in a certain direction. Having obtained the Hellmann-Feynman forces on each atom due to the displacement and performing this procedure for each atom and for each direction, one can build the force constant matrix. In practice, the symmetries of the systems are incorporated and the dynamical matrices are obtained using the Phonopy package (Togo and Tanaka 2015). In calculating the force constants, a $3 \times 3 \times 1$ super cell is used and for obtaining the phonon density of states the q-space is sampled with a $50 \times 50 \times 50$ mesh.

Figure 4.10 shows the comparison of the theoretical peaks and experimental peaks which were measured by DFT and Raman Spectroscopy, respectively. In other words, the observable peaks of the theoretical DFT method can be Raman active or not. So, some of the peaks cannot be seen in the Raman Spectroscopy. When the peaks of both methods were compared, one can realize the similarity between the peaks of Raman and DFT which are read as **564.8** and **563.5**, respectively. In addition to that Raman results have other remarkable peaks which are broader than the DFT peaks at the same frequency range. This width difference between the peaks of Raman and DFT can be arisen by temperature difference. DFT was performed at 0 K and the Raman Spectroscopy was performed at room temperature. So, it is well-known that the temperature increase is caused to observe the peaks as broader. For instance, the peaks as **107.4**, **119.4**, **245.2**, **380.3** and **973.1** which belong to DFT spectrum, are observed as **109**, **128.9**, **227.8**, **349** and **962.2** in Raman Spectrum with broader shape, respectively, at the same frequency range. It is considerable that these numerical differences are caused by temperature change, presence of peak-overlapping or peak-shifting. Also,

according to numerical observations, it can be said the peaks of DFT as **151.4, 460.3, 495.3, 663.6 and 733.5** are not raman active or are effected by the peak-overlapping and peak-shifting, because of their absence in Raman spectrum, with respect to their frequency scale. If you look at the Raman spectrum, you will see two remarkable peaks as **813.3 and 866.3** which do not take a place at DFT spectrum. These peaks point that there is a possibility of overtone of other excitations.

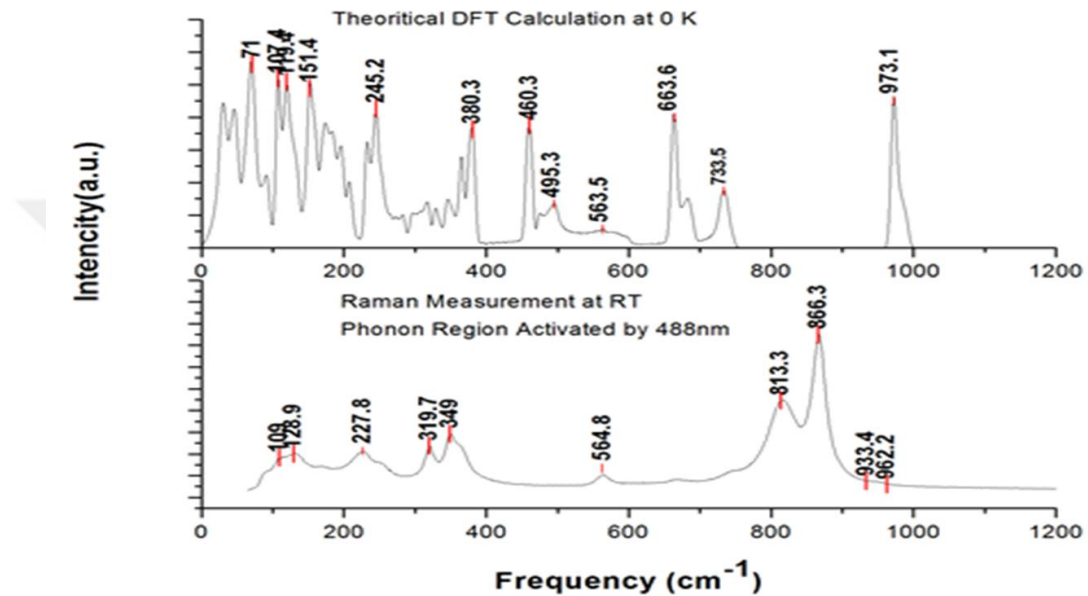


Figure 4.10. Phonon calculation plots of PbVO₃Cl; therotical DFT analysis and Raman Spectroscopy.

4.5. PbVO₃Cl in the new designed PWS system

The main reason for the detailed investigation on PbVO₃Cl is that the new designed mini photoreactor for PWS applications, which was mentioned in the previous chapters, is to be tested with any semiconducting material. After determining the particular characteristics of PbVO₃Cl, it was measured how this material would react in the designed system in a PWS reaction. For this purpose, experimental procedures were carried out with various light sources (Figure 4.11) in the presence and absence of co-catalyst material (Pt), including the magnetic stirrer in the proposed experimental setup.




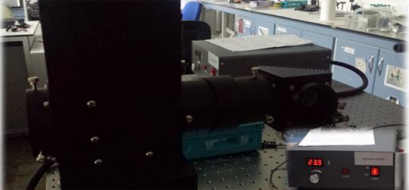
White Led Light		~1300 W/m ²	(430-600 nm)
Green Laser		~2200 W/m ²	(532 ± 10 nm)
Sun Light (AM1.5D)		~1000 W/m ²	(400-1200 nm)
Xenon Lamp		~2800 W/m ²	(185-2000 nm)

Figure 4.11. The used light sources.

Since it is not known whether the band position of PbVO_3Cl is prone to hydrogen production or oxygen production, or whether it does not stay out of position at both bands, any co-catalyst was not used in the initial analysis with different light sources in order to observe the natural tendency of the substance. The first experiment was performed with a solar simulator because the photon source we wanted to study was the sun. However, as it can be seen from Figure 4.12a, no significant changes in temperature, pH and gas concentrations were observed during the light on and off periods at intervals of ~1800 seconds (~30 min.). Later, the light sources were diversified towards the stronger ones and used as a photon source; white led light (Figure 4.12b) and green laser light (Figure 4.12c), respectively. In these two different light source experiments, it was tried to be a way to increase the frequency of opening and closing by keeping the light drain shorter, ~300 seconds, but again no results could be observed for the four parameters.

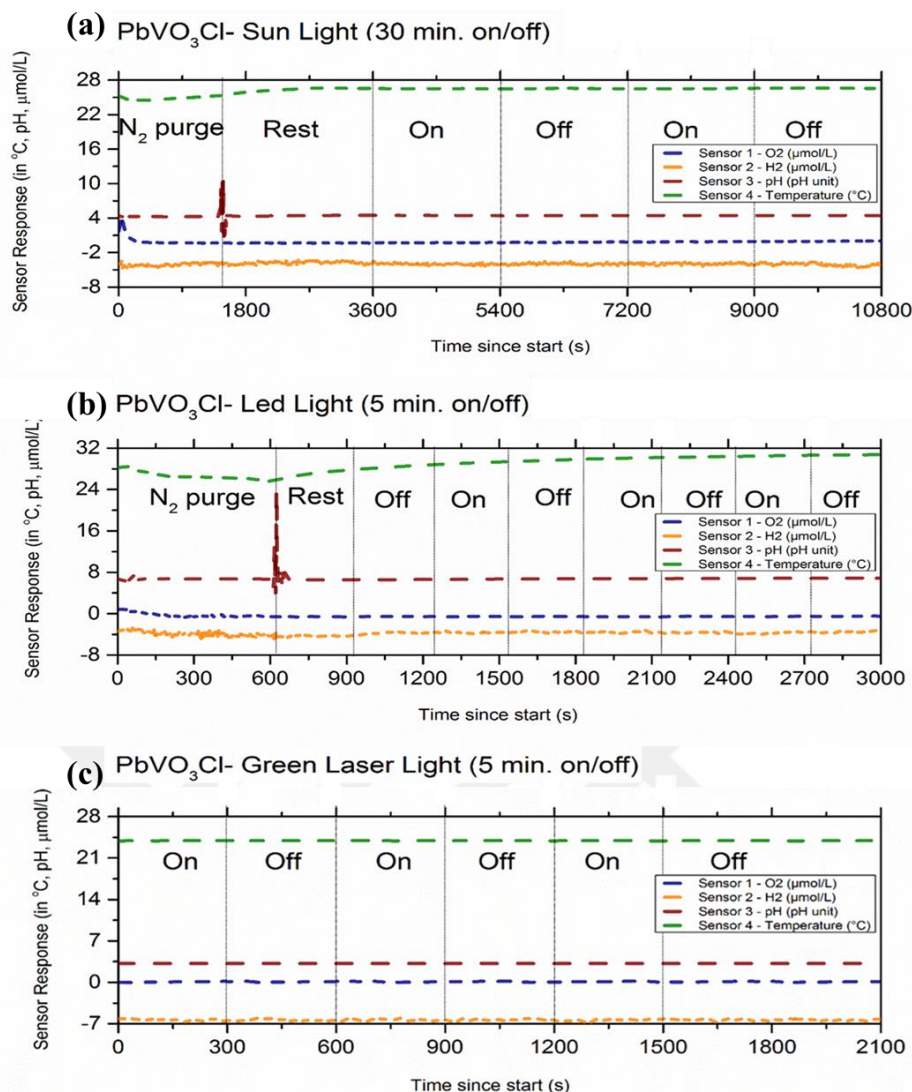


Figure 4.12. Response of PbVO₃Cl a) under sun light in pure water - 30 min. periods, b) under White led light in pure water - 5 min. periods, c) under green laser light in pure water - 5 min. periods.

As a result of the unobservable results, platinum was added to the aqueous PbVO₃Cl solution, wondering whether the use of the co-catalyst would make any difference, so a new trial was performed by exposing it to green laser light. Although the wavelength range of the green laser beam was not matched with the experimentally and theoretically calculated band gap of PbVO₃Cl, it was expected to observe its response with the co-catalyst effect. It can be seen from Figure 4.13a that photocatalytic results cannot be obtained again from the lead in the on/off light periods of ~30 minutes interval. As no result was obtained with this trial, finally a trial was made with xenon light which is a light source with a stronger power and wider wavelength range. However, the exposure frequency was again reduced to ~5 min. to avoid any sudden

temperature increase that could occur in the solution during long exposures because of the high power of the used light source (Figure 4.13b). It can be seen from the Figure 4.13 that the use of strong light power and co-catalyst does not work as well.

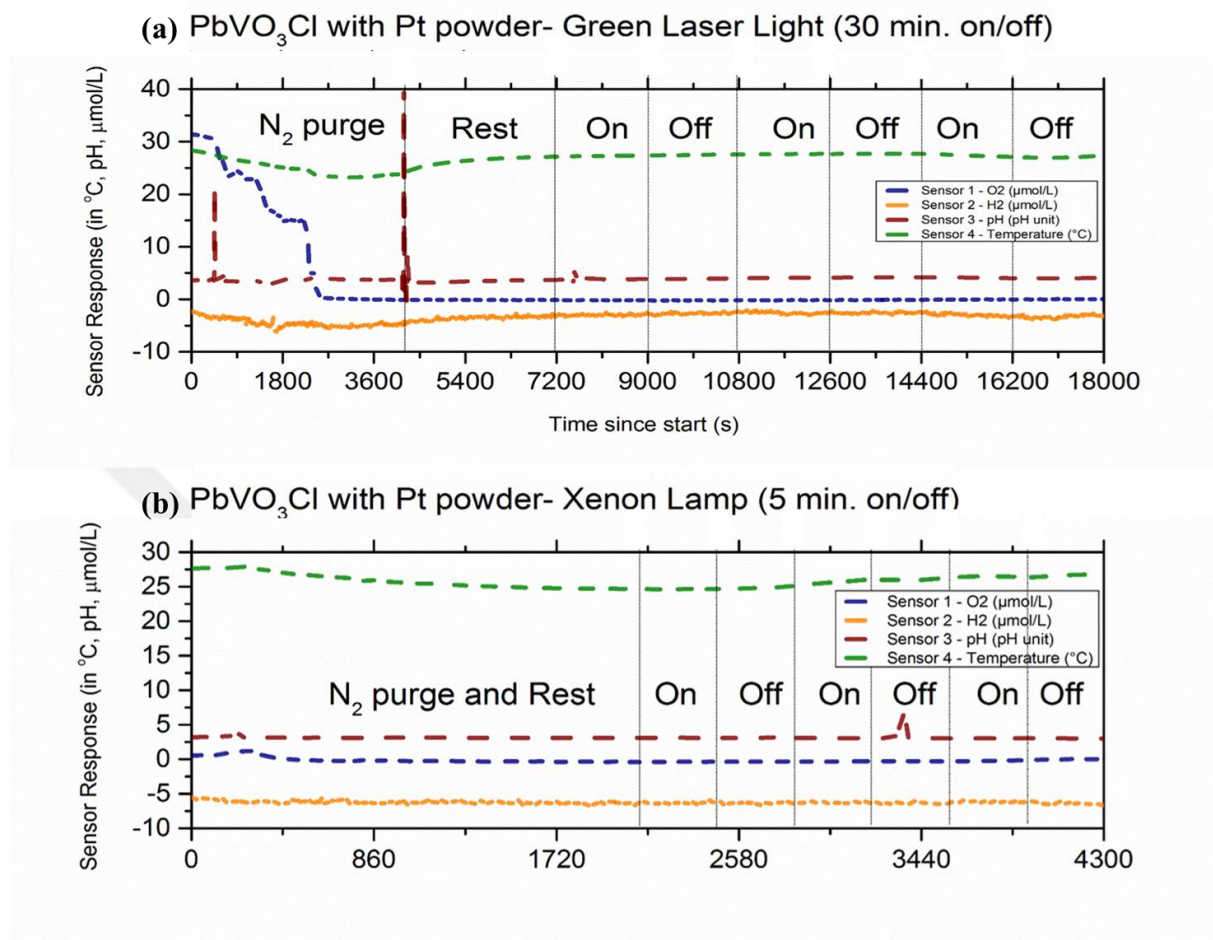


Figure 4.13. Response of PbVO₃Cl a) under green laser light in pure water - 30 min. periods, PbVO₃Cl with Pt powder, b) under Xenon light in pure water - 5 min. periods, PbVO₃Cl with Pt powder.

Although there is no meaningful conclusion to be made individually for the changes observed on the experimental results, it can be said in part that the PbVO₃Cl does not give any photocatalytic response under the Pt effect. Again, the band position of PbVO₃Cl is unknown, so it is possible that platinum is not a suitable co-catalyst for PbVO₃Cl. Besides, the PbVO₃Cl may not work in photocatalytic reactions experienced with water- though having sufficient band energy (~2.2 eV experimentally) for photocatalytic water splitting- even if it can be seen a good semiconducting material for the photocatalytic reactions. In order to be sure about all of these possibilities which are

true, PbVO_3Cl is needed to conduct with further investigations, especially its optical and photonic characteristics.

4.6. The Future Speculations about PbVO_3Cl

4.6.1. Theoretical Solar Efficiency Calculation for Single Layer PbVO_3Cl

The energy conversion efficiency of PbVO_3Cl is an important key to make a decision about the possibility of utilizing PbVO_3Cl as a prospective semiconductor in the applications of energy conversion devices. Figure 4.14 represents the total solar radiation power spectrum that strikes the Earth in the form of sunlight (Gueymard 2004, Murphy 2007). The radiation spectrum varied from 280 nm to 4000 nm (Gueymard 2004). Band absorption of the solar spectrum of PbVO_3Cl and commonly studied photoactive semiconductors such as TiO_2 and Si are highlighted by the shaded areas. The 4 optical band gaps determined by the Tauc plot calculation method were inserted into the solar spectrum (Figure 4.14). It is clearly seen that the calculated band gaps data for PbVO_3Cl occupied the highest intensity region of the total solar radiation spectrum. Positioning at the highest intensity region of the spectrum has proven to be beneficial for improving the photoactivity of the semiconductors. That is, higher radiation power ensures the higher efficiency in conversion of solar energy to another energy forms. Interestingly, PbVO_3Cl could be excited by visible light with wavelengths in a range between 544 nm and 576 nm, leading to the visible-light responsive photoactivity. This finding might help design a good photoelectrochemical cell that contained a photoanode and a photocathode on which anodic/cathodic reactions occur in the splitting of water for solar-fuel generation. In the light of the discussion mentioned, it must be borne in mind that the calculated 4 band gaps data did not still provide useful clues for specifying the exact value of the optical band gap of PbVO_3Cl . The computational methods have been studied and discussed in the Theoretical Calculation section of this study in order to define which optical band gap is closer one to the accurate value of the band gap of PbVO_3Cl .

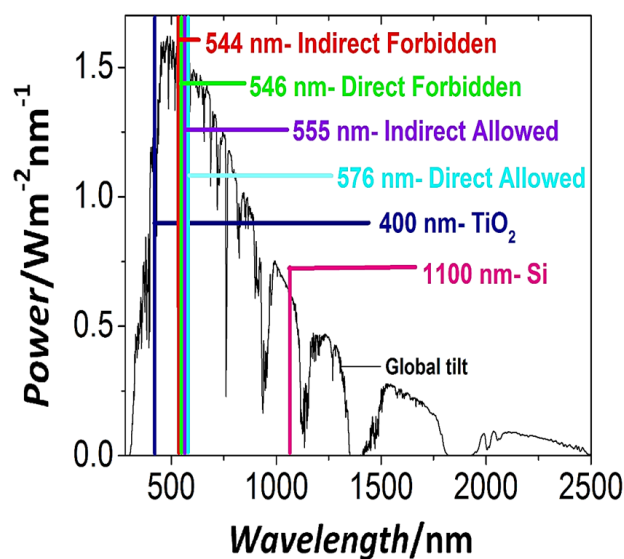


Figure 4.14. The Total Solar Radiation Power Spectrum was drawn with OriginPro by taking data from <https://www.pvlighthouse.com.au>.

On the other hand, the other two famous rivals—silicon (Si) and titaniumdioxide (TiO₂) are placed away from the range of maximum solar light wavelength. TiO₂ is placed at ~400 nm in the solar spectrum (Figure 4.14). TiO₂ exhibited direct but wide energy band gaps due to the low valence band position from the filled N 2p or o 2p states(Sun et al. 2014). However, its wide bandgap ($E_g = \sim 3.2$ eV) only allows TiO₂ to absorb photoenergy in the UV range, which is less than 3% of the whole solar light spectrum(Zhu et al. 2012). As a consequence, TiO₂ has very low efficiency (~2% (Roel van de Krol 2012))in the applications of the solar energy conversion devices as a semiconductor. The 1.12 eV band gap of crystalline Si allows effective light absorption at wavelengths from the UV to the near-infrared if the challenges of an indirect gap can be addressed (Figure 4.14). This results in a higher conversion efficiency (max. efficiency ~25% (Roel van de Krol 2012, Zhu et al. 2012)) compared to TiO₂, assuming a unity quantum efficiency. Si has an acceptable electron mobility, which leads to a wide application as a photoactive material for solar energy conversion(Sun et al. 2014). However, the small band gap energy of Si causes to high presence of thermalization waste as energy in the semiconductor when the photon comes with higher energy than its capacity.

It should be noted here that, the proportions concerning the area under the spectrum and the whole area of solar radiation were calculated by integration in order to define the solar energy efficiencies of each 4 mentioned transition types of PbVO₃Cl.

The efficiencies were computed for direct allowed transition, direct forbidden transition, indirect allowed transition and indirect forbidden transition as 30.1%, 25.6%, 26.9% and 25.3%, respectively. Taking into consideration the values of the efficiency obtained, the PbVO_3Cl promises a huge opportunity for the future studies when comparing with the other two competitors—Si and TiO_2 .

4.6.2. Theoretical Solar Efficiency of Double Layer Semiconductor

Tandem photoelectrochemical cells (PECs) have a multijunction design that consists of a photoanode/photocathode or a photoelectrode/photovoltaic configuration with a tunnel junction (Li and Wu 2015). As is well known from the literature that, (Van de Krol et al. 2012) in a tandem cell with a series connection, the overall photovoltage is the sum of individual junctions, but the overall photocurrent is determined by the minimum among all the individual junctions.

Figure 4.15 shows the Lewis structure which was proposed for increasing the energy efficiency of the semiconductors as a tandem device (Lewis and Nocera 2006). According to the Lewis structure, solar energy conversion efficiency over 80% was calculated theoretically using $\text{PbVO}_3\text{Cl}/\text{Si}$ tandem cell, as displaced in Table 4.3. Comparative performances are also summarized in Table 4.3. The flux of solar photons in the wavelength range from 547 nm to 280 nm represents 25.74% of the total solar photon flux, which is the maximum efficiency that has been predicted based on the bandgap of PbVO_3Cl , the solar spectrum, and various losses. A high efficiency of 54.70% was predicted for Si (Table 4.3). However, these efficiencies of energy conversion using a single bandgap material are too low to satisfy the requirements for an actual application. As a result, a more efficient configuration can be achieved using a tandem configuration of $\text{PbVO}_3\text{Cl}/\text{Si}$ with multiple bandgaps.

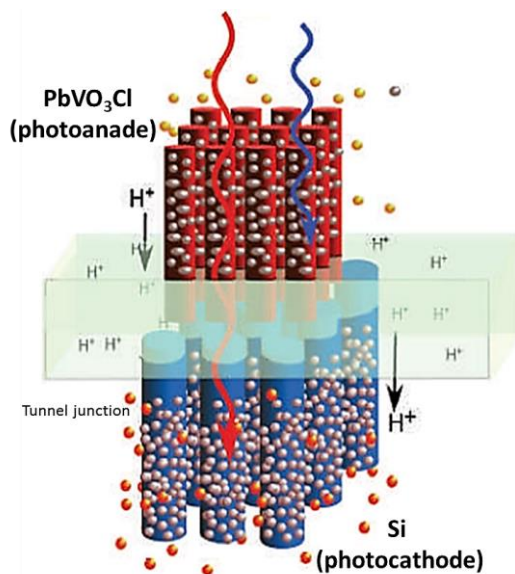


Figure 4.15. Lewis Structure in PEC cell. Reproduced with permission of the Nature Publishing Group (Nature Chemistry)(Gray 2009) 2009, Macmillan Publishers Limited.

Table 4.3. Electron energy efficiency result of PbVO₃Cl/Si tandem PEC device.

Device Layers	PbVO ₃ Cl	Si	Overall (Tandem device)
Wavelength range in photon absorption [nm]	280-547	547-1100	280-1100
Energy efficiency in photon absorption [%]	25.74	54.7	80.44
Thermalization Waste Energy[%]	15.21	17	32.21
Energy Efficiency in energy transportation from photon to electron [%]	10.53	37.7	48.23

When the white light comes to the tandem configuration of PbVO₃Cl/Si, firstly, PbVO₃Cl absorb the light up to ≤ 550 nm (25.74% of the photon energy) and then the Si continue to absorb lower intensity part of the light (≥ 1100 nm, 54.7% of the photon energy). Considering the efficiencies values for PbVO₃Cl and Si, the tandem efficiency is calculated as 80.44% for PbVO₃Cl/Si configuration.

It should be noted here that the band gap energies of PbVO₃Cl and Si allow transporting only 10.53% and 37.7% of the photon energy to the electron energy, respectively. Therefore, the overall tandem efficiency (efficiency of electron energy)

decreases to 48.23%. Nevertheless, 48.23% is a significant efficiency in comparison with other proposed PEC cells found in the literature, although the presence of the ~30% energy losses that caused by the thermalization process.

We theoretically demonstrated that the tandem configuration of $\text{PbVO}_3\text{Cl}/\text{Si}$ exhibited a 197% increase in efficiency relative to bare PbVO_3Cl , and 200% relative to bare Si, with almost a three-fold increase in current efficiencies at 500 nm. Hence, the overall light absorption spectral range of $\text{PbVO}_3\text{Cl}/\text{Si}$ is greatly extended. From the analysis of the results it can be said that tandem PEC cell can achieve much higher solar energy conversion efficiency than a single-junction-based PEC because of its higher photovoltage and larger light absorption spectral range.

4.6.3. How much voltage can be produced by designed device with PbVO_3Cl ? – The Band Position of PbVO_3Cl

Another key parameter for the semiconductors are the band positions. The band position helps to estimate the voltage production of the tandem system for photovoltaics and $\text{H}_2\text{-O}_2$ production of PEC cells for the water splitting process in solar fuel devices. Theoretically, for the well production of H_2 and O_2 in water splitting by using a semiconductor, the valance band and the conduction band of semiconductor must be at lower level than O_2 and higher level than H_2 , respectively. As can be seen from the Figure 4.16, the 1st position is the ideal position of $\text{PbVO}_3\text{Cl}/\text{Si}$ double layer semiconductor to use it in water splitting process (with respect to total voltage production of system), in spite of the 3rd position is seen that more efficient position for the $\text{H}_2\text{-O}_2$ production by PbVO_3Cl . Because of the valance band of Si (photocathode) and the conduction band of PbVO_3Cl (photoanode) are at the same energy level. In this situation, the electron transition occurs easily in tandem and the total voltage production of the system will be 3.3eV. The theoretical calculations show that the tandem efficiency will be 48.23% if the band position of PbVO_3Cl presences as the 1st position, in $\text{PbVO}_3\text{Cl}/\text{Si}$ device. However, the voltage production will be changed by the band position of photoanode. For instance, at the 2nd position, the electron transition occurs hardly and the total voltage production of system estimates as ~2.8 eV with ~0.5 eV waste energy (thermalization) due to band overlapping. Also, positioning at 4th makes the double layer system inefficient for water splitting because of being incapable of H_2 and O_2 production. These all possibilities for the band position of PbVO_3Cl should be

investigated by further studies to be ensured about the utility of the proposed device in solar energy conversion.

All in all, not only the band gap, but also the band positions are significant criteria in efficiency analysis of the tandem PECs to use in solar fuel devices. In this account, there is not any analysis about the band position of PbVO_3Cl , although the band gap of PbVO_3Cl was calculated by optical and theoretical methods. In further research, the band position of PbVO_3Cl will be analyzed. Also, future works of new solar fuel devices with respect to real band position of PbVO_3Cl will be proposed.

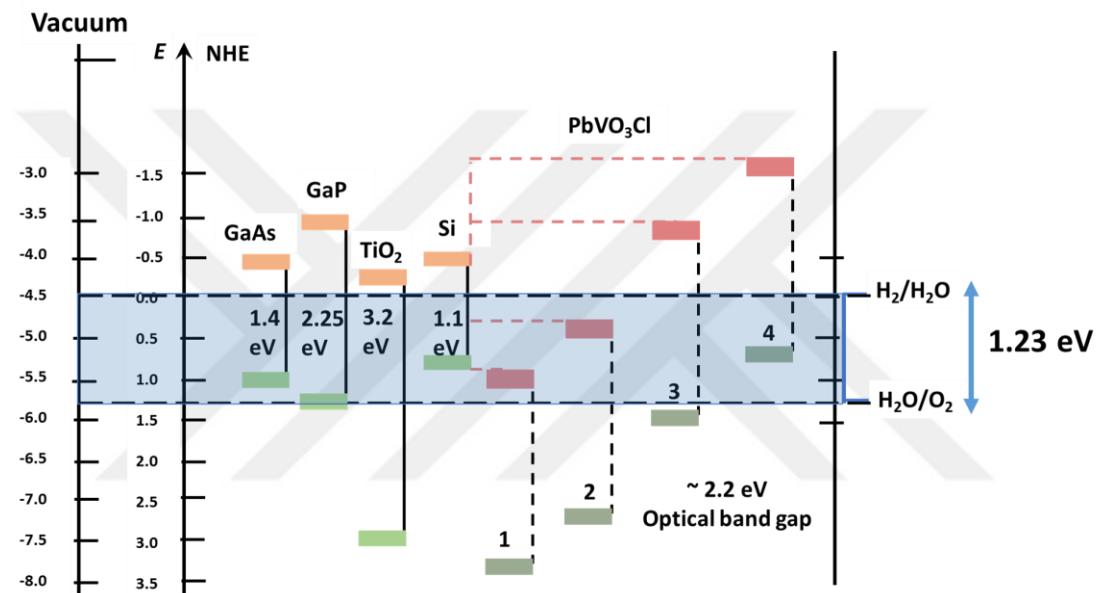


Figure 4.16. Band edge positions of selected semiconductors and 4 possible band edge positions of PbVO_3Cl .

4.6.4. Tecno-economic Analysis of PbVO_3Cl

Today, techno-economic analysis of products is based on principal and intermediate product prices. On the other hand, in PbVO_3Cl synthesis, only the material (elements) prices are taken as a basis. The reason is, NaVO_3 , PbCl_2 and B(OH)_3 , which are the materials used in synthesis of PbVO_3Cl , are mostly used in academical researches. This situation affects the price negatively because of non-commercialized structure. Since, rarity is a major parameter of cost, earth abundances of materials and production amounts have a big role on price(WebElements.com Archived from the original on 9 March 2007). Other two main parameters are the supply and demand levels. Table 4.4 shows the prices and earth abundancies of the main elements of

PbVO₃Cl, in 2012. A model was designed for Vanadium and Lead, because Chlorine and Oxygen prices are negligible (Chlorine is obtained from seas and Ozone can be produced/obtained with a minor negligible cost).

Table 4.4 Material list with respect to their earth abundancy and price.
(WebElements.com Archived from the original on 9 March 2007)

Elements	Price [\$ kg-1]	Earth Abundancy [%]
Pb (Lead)	1.9	0.00099
Cl (Chlorine)	1.5	0.017
V (Vanadium)	23	0.019
O (Oxygen)	0.003	46

As can be seen from Figure 4.17, exponential function of Vanadium and Lead, y , is used for extrapolation with a coefficient of determination (R^2) values. Both extrapolation models are based on exponential functions. It means that prices will tend to rise exponentially. According to extrapolation results, in 2020, the price forecast of Vanadium and Lead are around 23000 \$ unit tons⁻¹ and around 2000 \$ unit tons⁻¹, respectively. These values are the results of 0.77 and 0.87 R^2 values of vanadium and lead price estimations respectively.

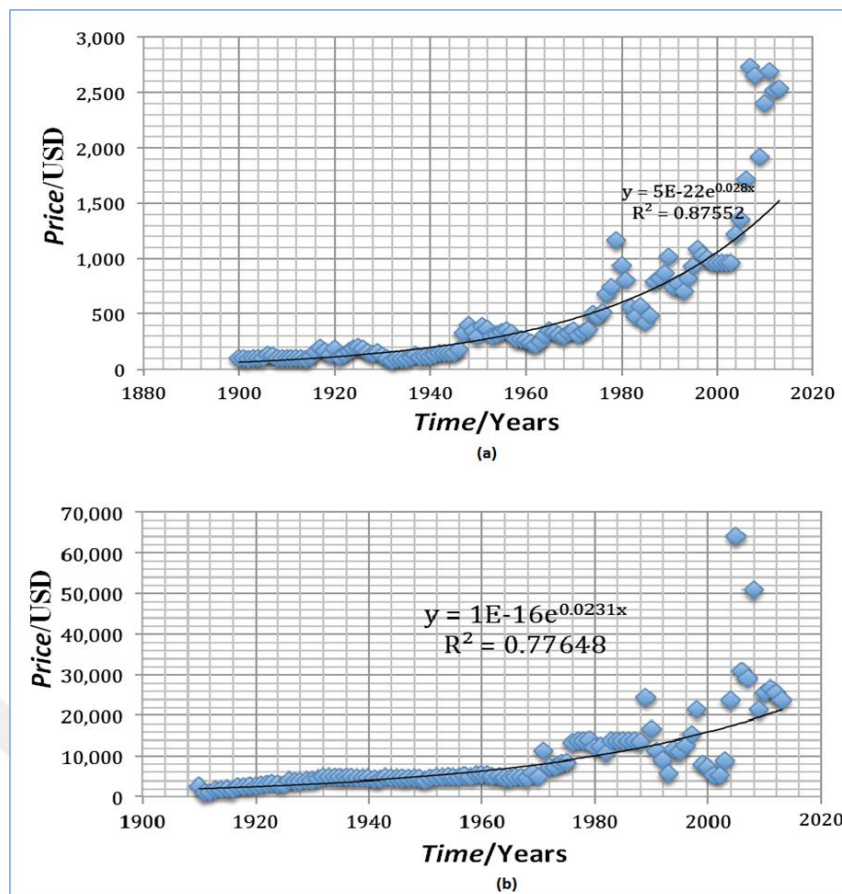


Figure 4.17. Plotting the price of a) Vanadium and b) Lead versus years (Service 2015). The tendency refers to forecasting in average price of the matter. The sharper temporal increase in price data may be caused by global wars or global crisis.

Regarding atomic weights, 1kg of $PbVO_3Cl$ will cost ~25 USD in 2020. As a conclusion, by using $PbVO_3Cl/Si$ device for future applications, the final price goal of novel solar fuel devices ($160\$ m^{-2}$) may be an achievable target.

Although $PbVO_3Cl$ did not give significant results in PWS experiments with various light sources, a price analysis was carried out in response to what would be the unit price for kWh for the efficient use of this produced hydrogen as fuel- if the hydrogen could be obtained from $PbVO_3Cl$ and water.

Primarily, it was assumed that 1 gram of $PbVO_3Cl$ yielded hydrogen from water in a 100% efficiency. Moreover, in Table 4.5, the amount of the needed substance, which use to obtain 1 kWh of energy for all fuel types, is shown in kg unit. According to hydrogen solubility in water values (Wiesenburg and Guinasso Jr 1979), max. 780.02 μmol of hydrogen dissolves in 1 L of water at 1 atm, at 25 °C and with 0 ‰ salinity. Namely, it means that $1.5723E-6$ kg of H_2 can be produced with a yield of 100% using 1

g of PbVO_3Cl in 1 L of water. As shown in the Table 4.5, for 1 kWh hydrogen energy can be obtained by 1 0.03003003 kg H_2 - means that the needed consumption amount of PbVO_3Cl should be 19.098 kg. According to estimated price/kg analysis of PbVO_3Cl , it is expected as 20\$ (USD) in 2016. Consequently, in order to obtain 1 kWh hydrogen energy by using PbVO_3Cl in PWS, it should be paid a price as 381.967 \$ (USD) when it is compared with other types of fuel, the financial cost to pay for 1kWh is considerably higher than the others.

Table 4.5. Comparison of hydrogen with other fuels that is based on their prices for 1 kWh, at 1 atm, at 25 °C, 1 atm.

FUELS	*Energy, kWh/kg	Mass in kg (to obtain 1kWh)	USD Price/kg (in 2016)	USD Price for 1 kWh (in 2016)
Hydrogen	33.3	0.03003003	20 (For PbVO_3Cl)	381.967 (For PbVO_3Cl)
Methane	12.8	0.078125	1.682	0.13125
Gasoline	12.4	0.080645161	1.02	0.082258064
Diesel	11.8	0.084745763	1.15	0.097457627
Methanol	5	0.2	1.6	0.32

*Same with Table 1.3 (Parthasarathy and Narayanan 2014).

4.7. Conclusion: Achievements of the chapter

PbVO_3Cl was synthesized by referencing from the research of Şahin A., and Emirdağ M. to be used as a photocatalyst in the designed experimental setup, and its unknown characteristics were tried to be determined by experimental and theoretical analyzes.

On that occasion, 4 optical band gaps were investigated and 3 theoretical band gaps were calculated. Whereby computational methods result, we had an agreement in transition type of PbVO_3Cl as an “indirect” transition. As a result of this, 2 optical band gaps were derived as 2.23 eV and 2.28 eV; and also, 3 theoretical band gaps as 1.65 eV, 2.05 eV, and 3.18 eV by using LDA, GGA, HSE06, respectively, however the HSE06 result (3.18 eV) was assumed more reliable result for a presumption in theoretical band gap energy of PbVO_3Cl . In addition to that the resistivity of PbVO_3Cl pellet was

measured and determined in average as 3.4 k Ω /cm and the phonon calculations were performed by using Raman Spectroscopy by DFT method.

After completing the characterization step, PbVO₃Cl was tried using various light sources and co-catalyst assistance in the new designed PWS system, but no significant results could be obtained. Additionally, a forecast - thought to be suitable for use as a photocatalyst due to its properties- was presented about efficiency of device which was designed (with respect to Lewis structure) with PbVO₃Cl as a photoanode and Si as a photocathode, even if no response was obtained by the PWS system. The photon absorption efficiency result of PbVO₃Cl/Si device was calculated as 80.44%, however 48.23% was transferred to electron, notably. When we compare 48.23% with other PEC devices, which are used in solar energy conversion, 48.23% looks promising percentage to investigate PbVO₃Cl in academical fields about solar energy conversion. Finally, an analysis was done due to hold a view about techno-economical position of PbVO₃Cl as ~25 USD/kg, in 2020.

CHAPTER 5

CONCLUSIONS AND FUTURE PERSPECTIVES

In this chapter, the conclusions of the work described in the previous chapters of this thesis are summarized. Moreover, several aspects are mentioned that can be useful for improvement of the new designed mini photoreactor for photocatalytic water splitting (PWS) applications.

This thesis is mainly focused on developing a new experimental set-up, which allows to work with smaller volumes in less time by using Unisense microsensors- four different microsensors (O₂, H₂, pH, T)- as a gas sensing method, for PWS applications. By considering the sizes of the microsensors, a mini photoreactor consisting of two parts, on which the sensors are stationary and which receives light directly into the solution in airtight environment, is designed by *Solidworks* and the physical modeling of the mini photoreactor was printed out successfully by 3D printer- *Objet30 Prime*.

The airtightness property required to enable the fabricated mini photoreactor to be used in PWS applications and the operation of the used microsensors as a gas sensing method in the light exposure of the designed mini photoreactor is performed with calibrated microsensors, and then, the system is tested by a common semiconductor, TiO₂-Degussa p25, to observe the changes, which are caused by photocatalytic effects, by the proposed PWS experimental set-up. The observations from experiments with TiO₂ confirmed that the proposed system in the co-operation of the fabricated mini photoreactor and microsensors is a functional experimental apparatus that can be used as an alternative apparatus for PWS applications.

Moreover, an attempt with a different semiconductor is presented by PbVO₃Cl, which was discovered in 2007 at IZTECH by M. Eanes and her research group, to diversify the examples in which is used by this alternative PWS apparatus. It is attempted to test some unknown optical characteristics of the material by using experimental and theoretical methods before testing by the proposed alternative experimental set-up, whether the new semiconducting material- PbVO₃Cl- has a function as a photocatalyst in PWS applications. As a result of these characterization analyzes, it is determined that PbVO₃Cl has a band structure of an “indirect” transition type and has a band gap energy experimentally and theoretically as ~2.2 eV ~3.18 eV,

respectively. Additionally, the resistivity of PbVO_3Cl , which its phonon calculations is performed by the comparison with DFT and Raman analysis, is determined in average as $3.4 \text{ k}\Omega/\text{cm}$ by Four Probe analysis.

After completing the characterization, PbVO_3Cl is tried using various light sources and co-catalyst (Pt) assistance in the new designed PWS system, but no significant results could be obtained. As known, the calculated efficiency limit of the system is between 0.0003814% and 0.000063567% , PbVO_3Cl may have a lower yield than this range in its photocatalytic reactions that carried out with water, therefore no activity is observed experimentally by the system. Besides, it is also possible that the platinum is not the right co-catalyst for needed help in H_2/O_2 production. There is another possibility that the material may not have the ability to produce hydrogen or oxygen since the band position is still unknown, although the it has sufficient band gap energy for PWS ($>1.23 \text{ eV}$).

Even if no response is obtained by the PWS system, a forecast- thought to be suitable for use it as a photocatalyst due to its properties- about the efficiency of device, which is designed wrt. Lewis structure by thick layer (indirect band structure) of PbVO_3Cl as a photoanode and silicon (Si) as a photocathode, is presented. Due to the fact that the applications of semiconductors in device design as a single crystal is easier and more significant, PbVO_3Cl can be called an ideal material for solar fuel device design, because PbVO_3Cl can be seen by naked eyes and be held by a tweezer to sever the needle crystals from each other if it needs. In the theory of this device, PbVO_3Cl can absorb the light up to $\leq 550 \text{ nm}$ (VIS region) of the solar irradiation and then Si can continue to absorb lower intensity part of the light (UV to N-IR, $\geq 1100 \text{ nm}$). Thus, the $\text{PbVO}_3\text{Cl}/\text{Si}$ device works with 48.23% of the photon absorption efficiency. In summary, when this efficiency value is compared with other PEC devices, which are used in solar energy conversion, it looks promising percentage to investigate and develop the usage of PbVO_3Cl , that its cost is expected to be $\sim 25 \text{ USD/kg}$ in 2020, in academical fields about solar energy conversion.

In conclusion, besides the success of the design, fabrication and measurement capability of the mini photoreactor, the proposed alternative experimental set-up, which is performed with the new designed mini photoreactor, provides solutions to the foreseen scientific problems in the PWS applications. Allowing for the measurement of small volumes, making it possible for a number of new photocatalysts, which are

difficult to synthesize or expensive to produce in a large scale, to be tested in PWS applications with a high number of repetitions. As the experimental solution, can be measured with four different parameters at the same time, it is possible to make a comment more accurately about the actual source of the change in the concentrations of oxygen and hydrogen that produced in the system. Therefore, the tendencies of the photocatalysts, which are tested in the system for PWS, can be analyzed more accurately. Besides, the fairly low efficiency limit of the system allows to observe and detect even the lowest O_2/H_2 productive photocatalysts. Furthermore, the new experimental apparatus for PWS application has another important output of the design work carried out, since it is one of the rare scientific studies using the three-dimensional printing technique. Consequently, the designed mini photoreactor for photocatalytic water splitting experiments in small volumes can be seen as a suitable and diversifiable part of the proposed PWS apparatus- which is introduced in this study- and it have a potential to be developed with innovative studies and it enables the usage areas to be replicated for the future applications.

REFERENCES

- Aguilar, Francisco X, and Warren Mabee. 2014. "A renewable source of energy." *Wood Energy in Developed Economies: Resource Management, Economics and Policy*:1.
- Allison, Ian, NL Bindoff, RA Bindschadler, PM Cox, Nathalie de Noblet, MH England, JE Francis, Nicolas Gruber, AM Haywood, and DJ Karoly. 2011. *The Copenhagen Diagnosis: Updating the world on the latest climate science*: Elsevier.
- Arnold, Mark A, and Mark E Meyerhoff. 1988. "Recent advances in the development and analytical applications of biosensing probes." *Critical Reviews in Analytical Chemistry* 20 (3):149-196.
- Atkins, Peter. 2010. *Shriver and Atkins' inorganic chemistry*: Oxford University Press, USA.
- Bak, T, J Nowotny, M Rekas, and CC Sorrell. 2002. "Photo-electrochemical hydrogen generation from water using solar energy. Materials-related aspects." *International journal of hydrogen energy* 27 (10):991-1022.
- Ball, P. 1999. "Reinventing the leaf." *Nature News*.
- Bamwenda, Gratian R, and Hironori Arakawa. 2001. "The visible light induced photocatalytic activity of tungsten trioxide powders." *Applied Catalysis A: General* 210 (1):181-191.
- Bank, Shodhganga Indian Thesis. Retrieved from: http://shodhganga.inflibnet.ac.in/bitstream/10603/21144/11/11_chapter%204.pdf
- Barber, James, and Phong D Tran. 2013. "From natural to artificial photosynthesis." *Journal of The Royal Society Interface* 10 (81):20120984.
- Bashouti, Muhammad Y, Gerald Brönstrup, Hossam Haick, Jordi Arbiol, Jürgen Ristein, Kasra Sardashti, Matthias Pietsch, Sanjay K Srivastava, Sebastian W Schmitt, and Silke Christiansen. 2012. *Hybrid silicon nanowires: from basic research to applied nanotechnology*: INTECH Open Access Publisher.
- Bencina, Metka, Matjaz Valant, Michael W. Pitcher, and Mattia Fanetti. 2014. "Intensive visible-light photoactivity of Bi- and Fe-containing pyrochlore nanoparticles." *Nanoscale* 6 (2):745-748. doi: 10.1039/C3NR04260J.
- Blöchl, P. E. 1994. "Projector augmented-wave method." *Physical Review B* 50 (24):17953-17979.
- Blok, Kornelis, and Evert Nieuwlaar. 2016. *Introduction to energy analysis*: Routledge.
- Bolton, James R, Stewart J Strickler, and John S Connolly. 1985. "Limiting and realizable efficiencies of solar photolysis of water." *Nature* 316:495.

- Borel, MM, J Chardon, A Leclaire, and B Raveau. 1999. "Chlorovanadates with Original Chain and Layered Structures: AVO_3Cl (A= Ba, Sr, Cd)." *Journal of Solid State Chemistry* 145 (2):634-638.
- Boris, D. Chernomordik, B. Russell Harry, Cvelbar Uros, B. Jasinski Jacek, Kumar Vivekanand, Deutsch Todd, and K. Sunkara Mahendra. 2012. "Photoelectrochemical activity of as-grown, α -Fe₂O₃ nanowire array electrodes for water splitting." *Nanotechnology* 23 (19):194009.
- Breyer, Christian, Dmitrii Bogdanov, Ashish Gulagi, Arman Aghahosseini, LSNS Barbosa, Otto Koskinen, M Baraza, Upeksha Caldera, Svetlana Afanasyeva, and Michael Child. 2016. "On the Role of Solar Photovoltaics in Global Energy Transition Scenarios." 32nd European Photovoltaic Solar Energy Conference.
- Brown, Laurie M. doi:. 1978. "The idea of the neutrino." *Physics Today* 9 (31):8-23. doi: 10.1063/1.2995181.
- Castellucci, Valeria, Mikael Eriksson, and Rafael Waters. 2016. "Impact of Tidal Level Variations on Wave Energy Absorption at Wave Hub." *Energies* 9 (10):843.
- Catalan, Lionel JJ, Victor Liang, and Charles Q Jia. 2006. "Comparison of various detection limit estimates for volatile sulphur compounds by gas chromatography with pulsed flame photometric detection." *Journal of Chromatography A* 1136 (1):89-98.
- Cody, GD, BG Brooks, and B Abeles. 1982. "Optical absorption above the optical gap of amorphous silicon hydride." *Solar Energy Materials* 8 (1):231-240.
- Cogdell, Richard J, Tatas HP Brotosudarmo, Alastair T Gardiner, Pedro M Sanchez, and Leroy Cronin. 2010. "Artificial photosynthesis—solar fuels: current status and future prospects." *Biofuels* 1 (6):861-876.
- Currao, Antonio. 2007. "Photoelectrochemical water splitting." *CHIMIA International Journal for Chemistry* 61 (12):815-819.
- Davids, Karel, and Carolus A Davids. 2012. *Religion, technology, and the great and little divergences: China and Europe compared, c. 700-1800*. Vol. 32: Brill.
- Davis, E. A., and N. F. Mott. 1970. "Conduction in non-crystalline systems V. Conductivity, optical absorption and photoconductivity in amorphous semiconductors." *Philosophical Magazine* 22 (179):0903-0922. doi: 10.1080/14786437008221061.
- Fujishima, Akira. 1972. "Electrochemical photolysis of water at a semiconductor electrode." *nature* 238:37-38.
- Furthmüller, J., J. Hafner, and G. Kresse. 1996. "Dimer reconstruction and electronic surface states on clean and hydrogenated diamond (100) surfaces." *Physical Review B* 53 (11):7334-7351.

- Garcia, Herncin E, and Louis I Gordon. 1992. "Oxygen solubility in seawater: Better fitting equations." *Limnology and oceanography* 37 (6):1307-1312.
- Giribabu, Krishnamoorthy, Ranganathan Suresh, Ramadoss Manigandan, Arunachalam Vijayaraj, Raju Prabu, and Vengidusamy Narayanan. 2012. "Cadmium sulphide nanorods: synthesis, characterization and their photocatalytic activity." *Bulletin of the Korean Chemical Society* 33 (9):2910-2916.
- Gray, Harry B. 2009. "Powering the planet with solar fuel." *Nature chemistry* 1 (1):7-7.
- Green, Martin A, Keith Emery, Yoshihiro Hishikawa, Wilhelm Warta, and Ewan D Dunlop. 2015. "Solar cell efficiency tables (Version 45)." *Progress in photovoltaics: research and applications* 23 (1):1-9.
- Griffiths, D. 2009. " Introduction to Elementary Particles." 2nd ed.:314-315.
- Grove, William Robert. 1874. *The Correlation of Physical Forces by WR Grove*: Longmans, Green.
- Gueymard, Christian A. 2004. "The sun's total and spectral irradiance for solar energy applications and solar radiation models." *Solar Energy* 76 (4):423-453. doi: <http://dx.doi.org/10.1016/j.solener.2003.08.039>.
- Heller, Adam. 1981. "Conversion of sunlight into electrical power and photoassisted electrolysis of water in photoelectrochemical cells." *Accounts of chemical research* 14 (5):154-162.
- Heller, Adam. 1984. "Hydrogen evolving solar cells." *Catalysis Reviews Science and Engineering* 26 (3-4):655-681.
- Hernández-Ramírez, Aracely, and Iliana Medina-Ramírez. 2014. *Photocatalytic Semiconductors: Synthesis, Characterization, and Environmental Applications*: Springer.
- Hohenberg, P., and W. Kohn. 1964. "Inhomogeneous Electron Gas." *Physical Review* 136 (3B):B864-B871.
- Hulanicki, Adam, Stanislav Glab, and FOLKE Ingman. 1991. "Chemical sensors: definitions and classification." *Pure and Applied Chemistry* 63 (9):1247-1250.
- Ivill, M, SJ Pearton, S Rawal, L Leu, P Sadik, R Das, AF Hebard, M Chisholm, John D Budai, and David P Norton. 2008. "Structure and magnetism of cobalt-doped ZnO thin films." *New Journal of Physics* 10 (6):065002.
- Jacobsson, T Jesper, and Tomas Edvinsson. 2012. "Photoelectrochemical determination of the absolute band edge positions as a function of particle size for ZnO quantum dots." *The Journal of Physical Chemistry C* 116 (29):15692-15701.
- Jensen, Carsten. 1999. *Controversy and consensus: nuclear beta decay 1911–1934*. Vol. 24: Springer Science & Business Media.

- Jerome, Harry. 1934. "Mechanization in industry." *NBER Books*.
- Jewett, John W, and Raymond A Serway. 2008. *Physics for scientists and engineers with modern physics*: Cengage Learning EMEA.
- Jo, Vinna, Min Kyung Kim, Il-Wun Shim, and Kang Min Ok. 2009. "Synthesis, structure, and characterization of a layered mixed metal oxychloride, PbVO₃Cl." *Bulletin of the Korean Chemical Society* 30 (9):2145-2148.
- Joachim, Harold Henry, and David Arthur Rees. 1953. "Aristotle: The Nicomachean Ethics."
- Joule, James P. 1845. "XXXI. On the existence of an equivalent relation between heat and the ordinary forms of mechanical power: To the editors of the Philosophical Magazine and Journal."
- K. Domen, S. Naito, M. Suma, T. Onishi, K. Tamaura 1980. *J. Chem. Soc. Chem. Commun.* (543).
- Kalyanasundaram, Kuppuswamy, and M Graetzel. 2010. "Artificial photosynthesis: biomimetic approaches to solar energy conversion and storage." *Current opinion in Biotechnology* 21 (3):298-310.
- Kampschreur, Marlies J, Wouter RL van der Star, Hubert A Wielders, Jan Willem Mulder, Mike SM Jetten, and Mark CM van Loosdrecht. 2008. "Dynamics of nitric oxide and nitrous oxide emission during full-scale reject water treatment." *Water Research* 42 (3):812-826.
- Kannammal, L., S. Palanikumar, B. Meenarathi, A. Yelilarasi, and R. Anbarasan. 2014. "Synthesis, characterization and band gap energy of poly(ϵ -caprolactone)/Sr-MSA nano-composite." *Journal of Physics D: Applied Physics* 47 (13):135109.
- Kim, Ki-Hyun. 2005. "Performance characterization of the GC/PFPD for H₂S, CH₃SH, DMS, and DMDS in air." *Atmospheric Environment* 39 (12):2235-2242.
- Kohn, W., and L. J. Sham. 1965. "Self-Consistent Equations Including Exchange and Correlation Effects." *Physical Review* 140 (4A):A1133-A1138.
- Kresse, G., and J. Furthmüller. 1996. "Efficient iterative schemes for *ab initio* total-energy calculations using a plane-wave basis set." *Physical Review B* 54 (16):11169-11186.
- Kresse, G., and J. Hafner. 1993. "Ab initio-molecular dynamics for liquid metals." *Physical Review B* 47 (1):558-561.
- Kresse, G., and J. Hafner. 1994. "Ab initio- molecular-dynamics simulation of the liquid-metal amorphous-semiconductor transition in germanium." *Physical Review B* 49 (20):14251-14269.

- Kudo, Akihiko, and Yugo Miseki. 2009. "Heterogeneous photocatalyst materials for water splitting." *Chemical Society Reviews* 38 (1):253-278.
- Lehn, Jean-Marie, and Raymond Ziessel. 1982. "Photochemical generation of carbon monoxide and hydrogen by reduction of carbon dioxide and water under visible light irradiation." *Proceedings of the National Academy of Sciences* 79 (2):701-704.
- Lehn, JM, JP Sauvage, and R Ziessel. 1980. Photochemical Water Splitting Continuous Generation of Hydrogen and Oxygen by Irradiation of Aqueous Suspensions of Metal Loaded Strontium-Titanate. GAUTHIER-VILLARS 120 BLVD SAINT-GERMAIN, 75280 PARIS CEDEX 06, FRANCE.
- Lewis, Nathan S. 2001. "Light work with water." *Nature* 414 (6864):589-590.
- Lewis, Nathan S., and Daniel G. Nocera. 2006. "Powering the planet: Chemical challenges in solar energy utilization." *Proceedings of the National Academy of Sciences* 103 (43):15729-15735. doi: 10.1073/pnas.0603395103.
- Li, Jiangtian, and Nianqiang Wu. 2015. "Semiconductor-based photocatalysts and photoelectrochemical cells for solar fuel generation: a review." *Catalysis Science & Technology* 5 (3):1360-1384.
- Liu, Xiao, Sitian Cheng, Hong Liu, Sha Hu, Daqiang Zhang, and Huansheng Ning. 2012. "A survey on gas sensing technology." *Sensors* 12 (7):9635-9665.
- Luca, Vittorio, Dugald J Maclachlan, James M Hook, and Ray Withers. 1995. "Synthesis and characterization of mesostructured vanadium oxide." *Chemistry of materials* 7 (12):2220-2223.
- Macquorn Rankine, William John. 1853. "XVIII. On the general law of the transformation of energy." *The London, Edinburgh, and Dublin Philosophical Magazine and Journal of Science* 5 (30):106-117.
- Malhotra, Vaibhav, José L Fernández Solís, Sarel Lavy, and Michael Neuman. 2010. "Feasibility of an Off-Grid Renewable Energy Source for the Mercantile Sector." *Journal of Green Building* 5 (1):71-87.
- Martinot, Eric, and Janet L Sawin. 2012. "Renewables 2012 global status report." *Renewable Energy Policy Network for the 21st Century*.
- Masamoto, Kazuto, Alberto Vazquez, Ping Wang, and Seong-Gi Kim. 2009. "Brain Tissue Oxygen Consumption And Supply Induced By Neural Activation." In *Oxygen Transport to Tissue XXX*, 287-292. Springer.
- Mentré, Olivier, Marielle Huvé, and Francis Abraham. 1999. "Bidimensional Cationic Ordering and Thermal Dependence in β -Pb x V 2 O 5 Bronzes." *Journal of Solid State Chemistry* 145 (1):186-196.

- Millero, Frank J, and Alain Poisson. 1981. "International one-atmosphere equation of state of seawater." *Deep Sea Research Part A. Oceanographic Research Papers* 28 (6):625-629.
- Monkhorst, Hendrik J., and James D. Pack. 1976. "Special points for Brillouin-zone integrations." *Physical Review B* 13 (12):5188-5192.
- More, Charles. 2002. *Understanding the industrial revolution*: Routledge.
- Moriarty, Patrick, and Damon Honnery. 2009. "Hydrogen's role in an uncertain energy future." *International Journal of Hydrogen Energy* 34 (1):31-39.
- Morrison, Stanley Roy. 1980. "Electrochemistry at semiconductor and oxidized metal electrodes."
- Mott, NF, and EA Davis. 1979. "Electronic processes in non-crystalline solids." *Clarendon, Oxford*:465.
- Murphy, A. B. 2007. "Band-gap determination from diffuse reflectance measurements of semiconductor films, and application to photoelectrochemical water-splitting." *Solar Energy Materials and Solar Cells* 91 (14):1326-1337. doi: <http://dx.doi.org/10.1016/j.solmat.2007.05.005>.
- Navarro Yerga, Rufino M, M Consuelo Álvarez Galván, F Del Valle, José A Villoria de la Mano, and Jose LG Fierro. 2009. "Water Splitting on Semiconductor Catalysts under Visible-Light Irradiation." *ChemSusChem* 2 (6):471-485.
- Nelson, Vaughn C, and Kenneth L Starcher. 2015. *Introduction to renewable energy*: CRC press.
- Nylander, C. 1985. "Chemical and biological sensors." *Journal of Physics E: Scientific Instruments* 18 (9):736.
- Oharazawa, Hideaki, Tsutomu Igarashi, Takashi Yokota, Hiroaki Fujii, Hisaharu Suzuki, Mitsuru Machide, Hiroshi Takahashi, Shigeo Ohta, and Ikuroh Ohsawa. 2010. "Protection of the retina by rapid diffusion of hydrogen: administration of hydrogen-loaded eye drops in retinal ischemia-reperfusion injury." *Investigative ophthalmology & visual science* 51 (1):487-492.
- Ohtani, B. 2010. "Photocatalysis A to Z—What we know and what we do not know in a scientific sense." *Journal of Photochemistry and Photobiology C: Photochemistry Reviews* 11 (4):157-178.
- Oppenheim, J, and ED Beinhocker. 2009. "Climate change and the economy: myths versus realities." *McKinsey & Company*, available at http://www.euractiv.com/25/images/Climate_change_myths.pdf (accessed on 15 July 2009).
- Painuly, Jyoti P. 2001. "Barriers to renewable energy penetration; a framework for analysis." *Renewable energy* 24 (1):73-89.

- Parthasarathy, Prakash, and K Sheeba Narayanan. 2014. "Hydrogen production from steam gasification of biomass: Influence of process parameters on hydrogen yield—A review." *Renewable Energy* 66:570-579.
- Pelaez, Miguel, Nicholas T Nolan, Suresh C Pillai, Michael K Seery, Polycarpus Falaras, Athanassios G Kontos, Patrick SM Dunlop, Jeremy WJ Hamilton, J Anthony Byrne, and Kevin O'shea. 2012. "A review on the visible light active titanium dioxide photocatalysts for environmental applications." *Applied Catalysis B: Environmental* 125:331-349.
- Pellizetti, E, and N Serpone. 1989. *Photocatalysis, Fundamentals and Applications*. Wiley, New York.
- Perdew, J. P., and Alex Zunger. 1981. "Self-interaction correction to density-functional approximations for many-electron systems." *Physical Review B* 23 (10):5048-5079.
- Perdew, John P., Kieron Burke, and Matthias Ernzerhof. 1996. "Generalized Gradient Approximation Made Simple." *Physical Review Letters* 77 (18):3865-3868.
- Perez, Richard, and Marc Perez. 2009. "A fundamental look at energy reserves for the planet." *The IEA SHC Solar Update* 50 (2).
- Phuruangrat, Anukorn, Oranuch Yayapao, Titipun Thongtem, and Somchai Thongtem. 2014. "Preparation, characterization and photocatalytic properties of Ho doped ZnO nanostructures synthesized by sonochemical method." *Superlattices and Microstructures* 67:118-126.
- Pullen, Angelika. 2007. "Global wind energy markets continue to boom—2006 another record year." *Global Wind Energy Council Press Release, Brussels, Belgium*.
- Purchase, Robin, H Vriend, Huub de Groot, PFH Harmsen, and Harriëtte Louise Bos. 2015. *Artificial photosynthesis: for the conversion of sunlight to fuel*: Leiden University.
- Qasim, Mohammad. 2014. "The Fact of the Energy." Review of www.iiste.org. *Advances in Physics Theories and Applications* 29 (47).
- Rakowski Dubois, Mary, and Daniel L Dubois. 2009. "Development of molecular electrocatalysts for CO₂ reduction and H₂ production/oxidation." *Accounts of Chemical Research* 42 (12):1974-1982.
- Reeve, Charles David Chanel. 1992. "Practices of reason: Aristotle's Nicomachean ethics."
- Rehman, Shama, Ruh Ullah, AM Butt, and ND Gohar. 2009. "Strategies of making TiO₂ and ZnO visible light active." *Journal of Hazardous Materials* 170 (2):560-569.

- Rider, Christine. 2007. *Encyclopedia of the Age of the Industrial Revolution, 1700-1920: OZ and primary documents*. Vol. 2: Greenwood Publishing Group.
- Roeb, Martin, Nils Gathmann, Martina Neises, Christian Sattler, and Robert Pitz-Paal. 2009. "Thermodynamic analysis of two-step solar water splitting with mixed iron oxides." *International Journal of Energy Research* 33 (10):893-902.
- Roel van de Krol, Michael Grätzel. 2012. "Photoelectrochemical Hydrogen Production." *Springer US* 102:239-318. doi: 10.1007/978-1-4614-1380-6.
- Sahin, Aytac, and Mehtap Emirdag-Eanes. 2007. "Crystal structure of lead (II) trioxovanadate (V) chloride, Pb [VO₃] Cl." *Zeitschrift für Kristallographie-New Crystal Structures* 222 (3):159-160.
- Sato, Shinri, and John M White. 1980. "Photocatalytic production of hydrogen from water and Texas lignite by use of a platinized titania catalyst." *Industrial & Engineering Chemistry Product Research and Development* 19 (4):542-544.
- Serpone, Nick, and Ezio Pelizzetti. 1989a. *Photocatalysis: fundamentals and applications*. Vol. 251: Wiley New York.
- Serpone, Nick, and Ezio Pelizzetti. 1989b. *Photocatalysis: fundamentals and applications*: Wiley-Interscience.
- Service, Argus Media. 2015. "Metal Price Historical Database 1990-2015." <http://www.metalprices.com/historical/database>.
- Setyawan, Wahyu, and Stefano Curtarolo. 2010. "High-throughput electronic band structure calculations: Challenges and tools." *Computational Materials Science* 49 (2):299-312.
- Shang, Meng, Wenzhong Wang, Ling Zhang, and Haolan Xu. 2010. "Bi₂WO₆ with significantly enhanced photocatalytic activities by nitrogen doping." *Materials chemistry and physics* 120 (1):155-159.
- Sidén, Göran, Hylander Jonny, Charlotta Winkler, and Christian Stenqvist. 2016. 100 procent förnybar elenergi år 2020–2025–2030? : Högskolan i Halmstad.
- Sinha, Subrata, and S Chattopadhyay. 2015. "A Study on Application of Renewable Energy Technologies for Mitigating the Adverse Environmental Impacts Generated from Power Generation Units in Himalayan Region." *Population (millions)* 2030:2050-2100.
- Smil, Vaclav. 1994. "Energy in world history."
- Smil, Vaclav. 2000. "Perils of long-range energy forecasting: reflections on looking far ahead." *Technological Forecasting and Social Change* 65 (3):251-264.
- Smith, Crosbie. 1998. *The science of energy: A cultural history of energy physics in Victorian Britain*: University of Chicago Press.

- SourceOECD. 2006. *World energy outlook: OECD/IEA*.
- Spitzer, WG, MI Gershenzon, CJ Frosch, and DF Gibbs. 1959. "Optical absorption in n-type gallium phosphide." *Journal of Physics and Chemistry of Solids* 11 (3):339-341.
- Stearns, Peter N. 1993. *The Industrial Revolution in World History*., 1998. Westview Press, Boulder, CO.
- Steinfeld, Aldo, and Anton Meier. 2004. "Solar fuels and materials." *Encyclopedia of energy* 5:623-637.
- Sun, Ke, Shaohua Shen, Yongqi Liang, Paul E Burrows, Samuel S Mao, and Deli Wang. 2014. "Enabling silicon for solar-fuel production." *Chemical reviews* 114 (17):8662-8719.
- Sze, SM. 1981. "Physics of semiconductor devices Wiley Eastern." *New York*.
- Takeuchi, Masato, Yukari Shimizu, Hiromasa Yamagawa, Tomoyoshi Nakamuro, and Masakazu Anpo. 2011. "Preparation of the visible light responsive N³⁻-doped WO₃ photocatalyst by a thermal decomposition of ammonium paratungstate." *Applied Catalysis B: Environmental* 110:1-5.
- Tang, Junwang, Defa Wang, Zhi Gang Zou, and Jin Hua Ye. 2003. "Modification of photophysical properties of WO₃ by doping different metals." *Materials Science Forum*.
- Tauc, J, R Grigorovici, and A Vancu. 1966. "Optical properties and electronic structure of amorphous germanium." *physica status solidi (b)* 15 (2):627-637.
- Tauc, Jan. 1966. "The optical properties of solids." *The Optical Properties of Solids*.
- Thorsteinsson, Hildigunnur, C Augustine, BJ Anderson, MC Moore, and JW Tester. 2008. "The impacts of drilling and reservoir technology advances on EGS exploitation." *Proceedings, Thirty-Third Workshop on Geothermal Reservoir Engineering, Institute for Sustainable Energy, Environment, and Economy (ISEEE)*.
- Togo, Atsushi, and Isao Tanaka. 2015. "First principles phonon calculations in materials science." *Scripta Materialia* 108:1-5.
- Turner, JA. 1999. "A realizable renewable energy future (vol 285, pg 687, 1999)." *Science* 285 (5433):1493-1493.
- Ulstrup, Karin E, Ross Hill, and Peter J Ralph. 2005. "Photosynthetic impact of hypoxia on in hospite zooxanthellae in the scleractinian coral *Pocillopora damicornis*." *Marine Ecology Progress Series* 286:125-132.
- Van de Krol, Roel, and Michael Grätzel. 2012a. "Photoelectrochemical hydrogen production." *Springer US*:17-18.

- Van de Krol, Roel, and Michael Grätzel. 2012b. *Photoelectrochemical hydrogen production*. Vol. 90: Springer.
- Van de Krol, Roel, Michael Grätzel, Michael Grätzel, and Michael Grätzel. 2012. *Photoelectrochemical hydrogen production*: Springer.
- Vannier, RN, G Mairesse, G Nowogrocki, F Abraham, and JC Boivin. 1992. "Electrical and structural investigations on a new bismuth lead vanadium oxide solid electrolyte." *Solid state ionics* 53:713-722.
- Viezbicke, Brian D., Shane Patel, Benjamin E. Davis, and Dunbar P. Birnie. 2015. "Evaluation of the Tauc method for optical absorption edge determination: ZnO thin films as a model system." *physica status solidi (b)* 252 (8):1700-1710. doi: 10.1002/pssb.201552007.
- Walsh, Bryan. 2008. "Solar power's new style." *Time* 171 (25):62-63.
- Walter, Michael G, Emily L Warren, James R McKone, Shannon W Boettcher, Qixi Mi, Elizabeth A Santori, and Nathan S Lewis. 2010. "Solar water splitting cells." *Chemical reviews* 110 (11):6446-6473.
- WebElements.com. Archived from the original on 9 March 2007. "Abundance in Earth's Crust."
- Werle, Peter, Franz Slemr, Karl Maurer, Robert Kormann, Robert Mücke, and Bernd Jänker. 2002. "Near-and mid-infrared laser-optical sensors for gas analysis." *Optics and lasers in engineering* 37 (2):101-114.
- Wiesenburg, Denis A, and Norman L Guinasso Jr. 1979. "Equilibrium solubilities of methane, carbon monoxide, and hydrogen in water and sea water." *Journal of Chemical and Engineering Data* 24 (4):356-360.
- Wilson, Fred L. 1968. "Fermi's theory of beta decay." *American Journal of Physics* 36 (12):1150-1160.
- WITTMER, DALE E, and RELVA C BUCHANAN. 1981. "Low-Temperature Densification of Lead Zirconate-Titanate with Vanadium Pentoxide Additive." *Journal of the American Ceramic Society* 64 (8):485-490.
- Young, Thomas. 1807. *A course of lectures on natural philosophy and the mechanical arts*. Vol. 2: Johnson.
- Yu, Yingchun, Youxian Ding, Shengli Zuo, and Jianjun Liu. 2010. "Photocatalytic activity of nanosized cadmium sulfides synthesized by complex compound thermolysis." *International Journal of Photoenergy* 2011.

Zhu, Liying, Woo-Jin An, Joseph W. Springer, Luis B. Modesto-Lopez, Sravani Gullapalli, Dewey Holten, Michael S. Wong, and Pratim Biswas. 2012. "Linker-free quantum dot sensitized TiO₂ photoelectrochemical cells." *International Journal of Hydrogen Energy* 37 (8):6422-6430. doi: 10.1016/j.ijhydene.2012.01.028.

